SOME STUDIES RELATING TO LOG-PERIODIC AND ASYMMETRIC DIPOLE ANTENNAS

THESIS SUBMITTED IN
PARTIAL FULFILMENT OF THE
REQUIREMENT FOR THE DEGREE OF

DOCTOR OF PHILOSOPHY

IN

PHYSICS

by

P. K. BANERJEE

at

BIRLA INSTITUTE OF TECHNOLOGY & SCIENCE

PILANI, RAJASTHAN, INDIA

1972

BIRLA INSTITUTE OF TECHNOLOGY & SCIENCE

PILANI (RAJASTHAN)

SUPERVISOR'S NOTE

The thesis entitled "SOME STUDIES RELATING TO LOG- PERIODIC DIPOLE AND ASYMMETRIC DIPOLE ANTENNAS" submitted by Mr. P. K. Banerjee, M. Sc., in partial fulfilment of the degree of Doctor of Philosophy, embodies the results of the investigations done under my supervision and I certify that the work is original.

Subrahmaniam

(V. Subrahmaniam)

PREFACE

It is the purpose of this thesis to present a study of the effect of feed point displacement on the electrical characteristics of asymmetric dipole antenna. An effort has been made to give a detailed analysis for deriving expressions for various important parameters of the antenna system mentioned above. The analysis presented in chapter 2 has been utilised in chapter 5 to suggest a new type of log-periodic structure, namely, the log-periodic structure consisting of asymmetric dipole elements. The study of the displaced dipole antenna system has been extended to investigate the effect of the plasma medium on the displaced asymmetric dipole antenna.

With a deep sense of gratitude, the author wishes to convey his heartfelt thanks to Dr. V. Subrahmanium, Assistant Professor, Department of Physics, Birla Institute of Technology and Science, for supervising the work.

It gives him immense pleasure to acknowledge the encouragement given by Dr. A. K. Dutta Gupta, Dean Faculty of Science and Dr. J. S. Verma, Head, Dept. of Physics, Birla Institute of Technology & Science. The facilities for the experimental work provided by Prof. K. V. Ramanan, Head, Department of Electrical & Electronics Engineering, Birla Institute of Technology & Science, is also gratefully acknowledged. The active help given by Mr. S. V. N. Rao, Department of Electrical and Electronics Engineering in carrying out the experimental investigations is also acknowledged.

It is the proud previlege of the author to acknowledge the vital help given by Mr. G. R. Rao, Mrs. G. Banerjee, Mr. N. K. Joshi, Mr. Chandra Shekhar Sharma, Mr. B. K. Kaushik, Miss V. L. Dewan and Mr. D. P. Sharma, Department of Physics, Birla Institute of Technology & Science, Pilani. The author is also thankful to Mr. S. K. Sinha for typing the manuscript. The facilities for the fabrication of the antenna system used in experimental work given by the Central Workshop, Pilani is greatly appreciated. The author also appreciates the help and cooperation given by Mr. S. Raghunath, C.S.D. , C.E.E.R.I., Pilani during the various stages of the work reported in this thesis. The co-operation given by the staff members , Department of Physics and all others involved directly or indirectly is worth appreciting .

Finally the author wishes to thank the University Grants Commission, New Delhi for providing financial assistance in the form of J.R.F. and the Information Processing Centre, B.I.T.S., Pilani for providing computations facilities.

P. K. Banerjee.

•••

TABLE OF CONTENTS

***

C H A P T E R - 1

INTRODUCTION

§ 1.1 LITERATURE SURVEY

1.1.1 A Linear Dipole Antenna:- A linear dipole antenna is widely used and well studied antenna. Depending on the type of feeding arrangement, there result two types of dipole antennas namely, the centrefed dipole or symmetric dipole and the asymmetric dipole whose feeding point is not at the centre. A large amount of theoretical and experimental work is available in standard texts written by King (1), Kraus (2), Schelkunoff (3) and Jordan (4).

Smith (5) observed that the theoretical and experimental results obtained for input impedance of a half wave dipole do not agree with each other, mainly due to the differences in the feeding arrangements used. R.A. Smith and C.H. Smith (6) have shown experimentally that the resistive part of the impedance of the antenna depends on the spacing at the centre of the dipole and on the method of feeding by the transmission line. Schelkunoff (7) investigated the effect of the feed gap on the input impedance and predicted that the resistive part of the input impedance decreases with the increase in the spacing of the feed gap.

As stated above the feed gap plays an important role in determining the input impedance of the antenna system.

In order to study the effect of variations of this feed gap on the electrical characteristics of the system, Kosta (8) introduced the concept of feed point displacement in 1967. Since then the centre fed dipole with displaced feed points has been the subject of many investigations.

However, the scope of the feed point displacement method was limited in the sense that the feed point displacement more than 0.1.λ resulted in inaccurate results. The reason is attributed to the fact that the feed point displacement requires the inclusion of proper function to describe the appreciable field produced in the gap region resulting from such displacements. To avoid complications, this field in the gap region is usually neglected so far as the displacement is within the above range. However, varying the feed point displacement from 0.0 to 0.1.λ produced an appreciable scanning of the beam. Specially a particular configuration of displaced system, namely, the transversely displaced configuration was found useful in describing the Log-periodic array.

1.1.2 Log-periodic Dipole Array:- Log-periodic antennas are widely used for very wide band operations and were earlier referred to as frequency independent antennas. The electrical properties of these antennas, such as, the radiation pattern, the radiation resistance, etc. change to a

negligible extent with the operating frequency over a band which is only limited by the size of the lowfrequency elements and by the constructional accuracy at the high frequency end of the band. These antennas also yield a substantial directive gain and as such have an edge over directive radiators with a narrow band width operation. Since the inception of these aerials they are satisfactorily utilized in VHF, UHF and SHF bands.

Du-Hamel (9) invented a planar log-periodic antenna structure shown in the fig (1.3). The electrical performance of this structure repeats it self periodically with the logarithm of the frequency because of its geometry and hence the structure is called " Log-periodic ". After Isbell (10) introduced the nonplanar log-periodic structure, Du-Hamel and his coworkers (11) enhanced the practical value of Log-periodic antenna by using wire structures and extending applications from microwaves to high frequency band. The importance of the log-periodic antennas was given a further boost when in U.S.A. Isbell (12) introduced a novel design concept in the log-periodic dipole antennas. In England Radford(13) took the lead in the design and development of logarithmic antennas for communication systems. Since the inception of log-periodic antennas, various research workers in different countries were involved in the development

of the theory governing the properties of these antennas. Although the geometrical principles governing these antennas are quite simple, according to Rumsey (14), no well defined theory to explain the experimentally observed properties of these antennas is so far available. The Log-periodic design has largely been an art, an application of empiricism based on intuition and not really a science.

Carrel (15) has proposed an analysis of the log-periodic dipole antenna from the point of view of the linear array theory taking in to account the self and mutual coupling effects between eight dipoles. He has also taken in to consideration the unequal length of the dipoles in his theory. Many research workers such as Mittra and Jones (16), Mages, Deschamps and Patton (17) etc. studied the log-periodic dipole antenna from periodically loaded (loaded with dipoles) transmission line concept. Use of Brillouin diagram was also made by Mittra and Jones (16) to explain the performance of log-periodic dipole array. It was pointed out by them that the multimode propagation exists in the periodically loaded transmission line when mutual coupling terms are considered but analysis of log-periodic dipole structure based on periodically loaded transmission line concept can not explain fully the multimode type of pro-

pagation. In conclusion it was also stated that the argument behind this line of approach, has largely been heuristic and thoroughanalysis of the log-periodic structures was yet to be worked out. Kosta (18) in 1967 presented the simplified theory of the log periodic dipole antenna from simple consideration of the linear array theory. Although this analysis was quite approximate (valid for the active region only) in nature but it was found to be quite useful in engineering applications where simplicity is of primary importance within a tolerable percentage of error.

1.1.3 Effect of Plasma Medium on Dipole Radiation:- It is well known that performance of a radiating source immersed in a plasma medium is different from its performance in free space. In last few years many investigations have been carried out to predict the effect of plasma medium on the radiation characteristics of a centre fed dipole. Cohen (19) has shown that an electric source immersed in a homogeneous plasma of infinite extent can excite an electroacoustic wave in addition to the usual electromagnetic wave. In absence of static electric or magnetic field, the electromagnetic waves are uncoupled and can be separated in to two independent modes. The electromagnetic waves become an ordinary transverse magnetic wave and the electroacoustic wave becomes an ordinary longitudional wave at great distances from the source.

Chen (20) has shown that the radiation resistance of an antenna is seriously effected by the presence of electro-acoustic wave.

Later in 1966, Talekar (21) studied the effect of weakly ionized gas type plasma medium on the finite size half wave dipoles. He has shown that for source frequencies far-far greater than the plasma frequency, the e.m. mode radiation resistance remains almost uneffected while the acoustic mode has an appreciable part of radiation resistance. However, for source frequencies equal to the plasma frequency the question of mode propagation becomes meaningless because all far fields reduce to Fresnel zone fields owing to the great attenuation suffered by the waves. At source frequencies far far less than the plasma frequencies, the e.m. mode travels with attenuation. The plasma mode has an epperciable radiation resistance in this case.

To investigate the effect of plasma medium on the centre fed dipole with arbitrarily displaced feed points, Kosta and Singh (22) carried out the analysis for far field radiation pattern. These investigations have shown that the radiation characteristics in plasma has entirely different characteristics than that in free space. Such studies have been found extensively useful for applications in space vehicles and satellites passing through the ionosphere.

§ 1.2 SYNOPSIS OF THE THESIS

The present investigation is taken up with a view to study the effect of feed point gap and the medium on electrical properties of the asymmetric dipoles.

1.2.1 Asymmetric Dipole:- Chapter 2 has been devoted to the theoretical and experimental investigation of the Asymmetric dipole antenna with arbitrarily displaced feed points. Taking sinusoidal current distribution the analysis has been carried out. Variation of various parameters like, radiation pattern, radiation resistance, gain etc. with the feed point displacement $2R/\lambda$ has been predicted. The entire study has been carried out in three cases:

(i) Arbitrary Displacement: This case has been studied by taking arbitrary displacement angle $\theta_1 = \theta_2 = 45^\circ$, fig (1.1a), $\frac{h_1}{\lambda} = 0.25$ and $\frac{h_2}{\lambda} = 0.75$. Theoretical calculations have been carried out for various values of feed point displacement $\frac{2R}{\lambda} = 0.04$ to 0.16. It has been possible to obtain a small scanning of 5° of the beam max. with in the above range of variation of the feed point displacement. It is found that radiation resistance decreases with the increase in $\frac{2R}{\lambda}$ values while power gain increases with the increase in $\frac{2R}{\lambda}$ values.

(ii) Transverse Displacement: This is a special case of arbitrary displacement. By putting $\theta_1 = \theta_2 = \frac{\pi}{2}$, fig(1.1b),

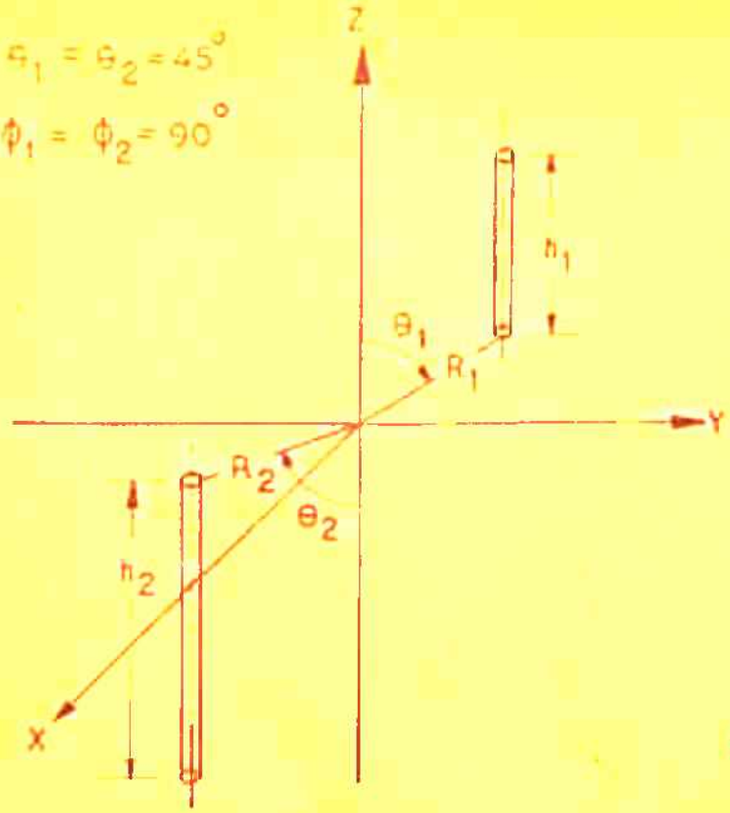

FIG. (1·1 a) ARBITRARILY DISPLACED ASY. DIPOLE ANTENNA.

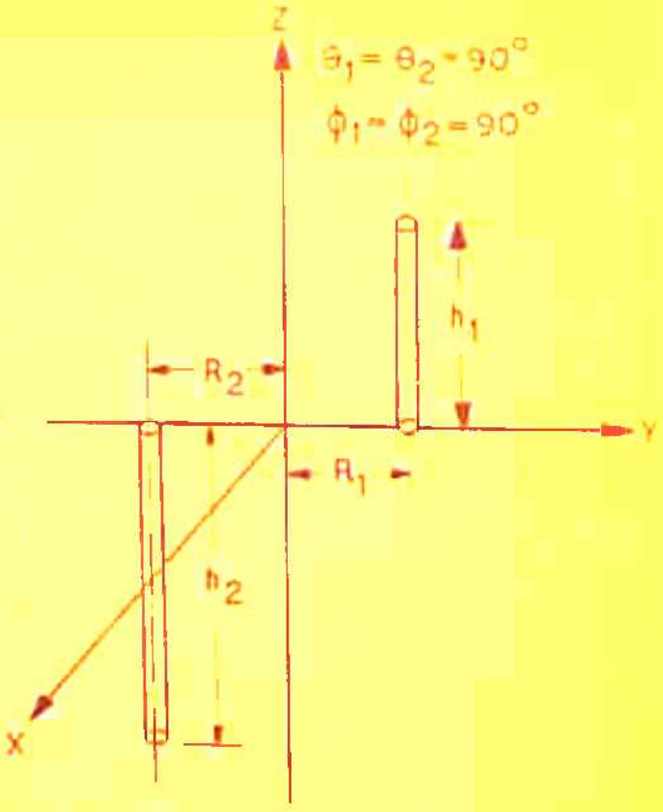

FIG. (1·1 b) TRANSVERSELY DISPLACED ASY. DIPOLE ANTENNA.

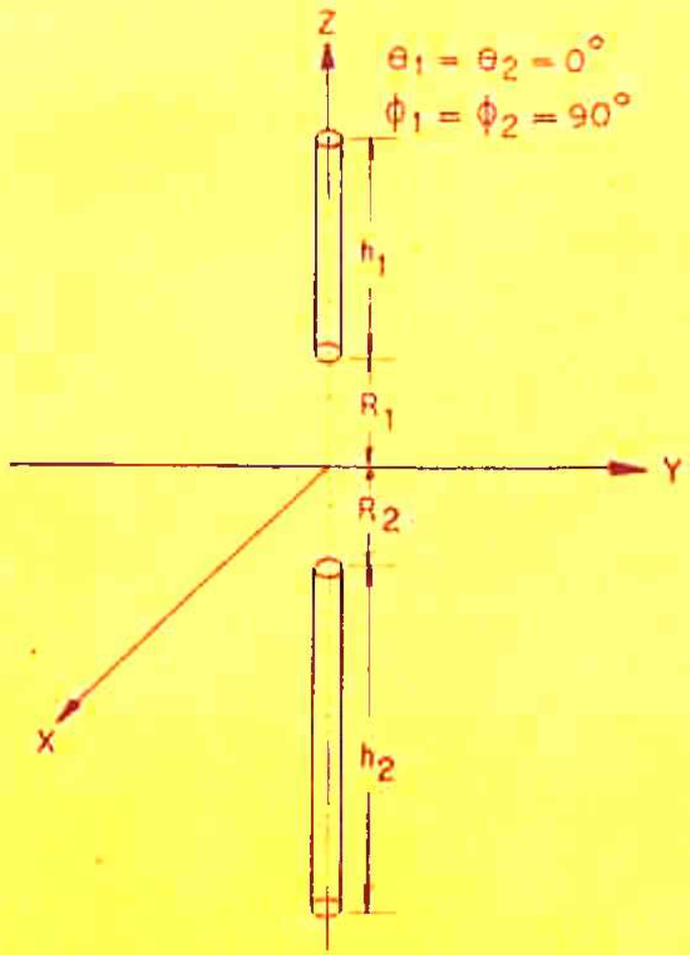

FIG. (1·1 c) AXIALLY DISPLACED ASY. DIPOLE ANTENNA.

one easily obtains the expression for the transversely displaced case. There also the whole pattern shifts by 5^{o} as $\frac{2R}{\lambda}$ values are varied in the above range. Variations of radiation resistance and gain are similar to the case of arbitrary displacement. This case is an important one as the analysis of this configuration forms the basis of explanation of the nonplanar log periodic dipole array with successive elements displaced transversely to their axis.

(iii) Axial Displacement: By putting $\theta_1 = \theta_2 = 0^{o}$, fig(1.1c), expressions for various parameters for axially displaced case are obtained. However in this case, unlike the arbitrarily and transversely displaced cases, the pattern remains unchanged for various values of $\frac{2R}{\lambda}$. Radiation resistance decreases with the increase in $\frac{2R}{\lambda}$ values while gain increases with the increase in $\frac{2R}{\lambda}$ values. Experimental investigations have also been carried out for transverse and axial displacements. The theoretical and experimental results are in good agreement. Experimental set up has been discussed in detail in this chapter.

1.2.2 Input Impedance of Transversely Displaced Asymmetric Dipole Antenna: Analysis of the input impedance of the transversely displaced asymmetric dipole antenna, fig(1.2b), has been presented in chapter 3. Input impedance has been studied as a function of the feed point displacement for various values of the displacement $\frac{2R}{\lambda}$ starting from 0.0

to 0.16. The input impedance has then been measured experimentally. Agreement between theoretical and experimental results is reasonably good.

1.2.3 Input Impedance and Gain of Log-periodic Dipole Antenna: A simple approach to explain the experimentally observed variation of the input impedance, radiation resistance and power gain for a non planar log-periodic dipole antenna ($\phi \neq 0^{\circ}$), fig.(1.2), has been discussed in chapter 4. Far-field expressions developed by Kosta (18) have been used to calculate the radiation resistance and power gain of the nonplanar LPD antenna. Power gain has been measured experimentally for various values of ϕ.

In addition a simple approach has been shown to explain the experimentally observed variations in input impedance shown by Monser (23). The nonplanar system has been treated as a periodically loaded transmission line. Using this concept, the expression for input impedance of the active region has been derived. The variation of this parameter as a function of ϕ (the separation angle between the two halves) has been studied both theoretically as well as experimentally.

1.2.4 A New Log-periodic Structure with Asymmetric Dipole Elements: In chapter 5 one of the configurations of the displaced system, namely, the transversely displaced

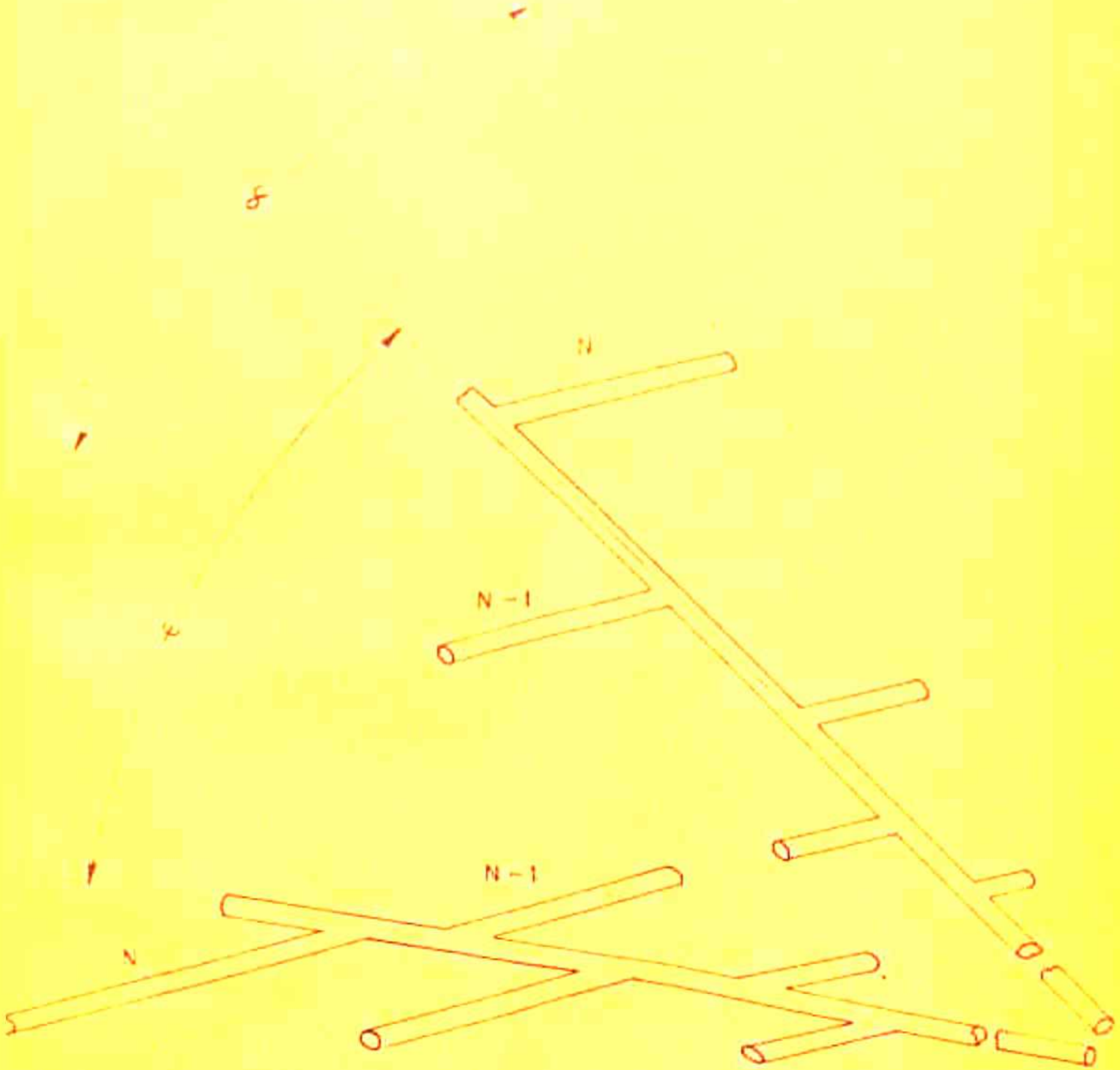

G.1.2. LOG-PERIODIC DIPOLE ANTENNA AND ITS PARAMETERS.

configuration has been used to explore a new log-periodic structure. In this new structure the conventional centre fed dipoles of the array have been replaced by the transversely displaced asymmetric dipoles. Expressions for the far field radiation pattern, radiation resistance and power gain have been developed using the conventional linear antenna array theory and the Poynting's vector method. A study of the various important antenna parameters (radiation pattern, radiation resistance and power gain etc.) have been made as a function of the separation angle ϕ between the two halves. In addition an approximate expression for the variation of input impedance of the active region has also been derived using the periodically loaded line concept and the perturbation technique. Theoretical as well as experimental results have been presented.

1.2.5 Some Studies of Arbitrarily Displaced Asymmetric Dipole Antenna Immersed in Weakly Ionised Plasma: A study of asymmetric dipole antenna system with arbitrarily displaced feed points immersed in weakly ionized plasma has been presented in chapter 6. Analysis has been carried out to predict the variation of radiation pattern of both the electromagnetic mode as well as the acoustic mode as functions of the feed point displacement $\frac{2R}{\lambda}$. It has been shown that for source frequencies far-far greater than the plasma frequency the electromagnetic mode radiation

is almost uneffected.

Conclusions are made in chapter 7, where the experimental agreement with the theory is discussed. Some suggestions for further work have also been given in this chapter.

C H A P T E R - 2

AN ASYMMETRIC DIPOLE ANTENNA WITH ARBITRARILY DISPLACED FEED POINTS

§ 2.1 INTRODUCTION

A careful examination of the log-periodic dipole antenna (for $\delta \neq 0^{\circ}$) with asymmetric dipoles as its elements, shown in fig.(2.1), reveals the fact that the constituent dipoles have their feed points displaced transverse to their axes. Hence, to study this type of array, one must first analyse its basic elements. The present chapter has been devoted to the analysis of the asymmetric dipole antenna with feed points displaced arbitrarily. Three possible configuration are discussed.

§ 2.2 DEVELOPMENT OF MATHEMATICAL EXPRESSIONS

2.2.1 Radiation Pattern

Fig (2.2) represents an asymmetrically fed dipole antenna with feed points displaced arbitrarily. SQ and S'Q' are the two constituent portions of the asymmetric dipole antenna which may be considered to be made of a large number of small current elements dz' each having a constant current I(z'). The radiation field due to such an element dz' is given by (24)

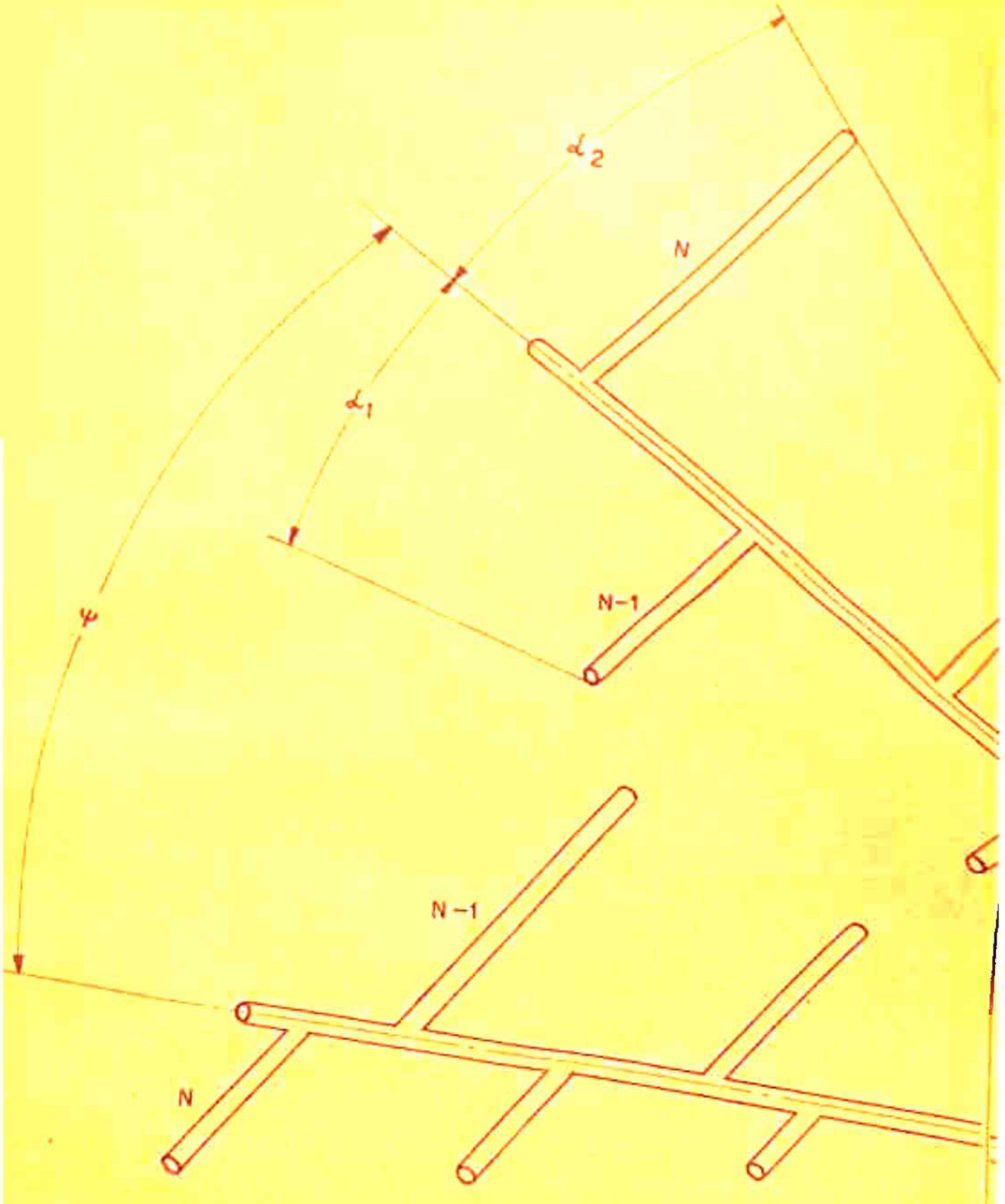

FIG.2·1. PARAMETER AND COORDINATE SYSTEM OF L P ASYMMETRIC DIPOLE ELEMENT

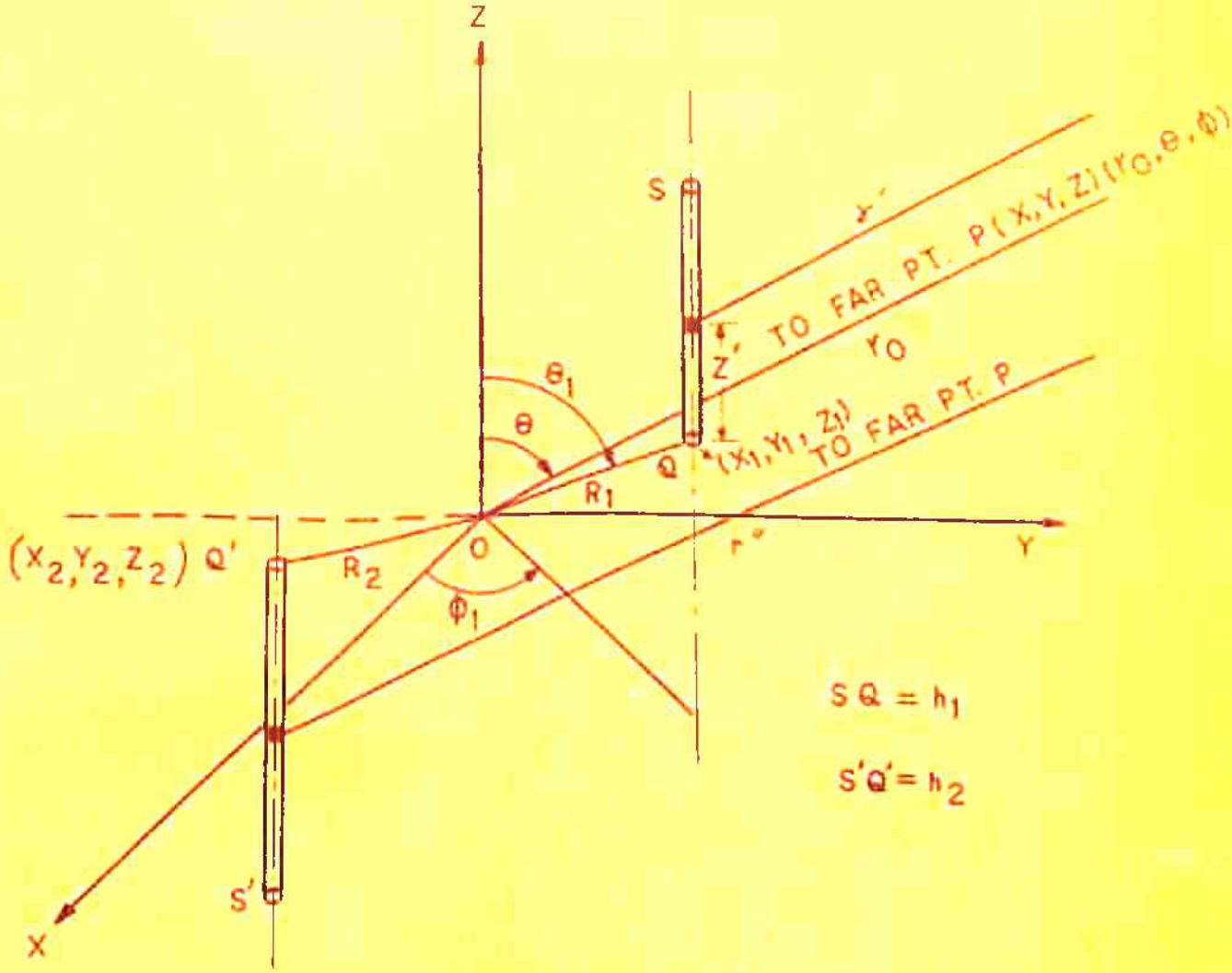

FIG. (2·2) LAYOUT AND COORDINATE SYSTEM OF ARBITRARILY DISPLACED ASY. DIPOLE.

$$dE_{SQ} = \frac{j\beta\eta\, I(z)\, e^{j(\omega t - r'/c)} \sin\theta\, dz'}{4\pi r'} \qquad (2.1)$$

From fig (2.2) it is obvious that

$$r' = [(x-x_1)^2 + (y-y_1)^2 + \{z - (z_1 + z')\}^2]^{1/2} \qquad (2.2)$$

where

$$x = r_o \sin\theta \cos\phi, \quad y = r_o \sin\theta \sin\phi,$$

$$z = r_o \cos\theta$$

and

$$x_1 = R_1 \sin\theta_1 \cos\phi_1, \quad y_1 = R_1 \sin\theta_1 \sin\phi_1,$$

$$z_1 = R_1 \cos\theta_1$$

Substituting these values of coordiantes, (2.2) results in

$$r' = r_o \left[1 + \frac{R_1^2 + 2R_1 z' \cos\theta + z'^2}{r_o^2} - \frac{2R_1}{r_o} (\sin\theta \sin\theta_1 \cos(\phi-\phi_1) + \cos\theta \cos\theta_1) - \frac{2z'}{r_o} \cos\theta \right]^{1/2}$$

which reduces to

$$r' = r_o - R_1 U_1 - z' \cos\theta \qquad (2.3)$$

where

$$U_1 = \sin\theta \sin\theta_1 \cos(\phi_1 - \phi) + \cos\theta \cos\theta_1 \qquad (2.4)$$

Similarly

$$r'' = r_o + R_2 U_2 - z' \cos\theta \qquad (2.5)$$

where

$$U_2 = \sin\theta \sin\theta_2 \cos(\phi_2 - \phi) + \cos\theta \cos\theta_2 \qquad (2.6)$$

Firstly, the current distribution of the following form is assumed.

$$I(z') = I_1 \sin[\beta(h_1 - z')], \quad z' > 0 \qquad (2.7)$$

$$= I_2 \sin[\beta(h_2 + z')], \quad z' < 0 \qquad (2.8)$$

where $\beta = 2\pi/\lambda$

Since

$I_1 \sin(\beta h_1) = I_2 \sin(\beta h_2)$ at $z' = 0$, this is possible only when

$$I_1 = I_m \sin(\beta h_2) \text{ and } I_2 = I_m \sin(\beta h_1)$$

Substituting these values of I_1 and I_2 in equations (2.7) and (2.8), the current distribution is

$$\begin{aligned} I(z') &= I_m \sin(\beta h_2) \sin[\beta(h_1 - z')], \quad z' > 0 \\ &= I_m \sin(\beta h_1) \sin[\beta(h_2 + z')], \quad z' < 0 \end{aligned} \qquad (2.9)$$

Inserting this current distribution in equation (2.1) and integrating, the radiation field due to the entire upper limb comes out to be

$$E_{SQ} = A \sin(\beta h_2) \int_0^{h_1} e^{-j\beta r_o + j\beta(R_1 U_1 + z' \cos\theta)} \sin[\beta(h_1 - z')] \sin\theta \, dz' \qquad (2.10)$$

where

$$A = \frac{j\beta\eta[I]}{4\pi r_o}, \quad [I] = I_m e^{j(\omega t - r_o/c)}$$

Simplifying

$$E_{SQ} = A' \sin(\beta h_2)\, e^{j\beta R_1 U_1} \int_0^{h_1} e^{j\beta z' \cos\theta} \sin\{\beta(h_1 - z')\}dz' \qquad (2.11)$$

where

$$A' = A \sin\theta$$

Using the standard integration formula

$$\int e^{ax} \sin(c+bx) = \frac{e^{ax}}{a^2 + b^2}[a \sin(c+bx) - b \cos(c+bx)]$$

and carrying out the integration

$$E_{SQ} = \frac{A'}{\beta \sin^2\theta} \sin(\beta h_2)\, e^{j\beta R_1 U_1} [e^{j\beta h_1 \cos\theta} - \{j \cos\theta \sin(\beta h_1) + \cos(\beta h_1)\}] \qquad (2.12)$$

Similarly for the lower limb

$$E_{S'Q'} = \frac{A'}{\beta \sin^2\theta} \sin(\beta h_1)\, e^{-j\beta R_2 U_2} [e^{-j\beta h_2 \cos\theta} + \{j \cos\theta \sin(\beta h_2) - \cos(\beta h_2)\}] \qquad (2.13)$$

Adding equations (2.12) and (2.13) the field due to the asymmetric dipole antenna with arbitrarily displaced feed points is

$$E(\theta, \phi) = K.[I].\ f(\theta, \phi) \qquad (2.14)$$

where

$$f(\theta , \phi) = \left[\begin{array}{l} \sin(\beta h_2)[e^{j\beta(R_1U_1 + h_1\cos\theta)} - e^{j\beta R_1U_1} \\ \{j \cos\theta \sin(\beta h_1) + \cos(\beta h_1)\}] \\ + \sin(\beta h_1)[e^{-j\beta(R_2U_2 + h_2\cos\theta)} + e^{-j\beta R_2U_2} \\ \{j \cos\theta \sin(\beta h_2) - \cos(\beta h_2)\}] \end{array} \right] \qquad (2.15)$$

and $K = \frac{j30}{r_0}$

Equation (2.14) is the most general expression for the far-field radiation pattern of the asymmetric dipole antenna with feed points displaced arbitrarily. This configuration is studied in the following three cases.

(i) Arbitrary Displacement:

This configuration is shown in fig.(2.3a). By putting $\phi_1 = \phi_2 = 90^0$ and $\theta_1 = \theta_2 = 45^0$ one obtains, from equation (2.14), the expression appropriate for this case.

$$E_{AR}(\theta , \phi) = K.[I].\ f_{AR}(\theta , \phi) \qquad (2.16)$$

where $U_1 = U_2 = \sin\theta \sin\theta_1 \sin\phi + \cos\theta \cos\theta_1$

and f_{AR} is obtained by inserting above values of U_1 and U_2 in equation (2.15). Calculations are carried out using the following data.

$\theta_1 = \theta_2 = 45^0$

$\phi = 90^0$ (for E-plane pattern)

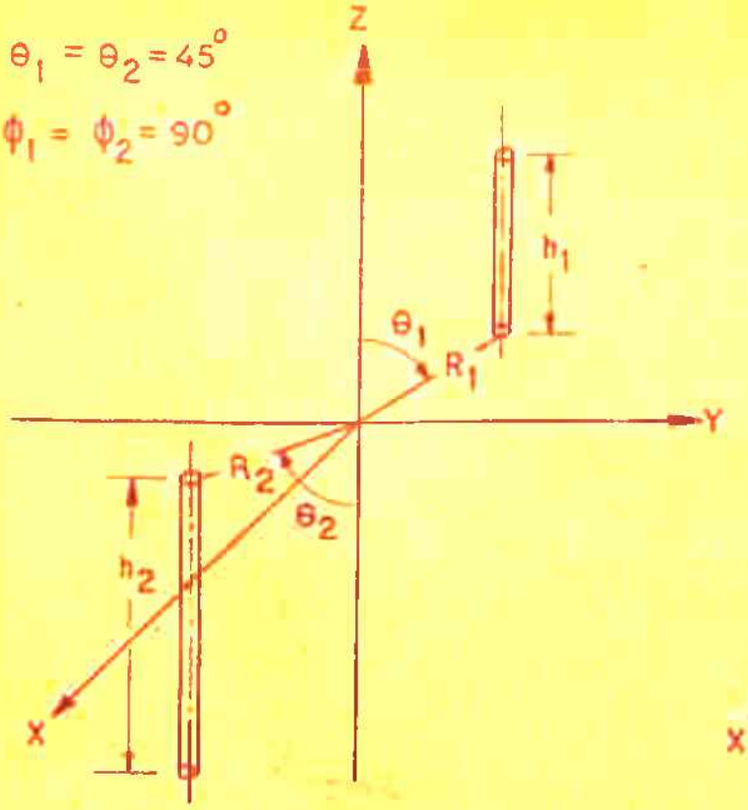

FIG. (2·3a) ARBITRARILY DISPLACED ASY. DIPOLE ANTENNA.

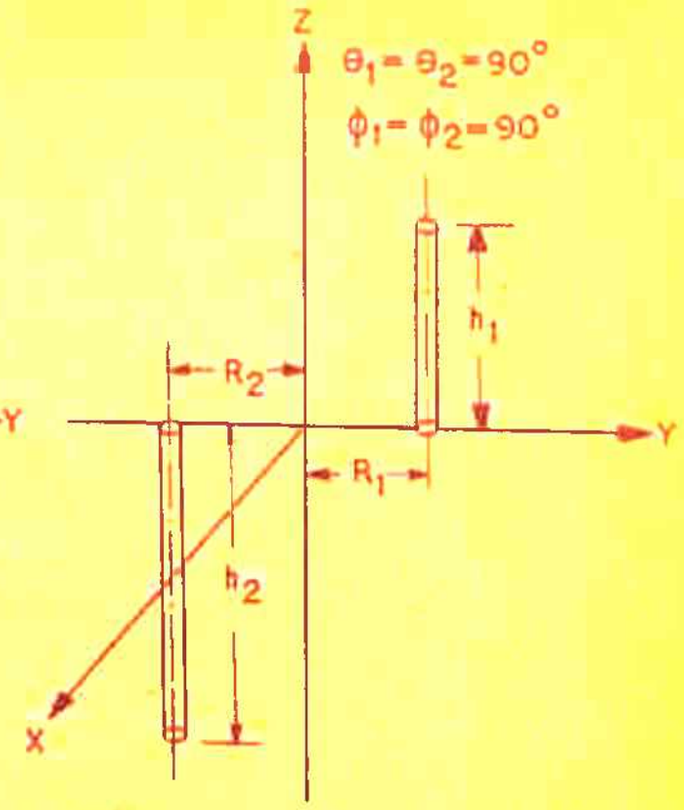

FIG. (2·4a) TRANSVERSELY DISPLACED ASY. DIPOLE ANTENNA.

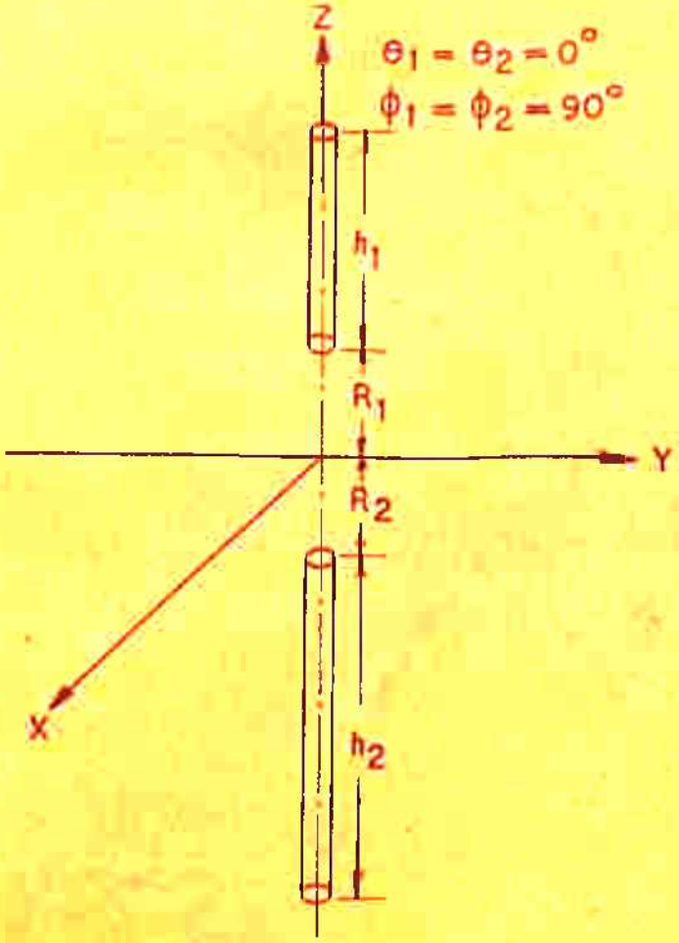

FIG. (2·5a) AXIALLY DISPLACED ASY. DIPOLE ANTENNA.

$\theta = 90^{\circ}$ (for H-pattern)

$\frac{h_1}{\lambda} = 0.25$

$\frac{h_2}{\lambda} = 0.75$

and $\frac{2R}{\lambda} = 0.04, 0.11, 0.16$

Plots of E and H-plane patterns are shown in fig.(2.3b)

(ii) Transverse Displacement:

On substitution of $\theta_1 = \theta_2 = 90^{\circ}$ and $\phi_1 = \phi_2 = 90^{\circ}$ [fig.(2.4a)] in equation (2.14), the expression for the far-field radiation pattern is obtained as

$$E_{TR}(\theta, \phi) = K.[I].\ f_{TR}(\theta, \phi) \qquad (2.17)$$

in which $U_1 = U_2 = \sin\theta \sin\phi$. f_{TR} can be obtained from equation (2.15) by using this value of U_1. Using equation (2.17), calculations have been done with the following parameters.

$\theta_1 = \theta_2 = 90^{\circ}$

$\phi_1 = \phi_2 = 90^{\circ}$

$\phi = 90^{\circ}$ (for E-plane pattern)

$\theta = 90^{\circ}$ (for H-plane pattern)

$\frac{h_1}{\lambda} = 0.25$

$\frac{h_2}{\lambda} = 0.75$

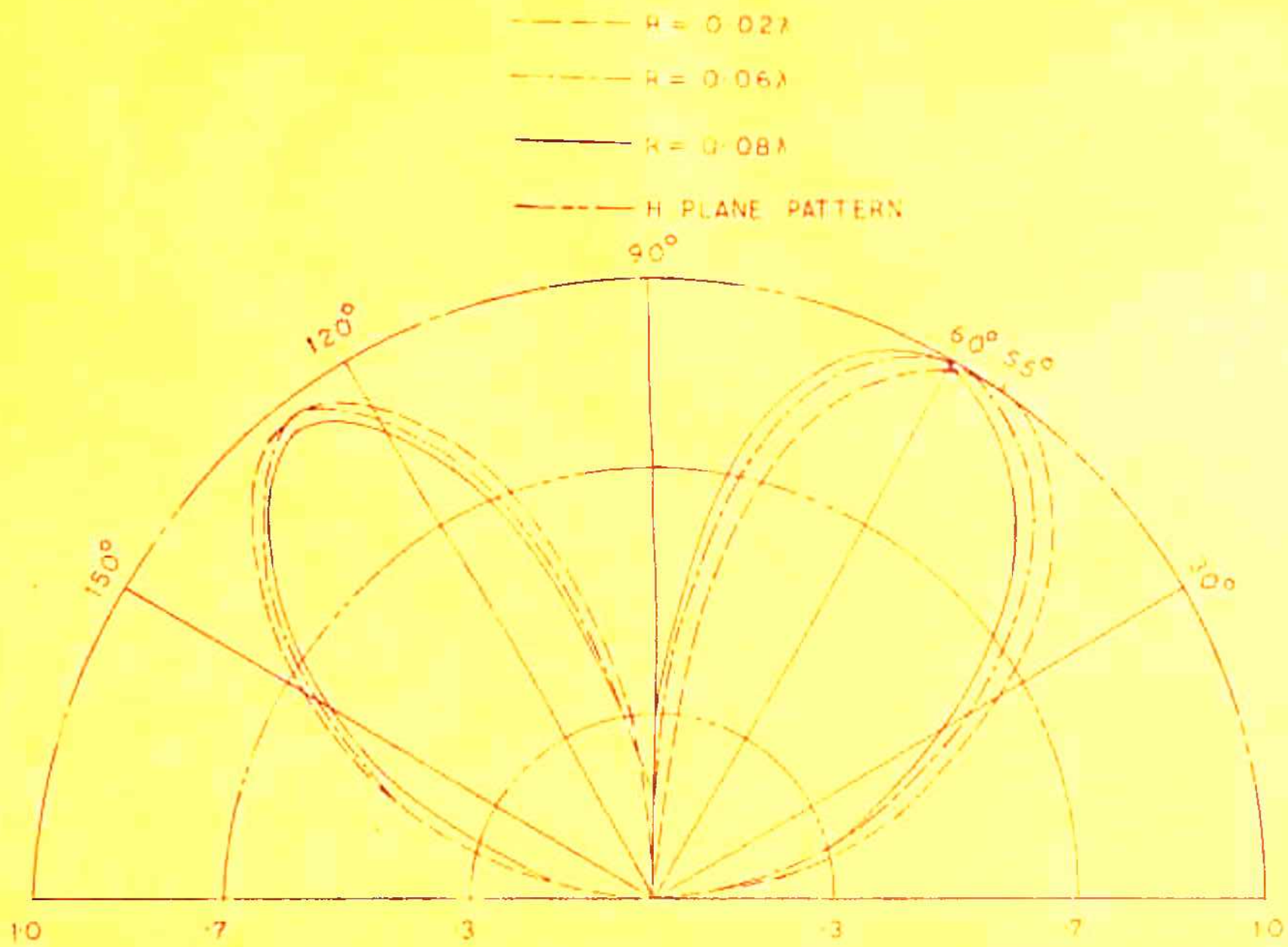

FIG. (2·3b) E & H PLANE PATTERNS OF ARBITRARILY DISPLACED CONFIGURATION.

and the values of $\frac{2R}{\lambda}$ mentioned in case (i)
Theoretical plots of E and H-plane patterns are shown in fig.(2.4b).

(iii) Axial Displacement:

Fig.(2.5a) shows this configuration. By substituting $\theta_1 = \theta_2 = 0^\circ$ and $\phi_1 = \phi_2 = 90^\circ$ in equation (2.14), the relevant expression for this case becomes

$$E_{AX}(\theta , \phi) = K.[I]. f_{AX}(\theta , \phi) \qquad (2.18)$$

where

$U_1 = U_2 = \cos \theta$

Equation (2.18) is the expression for the far-field radiation due to the asymmetrically driven dipole with axially displaced feed points. The following data is used to calculate the theoretical E and H-plane patterns.

$\theta_1 = \theta_2 = 0^\circ$

$\phi_1 = \phi_2 = 90^\circ$

$\frac{h_1}{\lambda} = 0.25$

$\frac{h_2}{\lambda} = 0.75$

and $\frac{2R}{\lambda} = 0.04, 0.12, 0.16$

Results are shown graphically in fig.(2.5b).

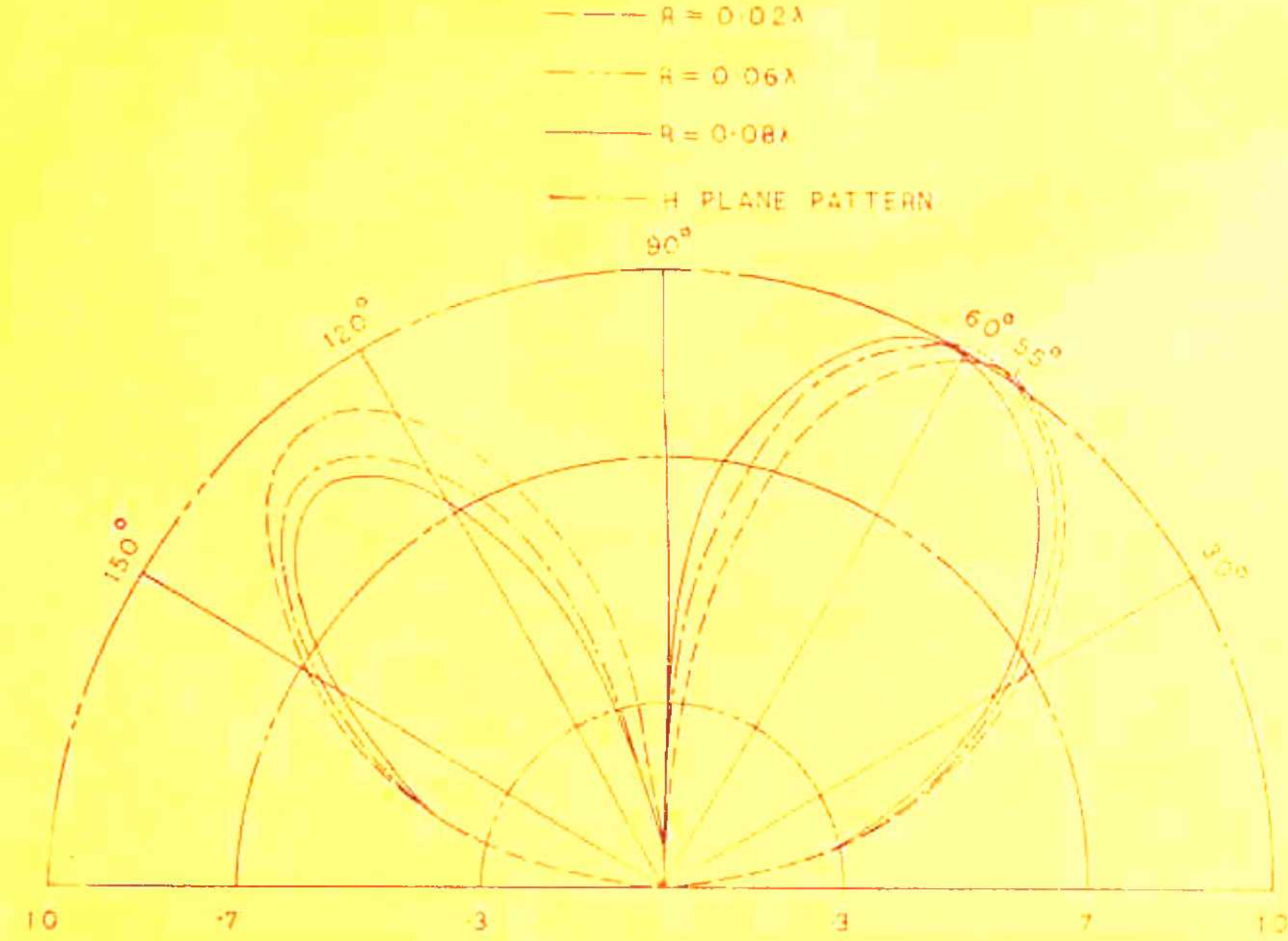

FIG. (24b) E & H PLANE PATTERNS OF TRANSVERSELY DISPLACED CONFIGURATION.

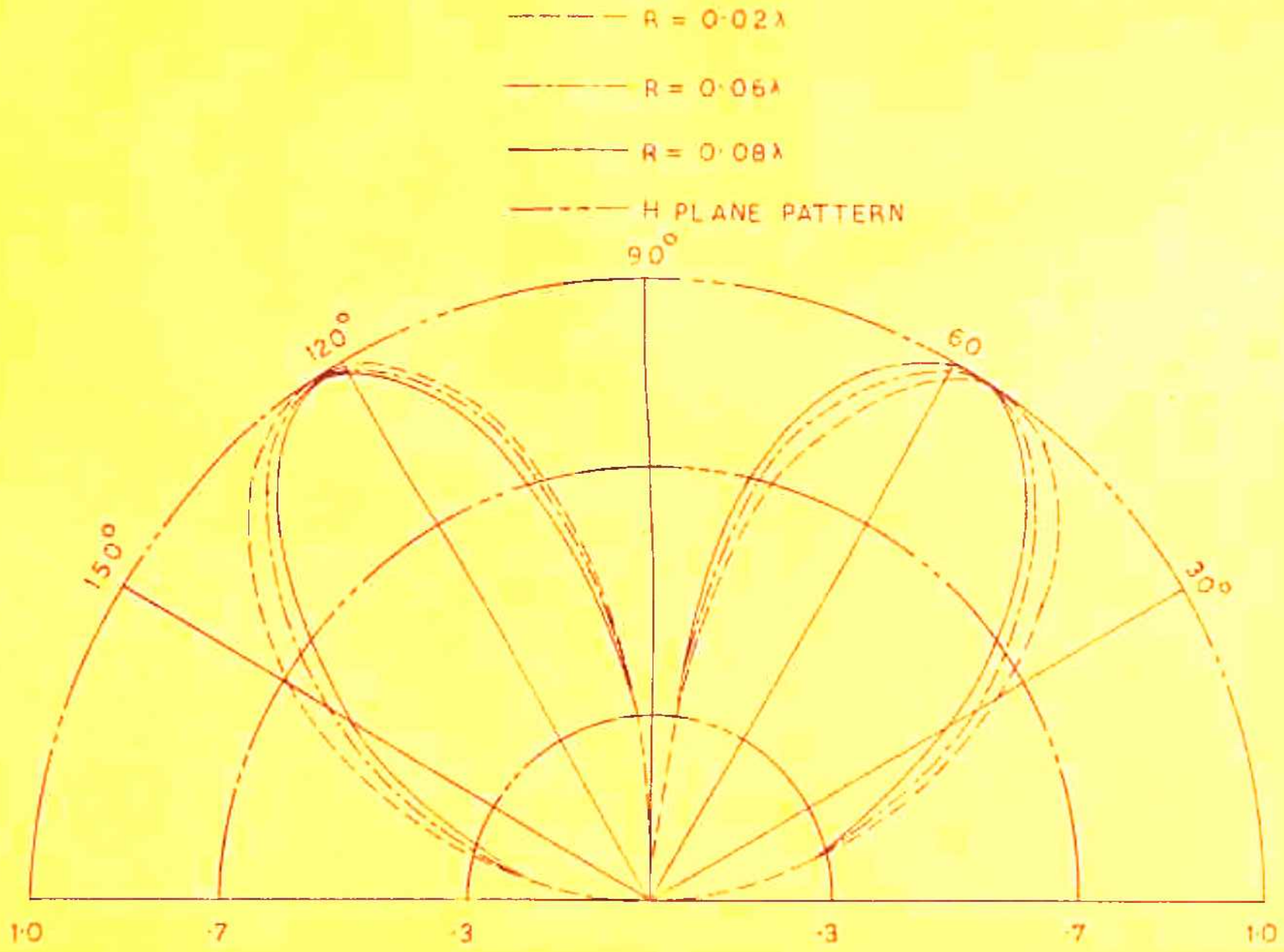

FIG. (2·56) E & H PLANE PATTERNS FOR AXIALLY DISPLACED CONFIGURATION.

2.2.2 Radiation Resistance:

The radiation resistance is obtained by integrating Poynting's vector over a large sphere yielding the total power radiated and equating this power to $I_m^2 R_o/2$, where R_o is the radiation resistance and I_m is the peak current. Expression for the total radiated power W is given by (25)

$$W = \frac{1}{2}\sqrt{(\mu_o/\epsilon_o)} \int_0^{2\pi} \int_0^{\pi} |H_\phi|^2 r_o^2 \sin\theta \, d\theta \, d\phi \qquad (2.19)$$

where

μ_o = free space permeability

ϵ_o = free space permittivity

$|H_\phi|$ = absolute value of magnetic field.

Using the relation

$$|H_\phi| = \frac{|E_\theta|}{\eta} = \frac{|f(\theta, \frac{\pi}{2})|}{\eta}$$

and $[I] = I_m$ in equation (2.19), the total radiated power W is

$$W = \frac{15 I_m^2}{2} \int_0^{\pi} |f(\theta, \tfrac{\pi}{2})|^2 \sin\theta \, d\theta$$

Equating this equation to $I_m^2 R_o/2$ and simplifying, the expression for the radiation resistance is obtained as

$$R_o = 15 \int_0^{\pi} |f(\theta, \pi/2)|^2 \sin\theta \, d\theta \qquad (2.20)$$

where $f(\theta , \frac{\pi}{2})$ is obtained from equation (2.15) by substituting $\phi = \frac{\pi}{2}$. Equation (2.20) gives the expression for radiation resistance of the arbitrarily displaced asymmetric dipole antenna.

As mentioned in sec. 2.2.1, radiation resistance may also be studied in three possible configurations discussed below.

(i) Arbitrary Displacement:

Radiation resistance for this case is given by

$$R_{OAR} = 15 \int_0^{\pi} |f_{AR}(\theta , \tfrac{\pi}{2})|^2 \sin \theta \, d\theta \qquad (2.21)$$

in which $f_{AR}(\theta , \frac{\pi}{2})$ is obtained by putting appropriate values of θ_1 and θ_2 and $\phi = \frac{\pi}{2}$ in the general expression of $f(\theta , \phi)$ given by equation (2.15).

(ii) Transverse Displacement:

For this configuration, the general expression of equation (2.20) reduces to

$$R_{OTR} = 15 \int_0^{\pi} |f_{TR}(\theta , \tfrac{\pi}{2})|^2 \sin \theta \, d\theta \qquad (2.22)$$

where $f_{TR}(\theta , \frac{\pi}{2})$ is obtained by substituting the appropriate values of U_1 and U_2 in equation (2.15).

(iii) Axial Displacement:

Radiation resistance for this case is given by

$$R_{OAX} = 15 \int_0^{\pi} |f_{AX}(\theta , \tfrac{\pi}{2})|^2 \sin\theta \, d\theta \qquad (2.23)$$

Theoretical calculations for the three cases discussed above have been carried out using the following parameters

$$\frac{h_1}{\lambda} = 0.25$$

$$\frac{h_2}{\lambda} = 0.75$$

and $\frac{2R}{\lambda}$ = 0.0, 0.025, 0.05, 0.08, 0.1, 0.12 and 0.18

Results are given in Table 2.1 and shown in fig.(2.6).

TABLE - 2.1

Feed Point Displacement 2R/λ	Radiation Resistance (in ohms)		
	Axial Displacement	Transverse Displacement	Arbitrary Displacement
0.0	93.43	93.43	93.43
0.025	94.86	93.35	93.78
0.05	95.98	93.09	94.50
0.08	96.91	92.55	94.94
0.10	97.29	92.05	94.98
0.12	97.48	91.45	94.81
0.18	96.98	89.01	93.00

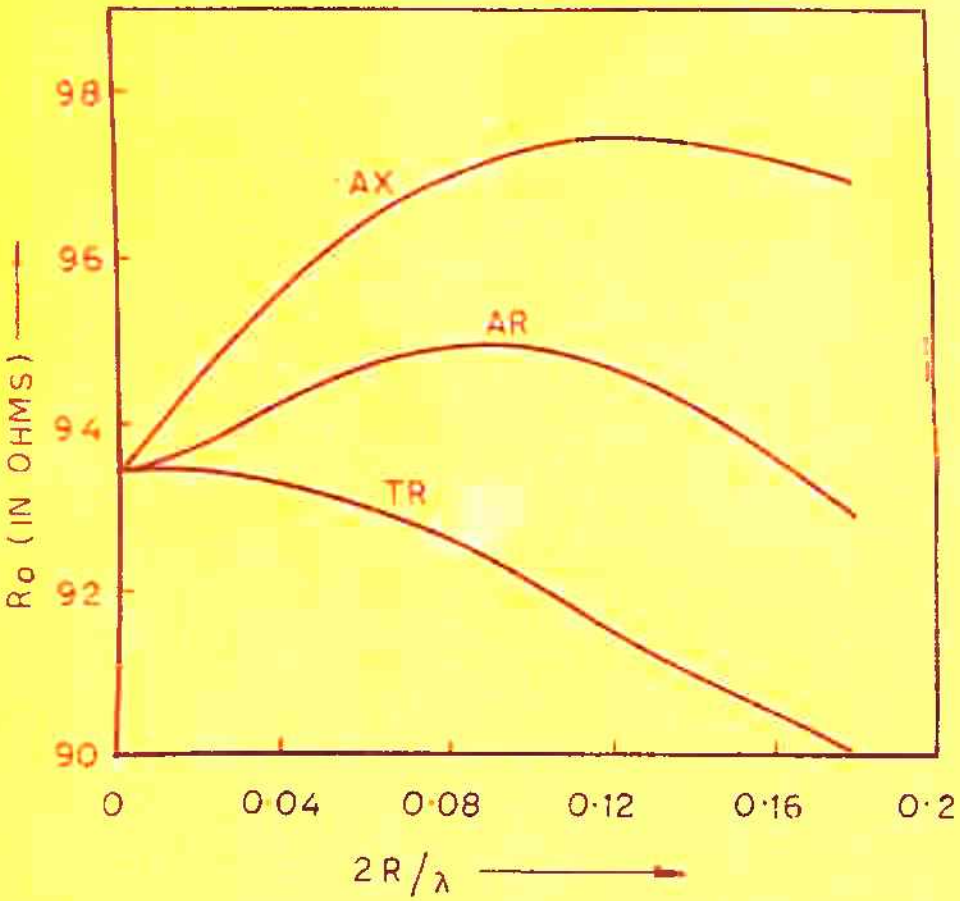

FIG. 2·6. RADIATION RESISTANCE AS FUNCTION OF FEED POINT DISPLACEMENT.

AX ≡ AXIAL DISPLACEMENT.

AR ≡ ARBITRARY DISPLACEMENT.

TR ≡ TRANSVERSE DISPLACEMENT

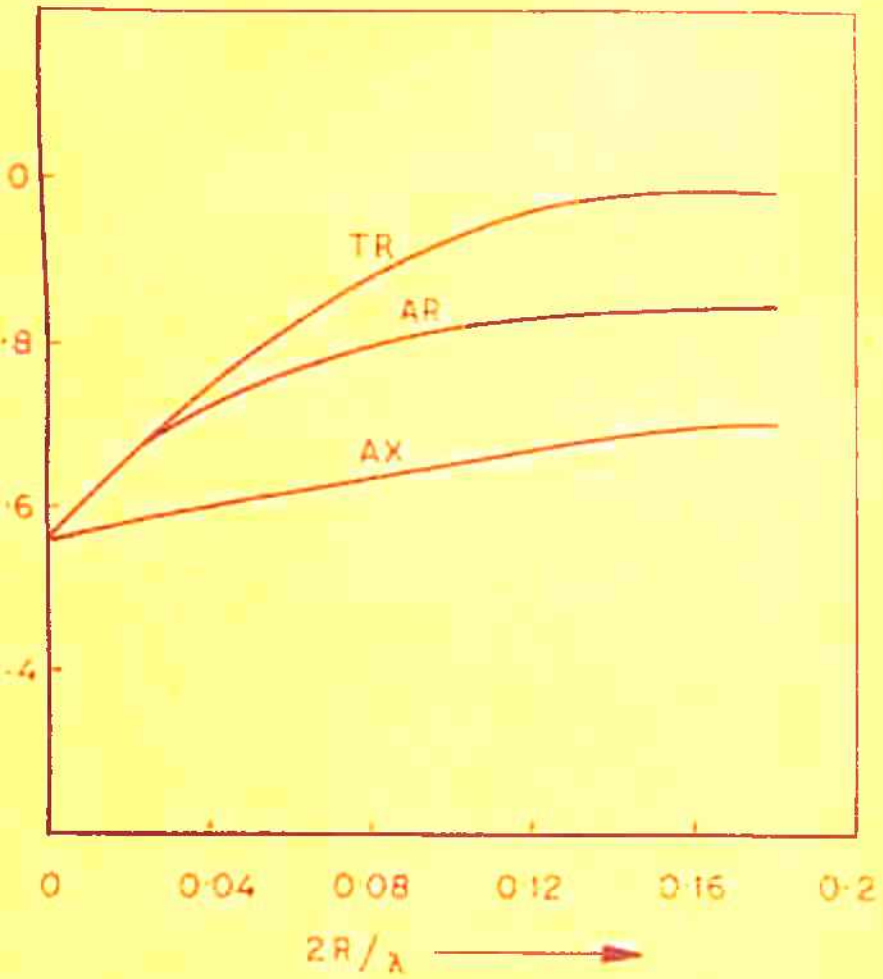

G. 2·7. POWER GAIN OF AXIALLY, TRANSVERSELY AND ARBITRARILY DISPLACED ASYMMETRIC DIPOLE ANTENNA AS A FUNCTION OF FEED POINT DISPLACEMENT $2R/\lambda$.

2.2.3 Power Gain:

For a given value of feed-point displacement 2R, the field $E(\theta , \frac{\pi}{2})$ and $E(\frac{\pi}{2} , \phi)$ will be maximum at an angle $\theta = \theta_m$ and $\phi = \phi_m$ respectively. Therefore

$$E_{max}(\theta_m) = K.[I]. f_{max}(\theta_m) \qquad (2.24)$$

Equation (2.24) gives the r.m.s. value of the field if I_m equals to the r.m.s. current at the location of current maximum (2). The antenna is supplied with the power $P = I_m^2 R_o$. Therefore

$$\frac{E_{max} \cdot r_o}{\sqrt{P}} = \left(\frac{30}{\sqrt{R_o}} \right) . f_{max}(\theta_m) \qquad (2.25)$$

A similar expression for the isotropic radiator is given in Page (26)

$$\frac{E_{iso.} r_o}{\sqrt{P}} = \sqrt{30} \qquad (2.26)$$

Dividing equation (2.25) by equation (2.26) and squaring, the power gain is

$$G = \left(\frac{30}{R_o}\right) f_{max}^2(\theta_m) \qquad (2.27)$$

where θ_m is the angle of maximum radiation for a specified value of 2R, the feed point displacement.

Equation (2.27) is a general expression which can be used for computing power gain by substituting the

appropriate functions $f_{max}(\theta_m)$ for the three configurations discussed in sec. (2.2.2). Computations have been done using data given in sec. (2.2.2). Results, so obtained, are given in Table 2.2 and shown in fig.(2.7).

TABLE - 2.2

Feed Point Displacement $2R/\lambda$	Power Gain (in dB)		
	Axial Displacement	Transverse Displacement	Arbitrary Displacement
0.0	2.56	2.56	2.56
0.025	2.582	2.688	2.688
0.05	2.603	2.792	2.751
0.08	2.632	2.880	2.786
0.10	2.646	2.919	2.796
0.12	2.660	2.967	2.836
0.16	2.695	3.077	2.840

2.2.4 Effective Aperture:

The effective aperture of an antenna is given by

$$G = \frac{4\pi A}{\lambda^2}$$

$$\text{or} \quad \frac{A}{\lambda^2} = \frac{G}{4\pi} \qquad (2.28)$$

where G = power gain

A = Effective aperature

λ = Operating wave length

TABLE - 2.3

Feed Point Displacement $2R/\lambda$	EFFECTIVE APERTURE		
	Axial Displacement	Transverse Displacement	Arbitrary Displacement
0.00	0.1434	0.1434	0.1434
0.025	0.1441	0.1477	0.1477
0.05	0.1449	0.1513	0.1499
0.08	0.1458	0.1544	0.1511
0.10	0.1463	0.1558	0.1511
0.12	0.1468	0.1575	0.1528
0.18	0.1480	0.1616	0.1530

This equation can be used to compute the effective aperture for various configurations discussed by substituting the respective values of power gain from sec. 2.2.3. Results are given in Table 2.3 and shown in Fig.(2.8)

§ 2.3 EXPERIMENTAL INVESTIGATIONS

2.3.1 Experimental Arrangement and Measurement Technique

The experimental investigations have been carried out for the measurement of the following.

(i) Voltage and Current distribution

(ii) Radiation pattern

(ii) Power gain and Effective aperture

(i) Voltage and Current Distribution Measurements:

An asymmetric dipole antenna at 300 Mc/S has been designed H/a = 143 where H is the total length of the dipole and 'a' is the radius of the Aluminium tube used. As the structure is a balanced one, a balun was developed to facilitate the impedance and radiation pattern measurements as the oscillator to be used is provided with coaxial out put. The experimental arrangement for voltage distribution measurements is shown in figs.(2.9a and 2.9b). Out put of the signal generator, comprising of a G.R. unit oscillator No. 1209-B modulated at a frequency of 1000 C.P.S. by G.R. audio-oscillator No. 1214-A is

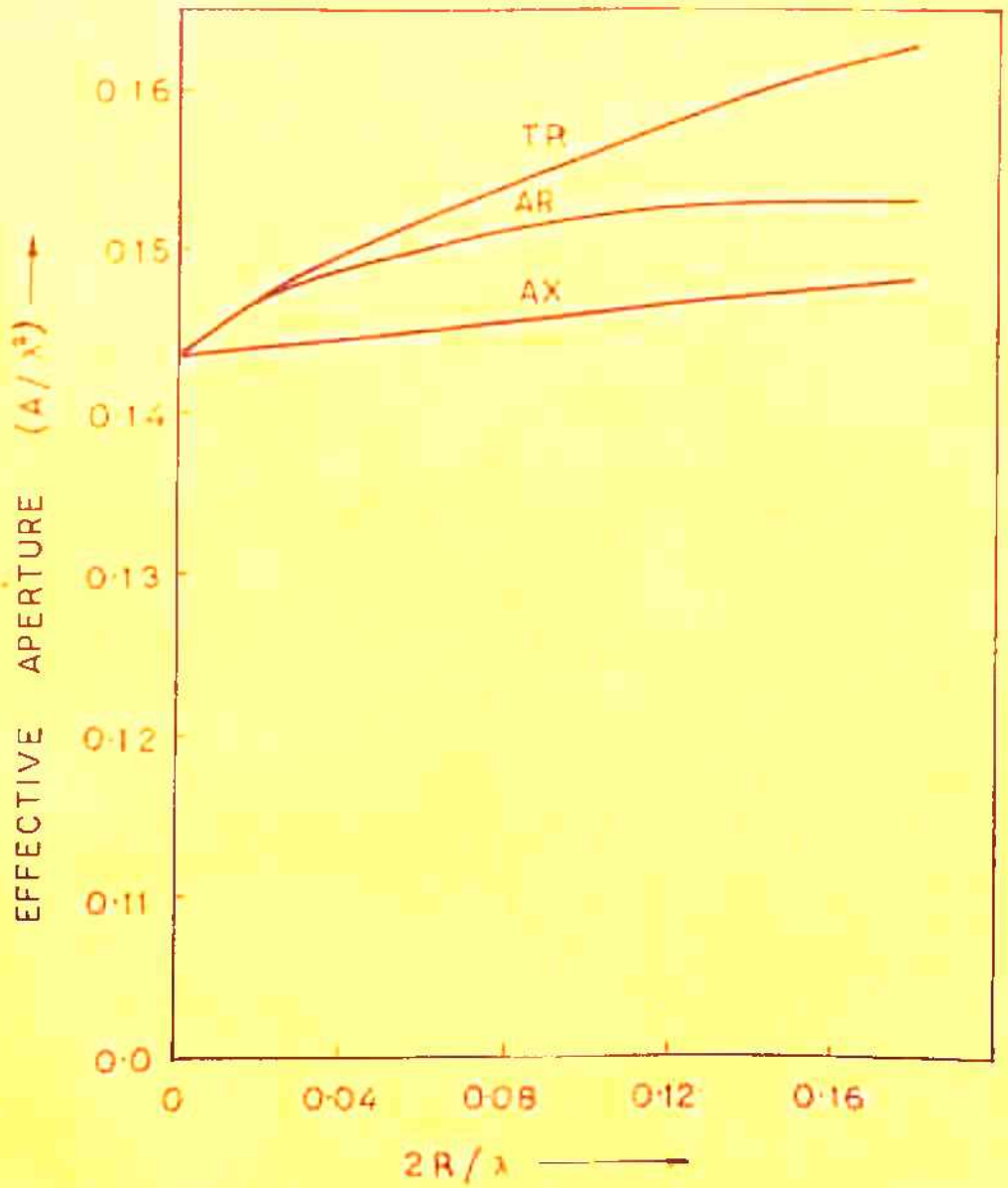

FIG. 2·8. EFFECTIVE APERTURE OF AXIALLY, TRANSVERSELY AND ARBITRARILY DISPLACED CONFIGURATION AS FUNCTION OF FEED POINT DISPLACEMENT $2R/\lambda$.

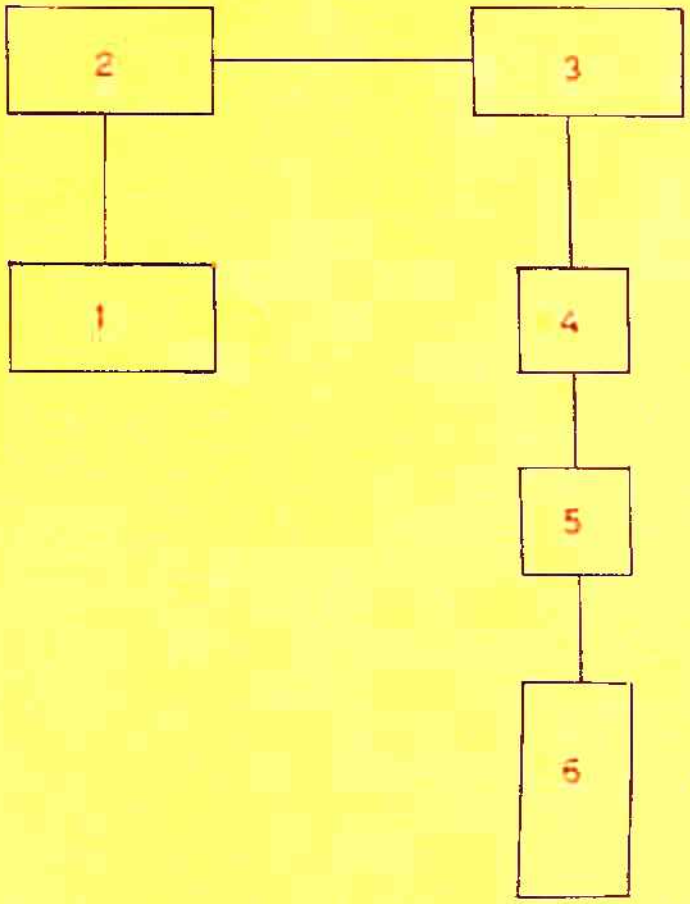

1 MODULATOR (TYPE 1214 – A)

2 G. R. UNIT OSCILLATOR (TYPE 1209 – B)

3 DISPLACED ASYMMETRIC DIPOLE

4 VOLTAGE PROBE

5 DETECTOR

6 SWR METER (TYPE HP 415 – B)

FIG. (2·9a) BLOCK DIAGRAM FOR VOLTAGE DISTRIBUTION MEASUREMENT.

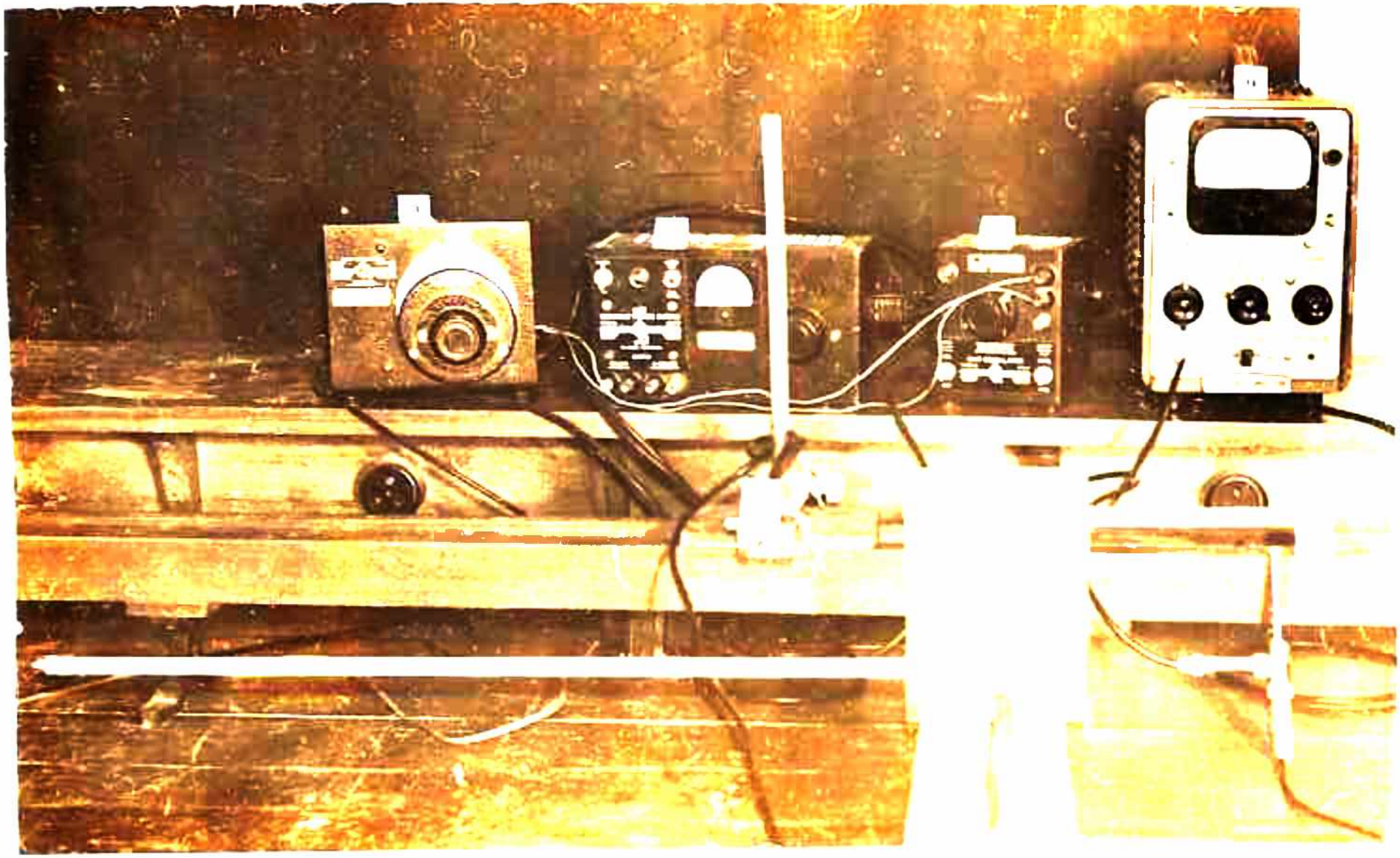

FIG.(2·9b) SETUP FOR VOLTAGE DISTRIBUTION MEASUREMENTS.

1. POWER SUPPLY 2. MODULATOR 3. G. R. UNIT OSCILLATOR 4. S. W. R. METER

5. CRYSTAL DETECTOR 6. PROBE DIPOLE 7. DISPLACED ASY. DIPOLE

fed to the dipole through a balun and a twin transmission line. A $\lambda/8$ dipole is used to sample the field as it moves on the probe carriage parallel to the dipole. The out put of the probe is connected to SWR meter (type HP 415-B) through crystal detector (No. 420-A HP). Measurements are done by moving the voltage probe over the entire length of the dipole. This procedure is repeated for various values of feed point displacement 2R. Results are shown graphically in figs.(2.10a and 2.10b) both for axial as well as transverse displacements.

For current distribution measurements, the voltage probe was replaced by a $\frac{\lambda}{8}$ circular loop. The experimental set up remains the same as in the voltage measurement. The loop is moved from one end to the other without touching the dipole. Results have been graphically shown in figs.(2.11a and 2.11b).

(ii) <u>Radiation Pattern Measurements:</u>

The block diagram and the photograph of the experimental arrangement used for the measurement of the radiation pattern are shown in figs.(2.12a, 2.12b). A centre-fed half wave dipole made of aliminium was used as the radiating source and the displaced antenna system was used as the receiving

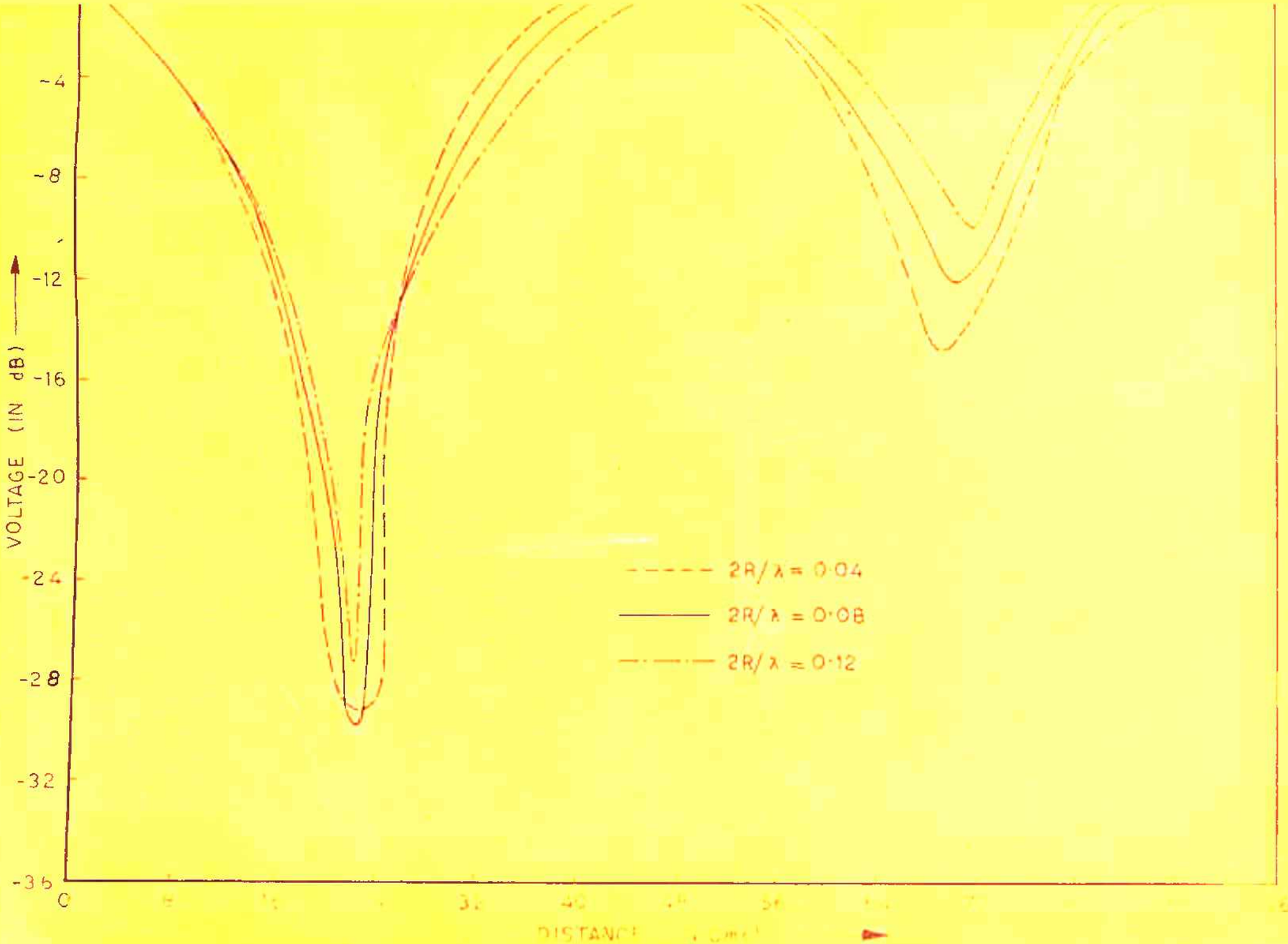

FIG. (2·10a) VOLTAGE DISTRIBUTION ON ASYMMETRIC DIPOLE ANTENNA WITH FEED POINTS DISPLACED TRANSVERSE

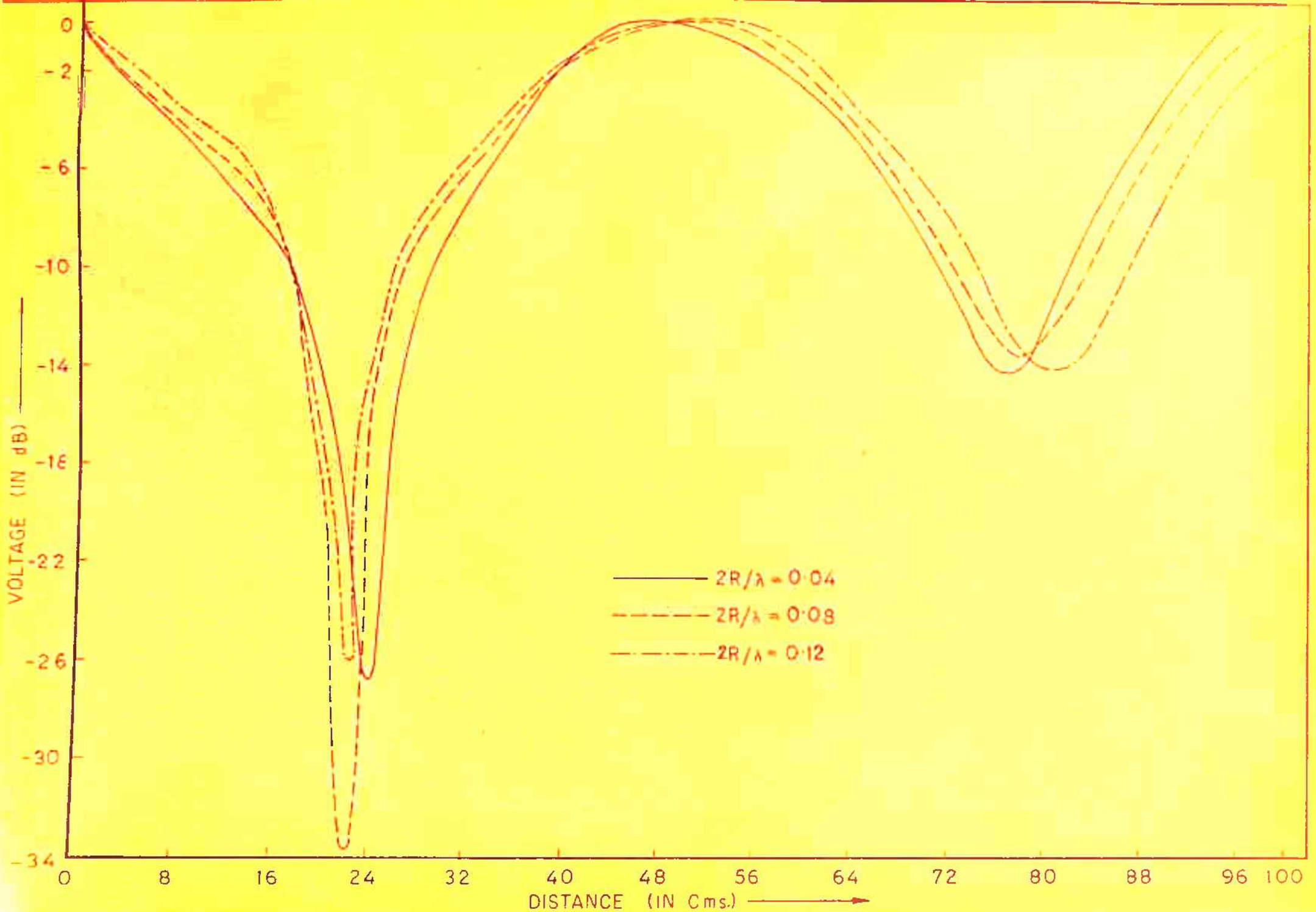

FIG. (2·10b) VOLTAGE DISTRIBUTION ON AXIALLY DISPLACED ASYMMETRIC DIPOLE ANTENNA.

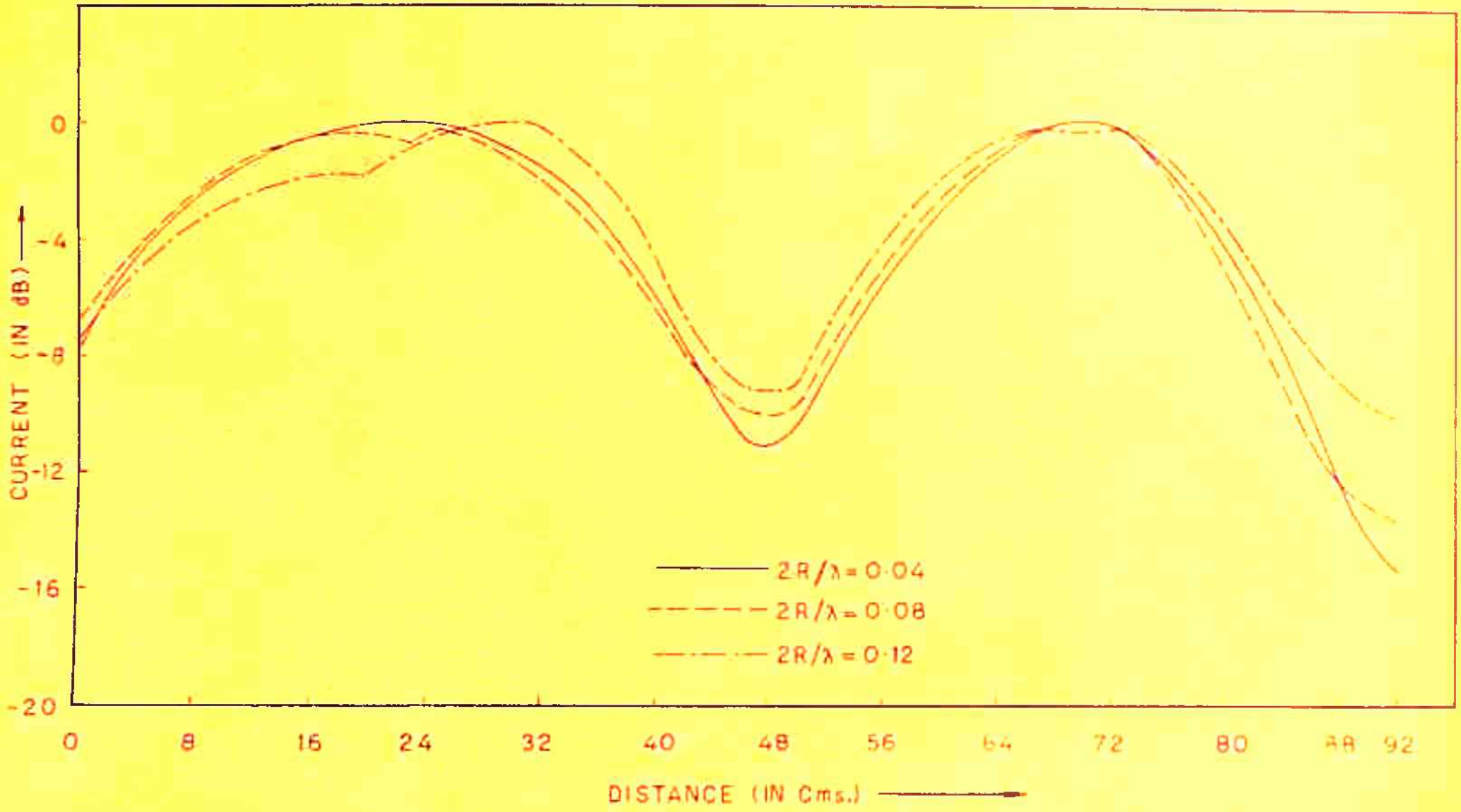

FIG. (2·11a) CURRENT DISTRIBUTION ON ASYMMETRIC DIPOLE ANTENNA WITH FEED POINTS DISPLACED TRANSVERSE TO THE AXIS.

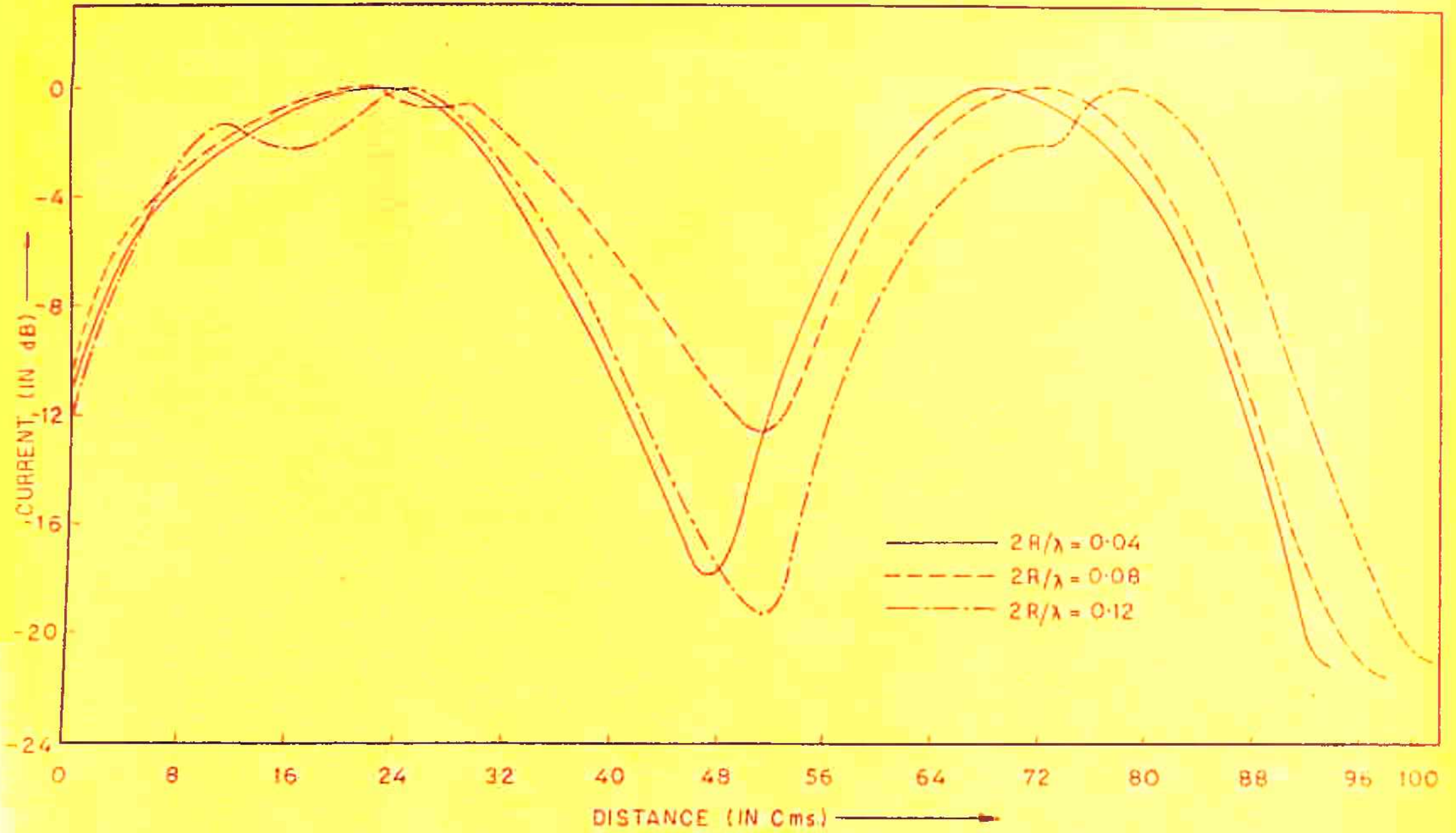

FIG.(2·11b) CURRENT DISTRIBUTION ON ASYMMETRIC DIPOLE ANTENNA WITH FEED POINTS DISPLACED AXIALLY.

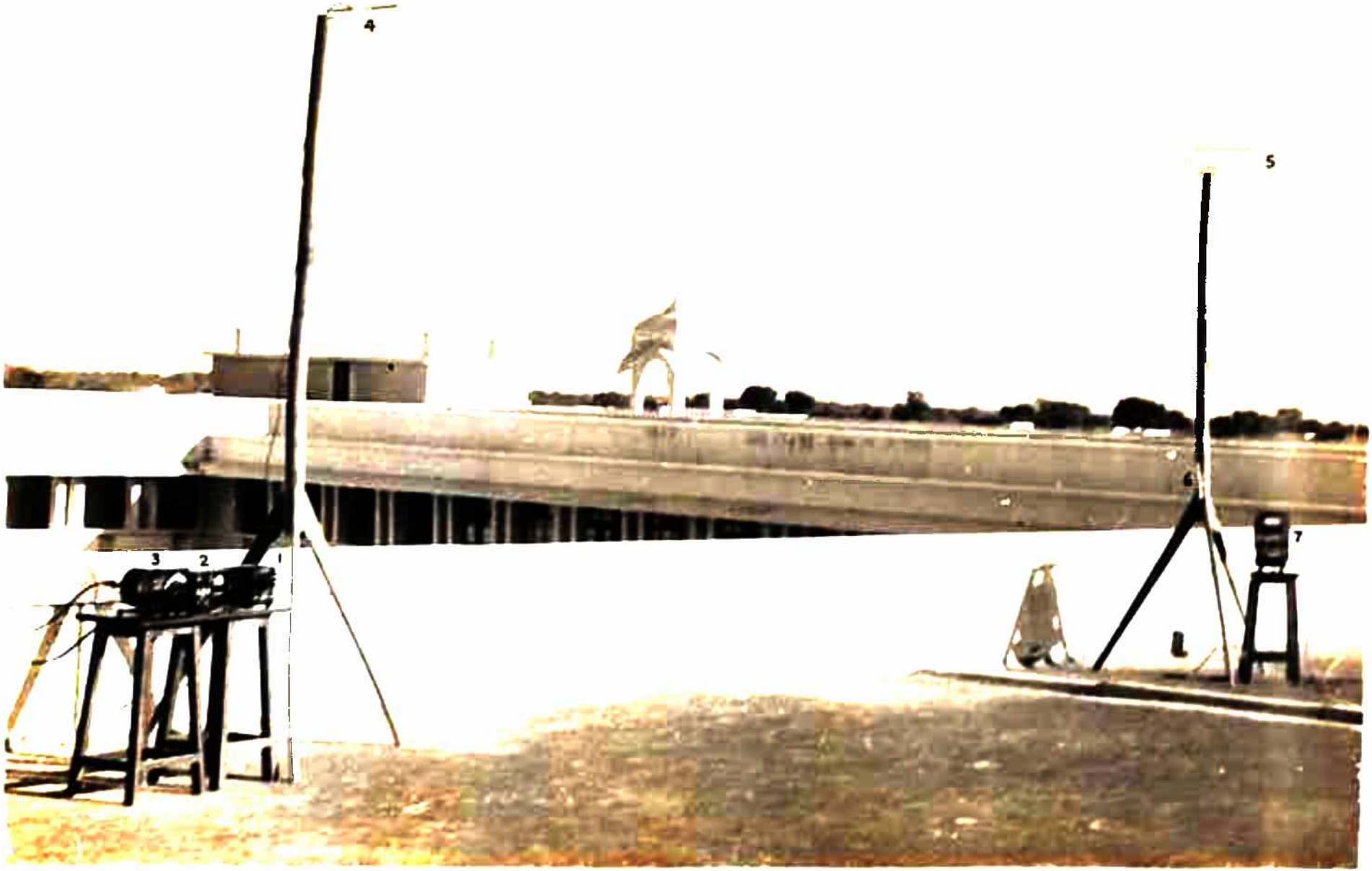

FIG. (2·12a) SETUP FOR RADIATION PATTERN MEASUREMENTS.

(1) MODULATOR (2) POWER SUPPLY (3) G.R. UNIT OSCILLATOR (4) TRANSMITTING DIPOLE (5) RECEIVING ASY. DIPOLE (6) CRYSTAL DETECTOR (7) S.W.R. METER.

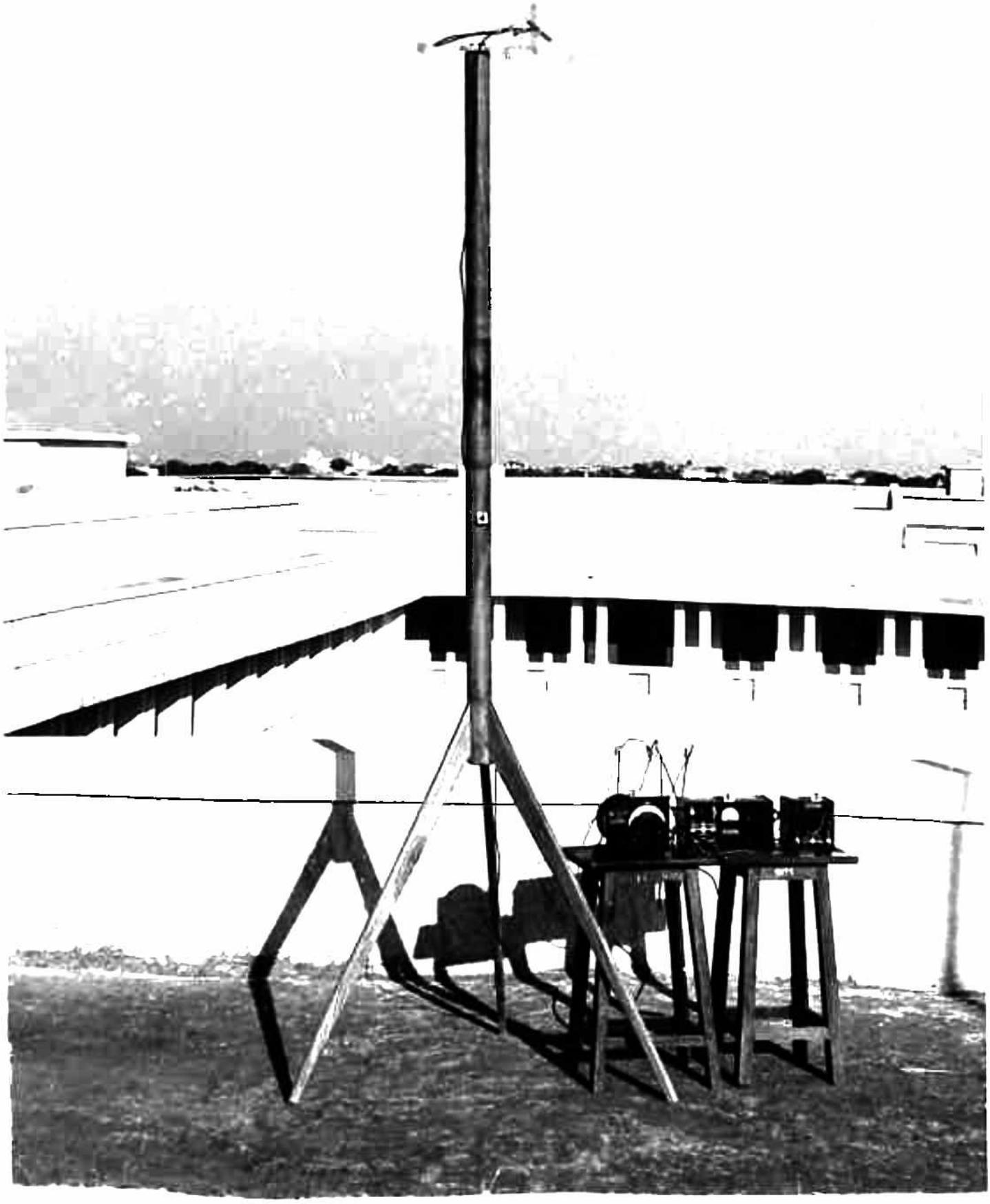

CLOSEUP OF TRANSMITTING DIPOLE

1. POWER SUPPLY 2. G. R. UNIT OSCILLATOR 3. MODULATOR

4. ANTENNA MAST. 5. TRANSMITTING DIPOLE

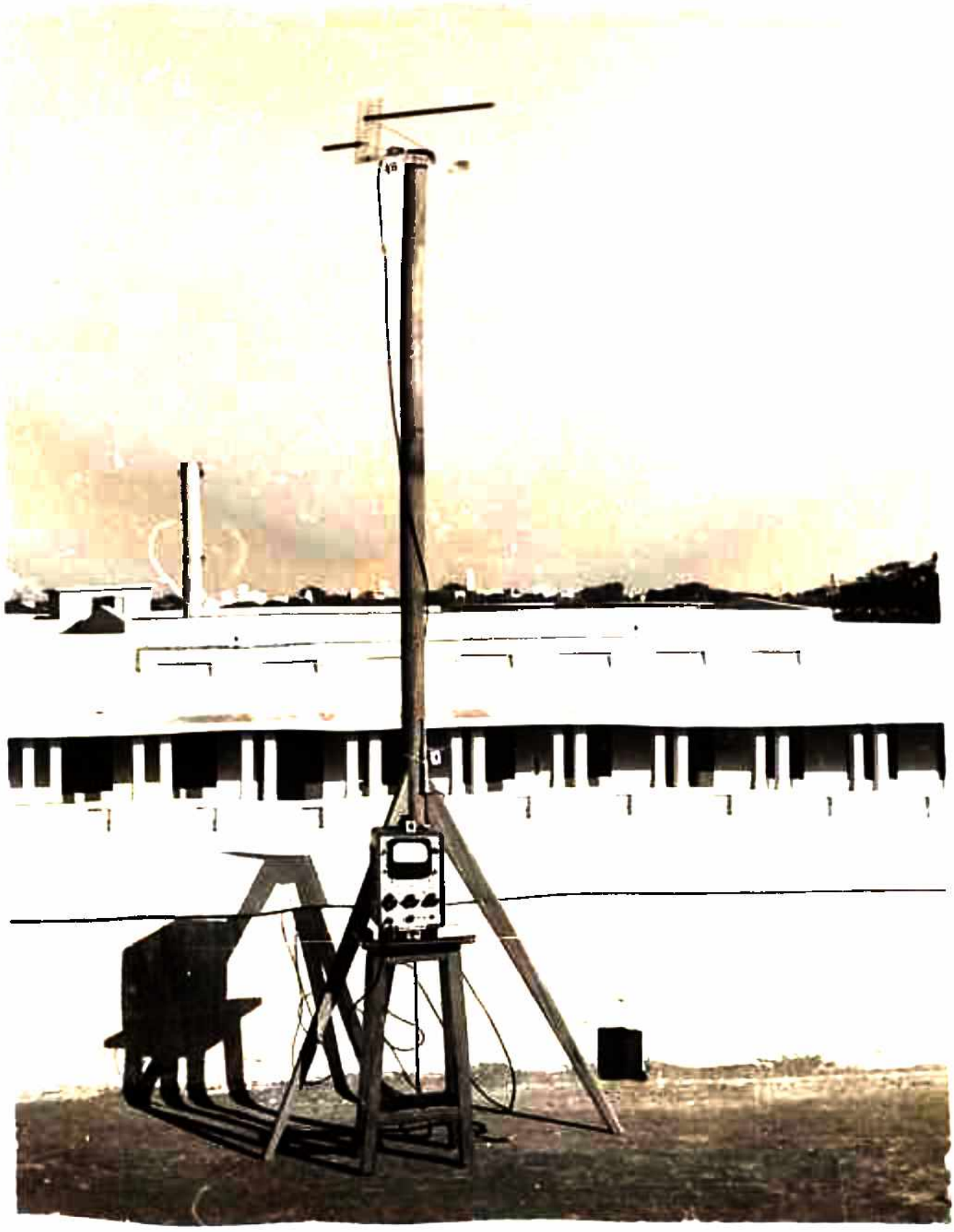

CLOSEUP OF RECEIVING ASY. DIPOLE ANTENNA

6. S. W. R. METER 7. CRYSTAL DETECTOR 8. RECEIVING DISPLACED DIPOLE

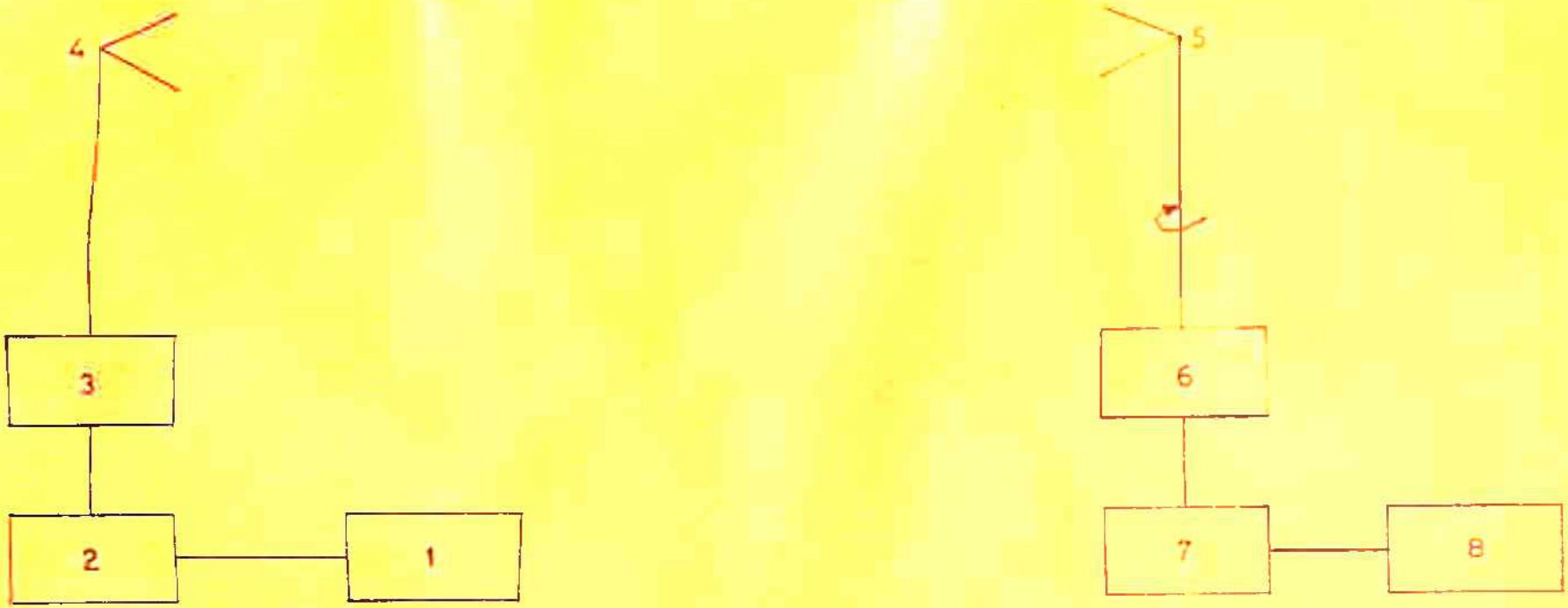

1 MODULATOR (TYPE 1214 – A)

2 G. R. UNIT OSCILLATOR (TYPE 1209 – B)

3 FILTER

4 TRANSMITTING ANTENNA

5 RECEIVING ANTENNA

6 ROTATING TABLE

7 DETECTOR

8 SWR METER (TYPE HP 415 – B)

FIG. (2·12b) BLOCK DIAGRAM FOR RADIATION PATTERN MEASUREMENT.

antenna. The radiating centre-fed dipole is connected through the line balun to the G.R.Unit oscillator (Type 1209-B) modulated by the 1000 C.P.S. G.R. audio oscillator (type 1214-A). Two masts, for mounting the transmitting and receiving antennas, of height 10 ft. and capable of rotation in the horizental plane have been designed and frabricated. A circular scale at the base of the rotating system is provided for noting the angular rotation. The displaced configuration is mounted on the masts. Figs.(2.12c, 3.2b) show the actual condition of the transversely and the axially displaced systems respectively during the measurements. Patterns were obtained for various feed point displacements at an operating frequency of 300 Mc/S. Radiation patterns (E and H-plane) are shown in figs.(2.13a ... 2.13f).

(iii) Power Gain and Effective Aperture:

For power gain measurements, the gain of the half wave centre fed dipole was first measured. This centre fed dipole was, then, replaced by the asymmetric dipole (displaced configuration) and the procedure was repeated. The difference of these two measurements gives the power gain.

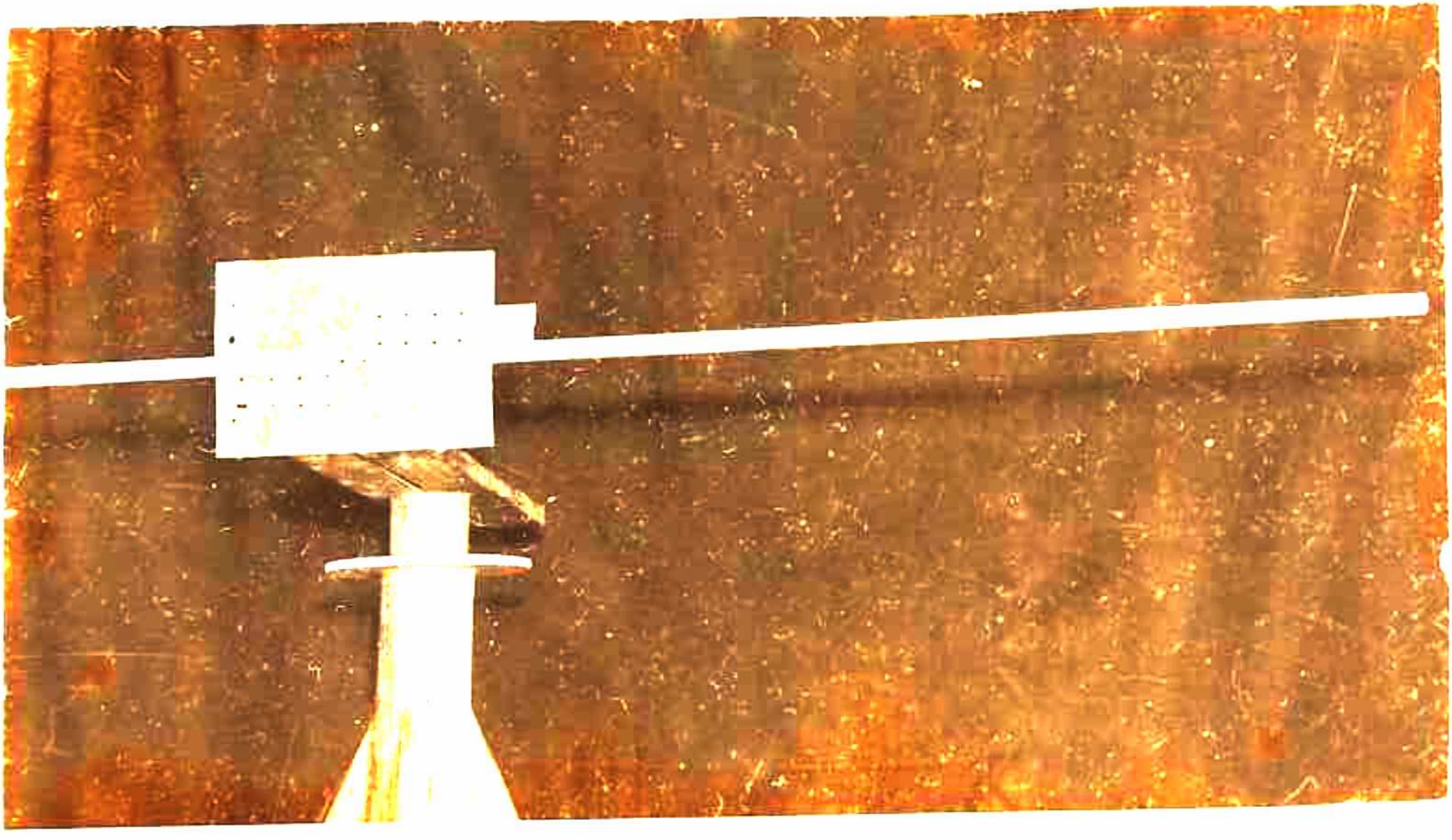

FIG.(2·12c) CLOSEUP OF AXIALLY DISPLACED ASY. DIPOLE ANTENNA.

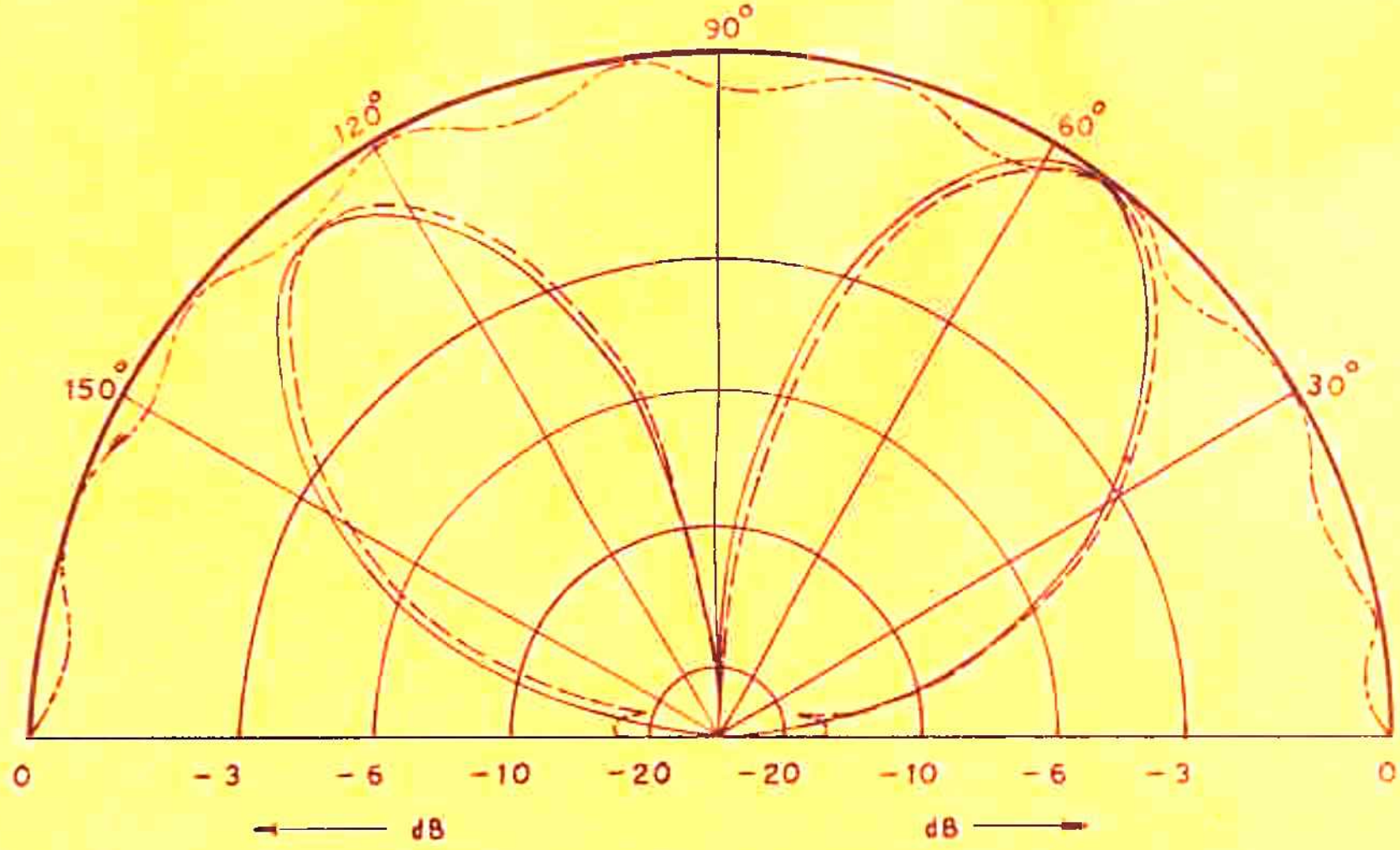

FIG. (2·13a) E AND H—PLANE PATTERNS OF TRANSVERSELY DISPLACED ASYMMETRIC DIPOLE ANTENNA FOR = 0·02λ.

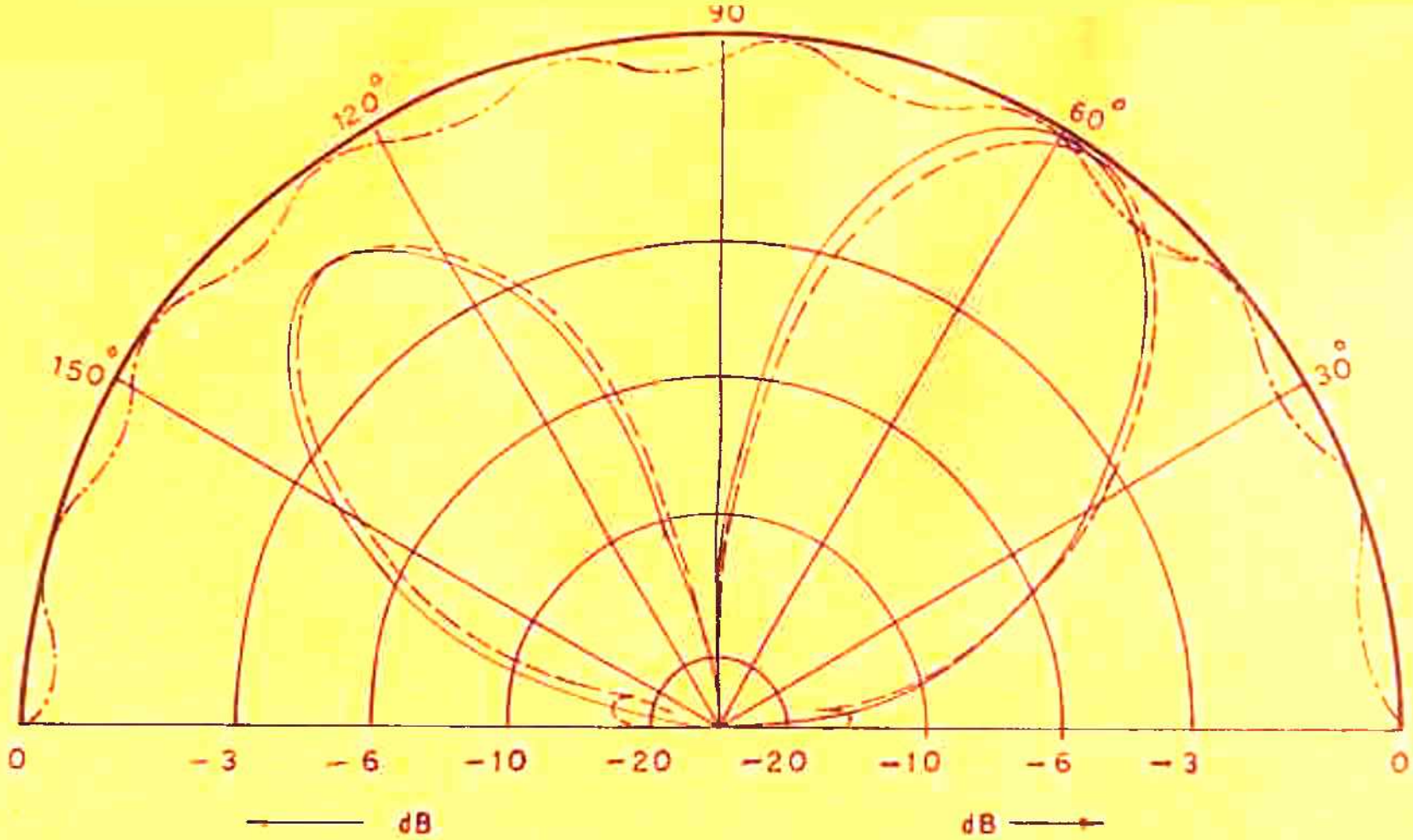

FIG. (2·13b) E AND H-PLANE PATTERNS OF TRANSVERSELY DISPLACED ASYMMETRIC DIPOLE ANTENNA FOR $R = 0.06\lambda$.

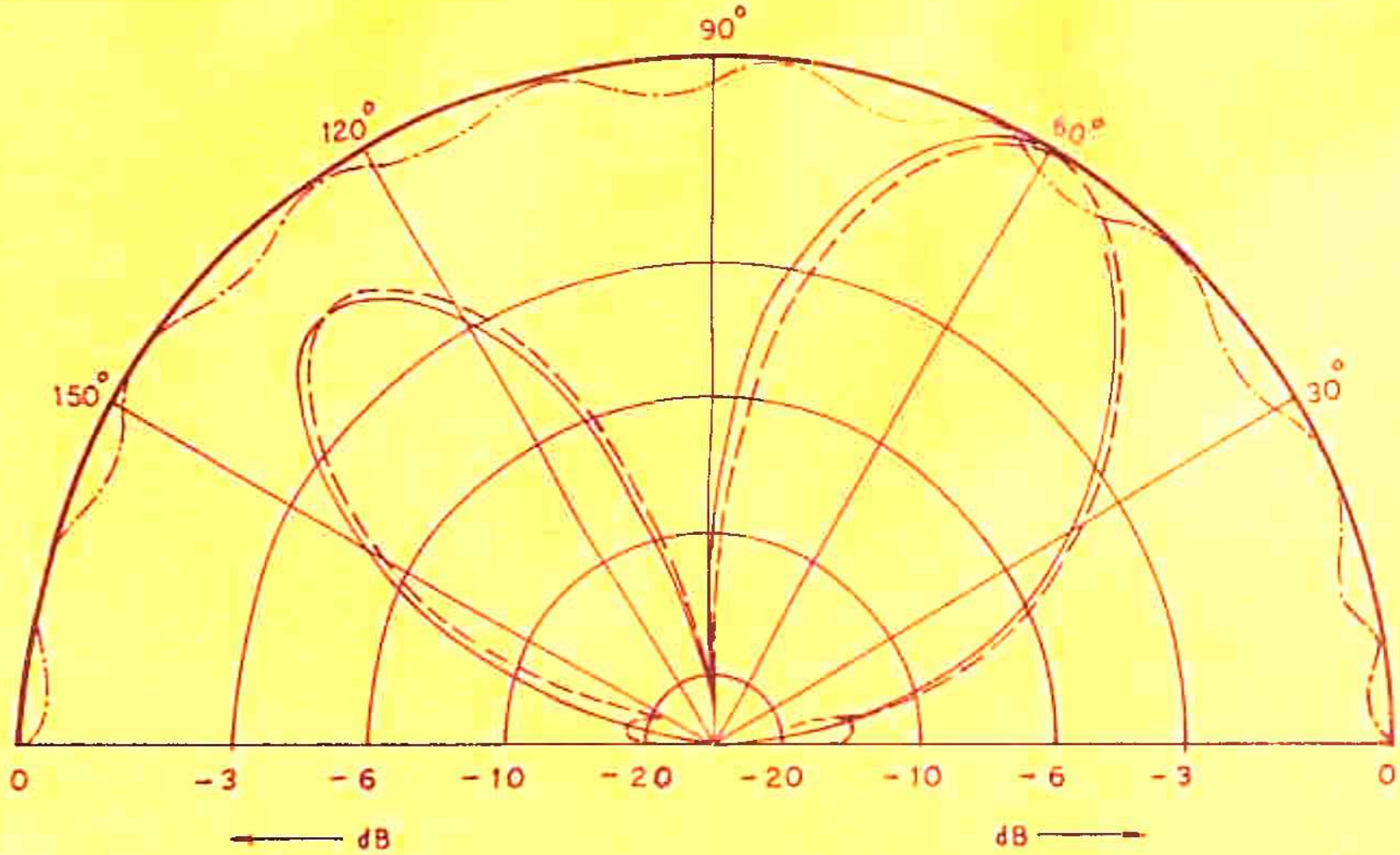

FIG. (2·13c) E AND H-PLANE PATTERNS OF TRANSVERSELY DISPLACED ASYMMETRIC DIPOLE ANTENNA FOR = 0·08λ.

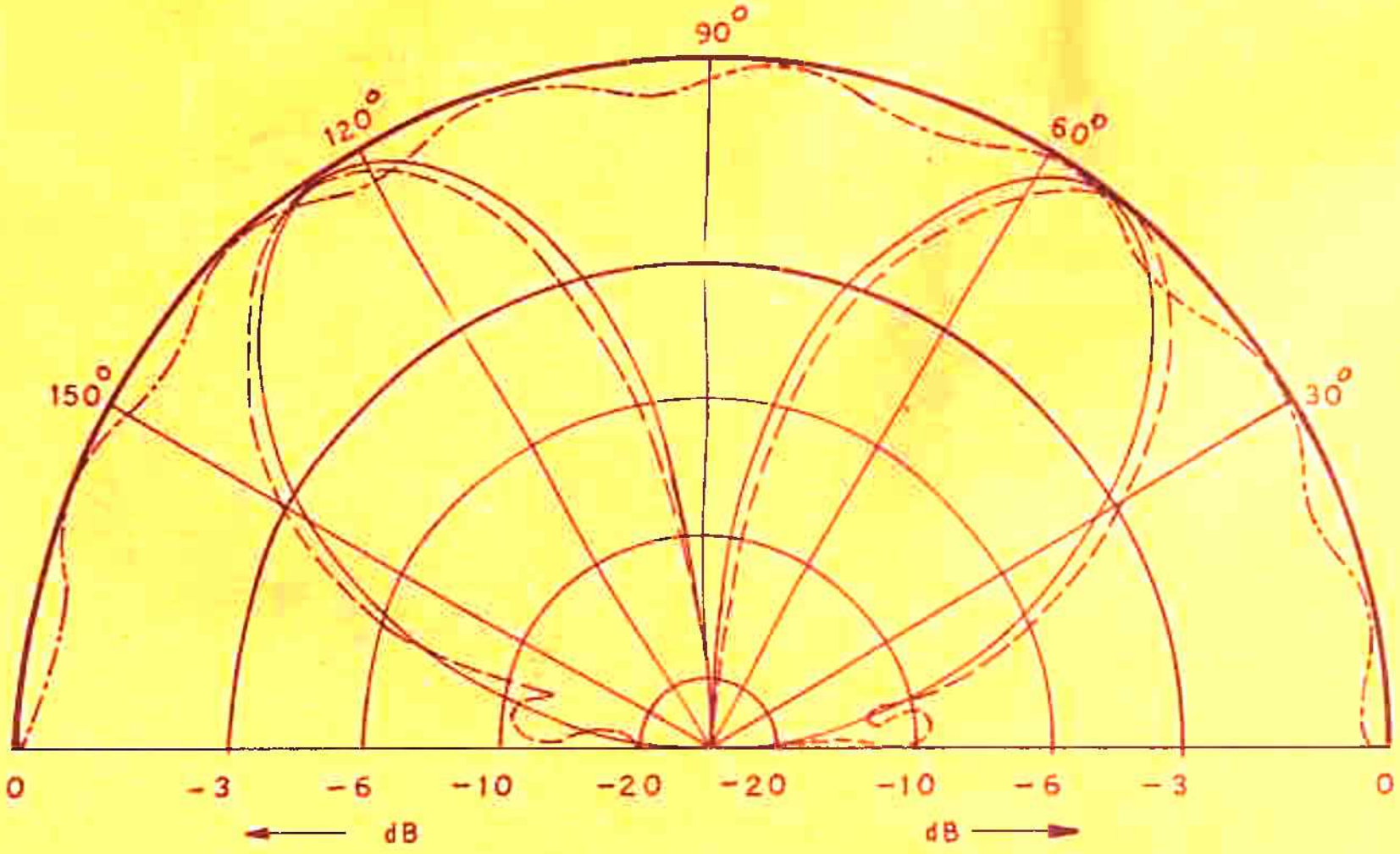

FIG. (2·13d.) E AND H-PLANE PATTERNS OF AXIALLY DISPLACED ASYMMETRIC DIPOLE ANTENNA FOR R = 0·02 λ .

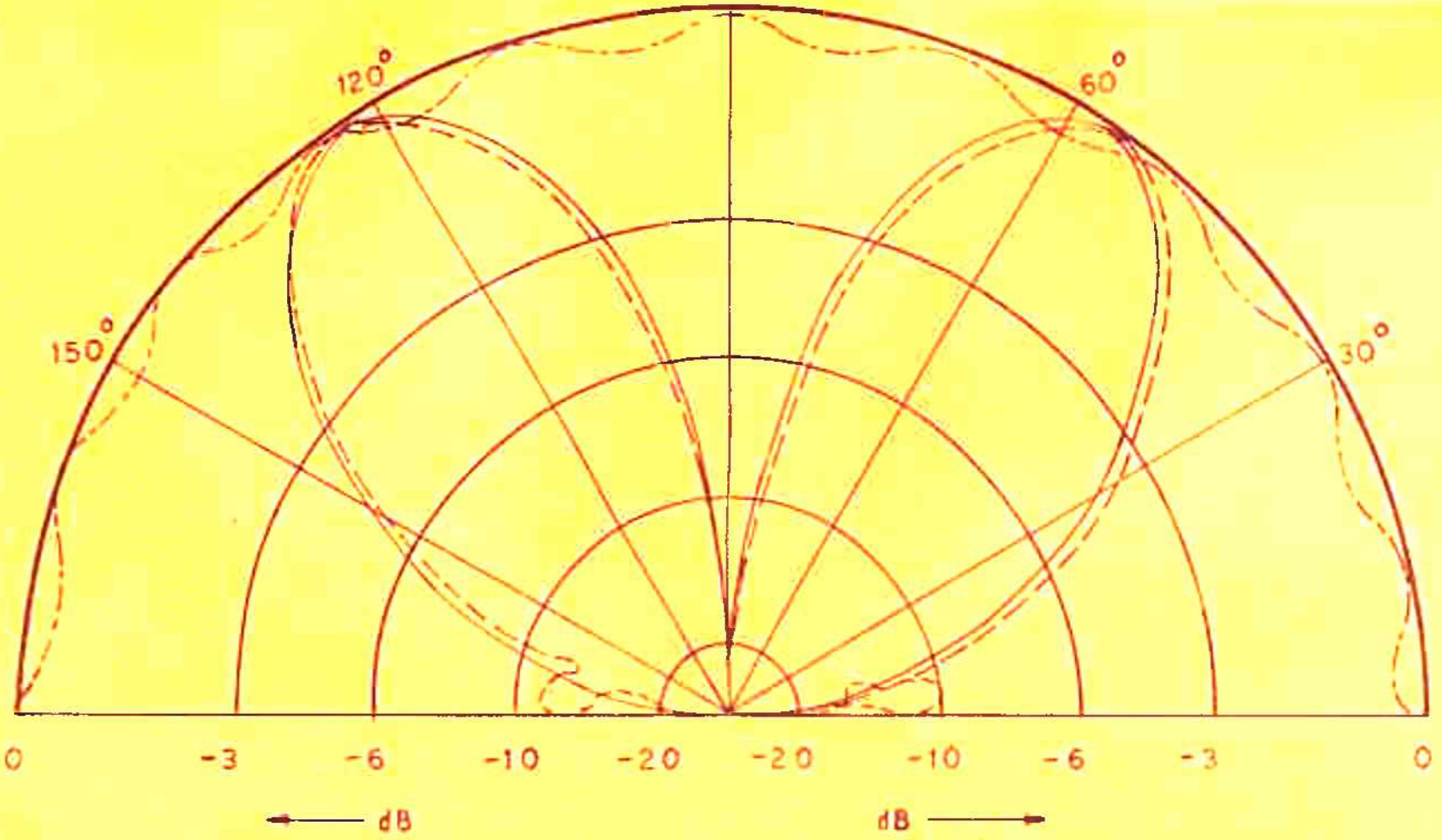

FIG. (2·13e) E AND H-PLANE PATTERNS OF AXIALLY DISPLACED ASYMMETRIC DIPOLE ANTENNA FOR $R = 0.06\lambda$.

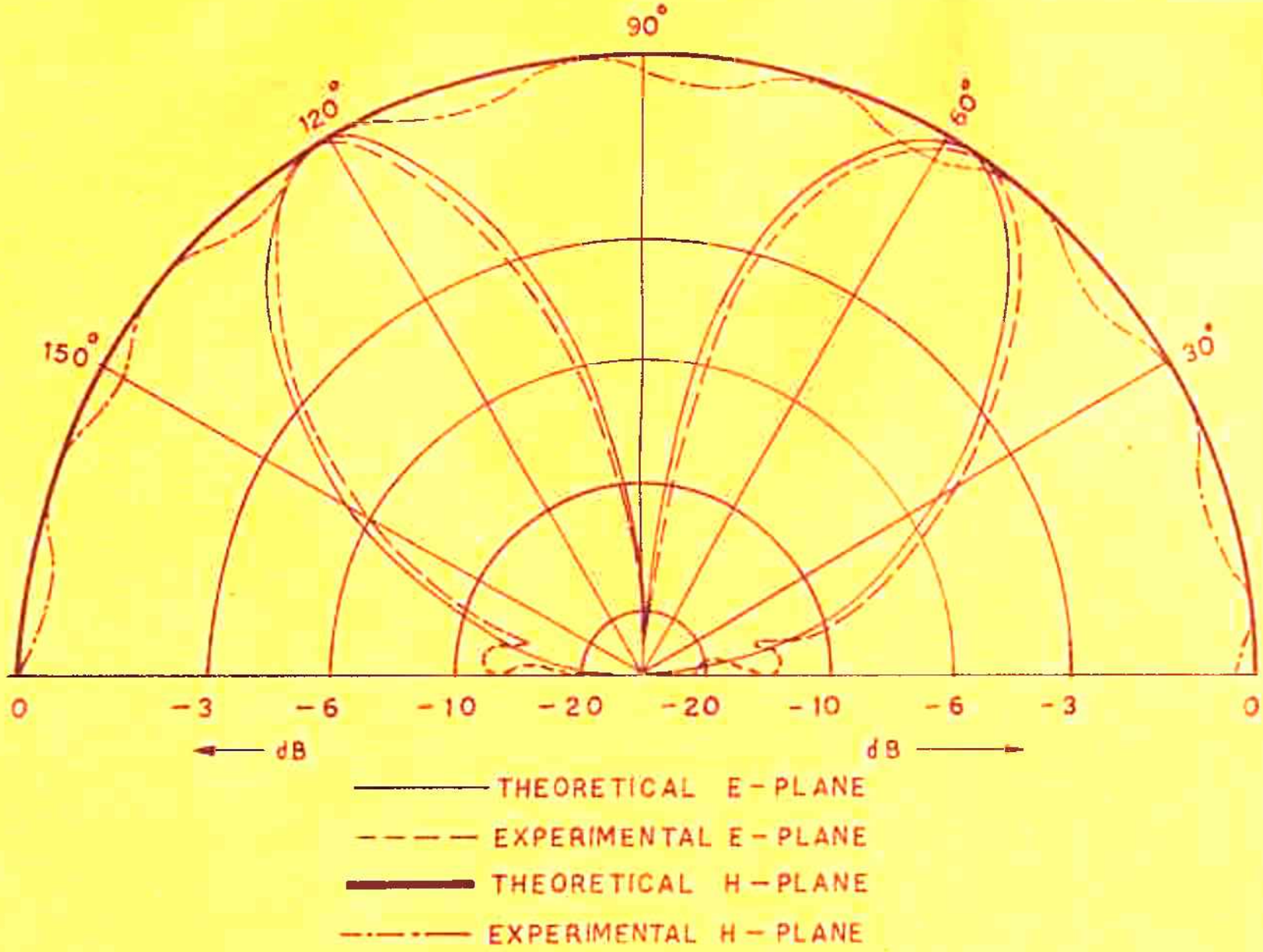

FIG. (2·13f) E AND H-PLANE PATTERNS OF AXIALLY DISPLACED ASYMMETRIC DIPOLE ANTENNA FOR R = 0·08λ.

In sec. 2.2.4, the effective aperture is defined as

$$\frac{A}{\lambda^2} = \frac{G}{4\pi}$$

Using the values of power gain determined experimentally, the effective aperture can be calculated. Results of the power gain and effective aperture measurements are given in Table 2.4 and shown graphically in fig.(2.14) and fig.(2.15).

TABLE - 2.4

Feed Point Displacement $2R/\lambda$	Power Gain (in dB)		Effective Aperture A/λ^2	
	Axial Displacement	Transverse Displacement	Axial Displacement	Transverse Displacement
0.0	3.0	3.0	0.143	0.143
0.04	2.66	2.85	0.144	0.148
0.08	2.69	2.94	0.145	0.153
0.12	2.71	3.03	0.146	0.158
0.16	2.75	3.14	0.147	0.161

§ 2.4 CONCLUSIONS AND DISCUSSIONS

2.4.1 Radiation Patterns

It is seen from the pattern plots for transversely displaced case that the direction of maximum radiation shifts by 5° as $2R/\lambda$ is increased from 0.04 to 0.16.

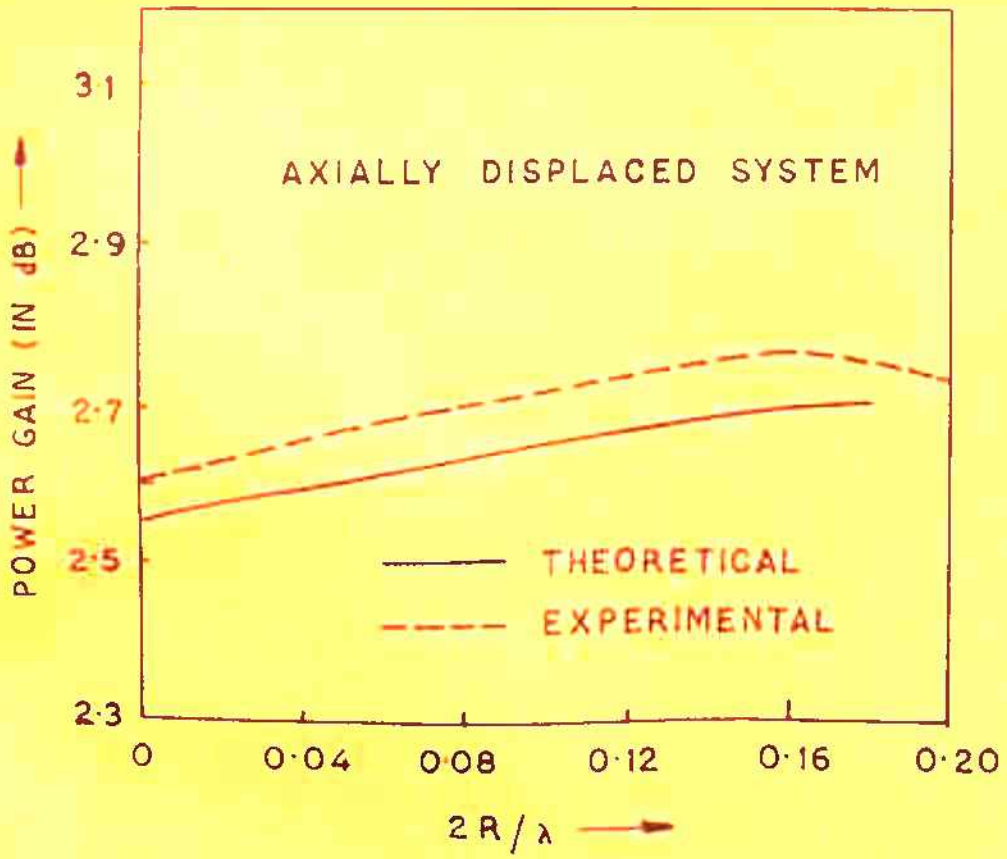

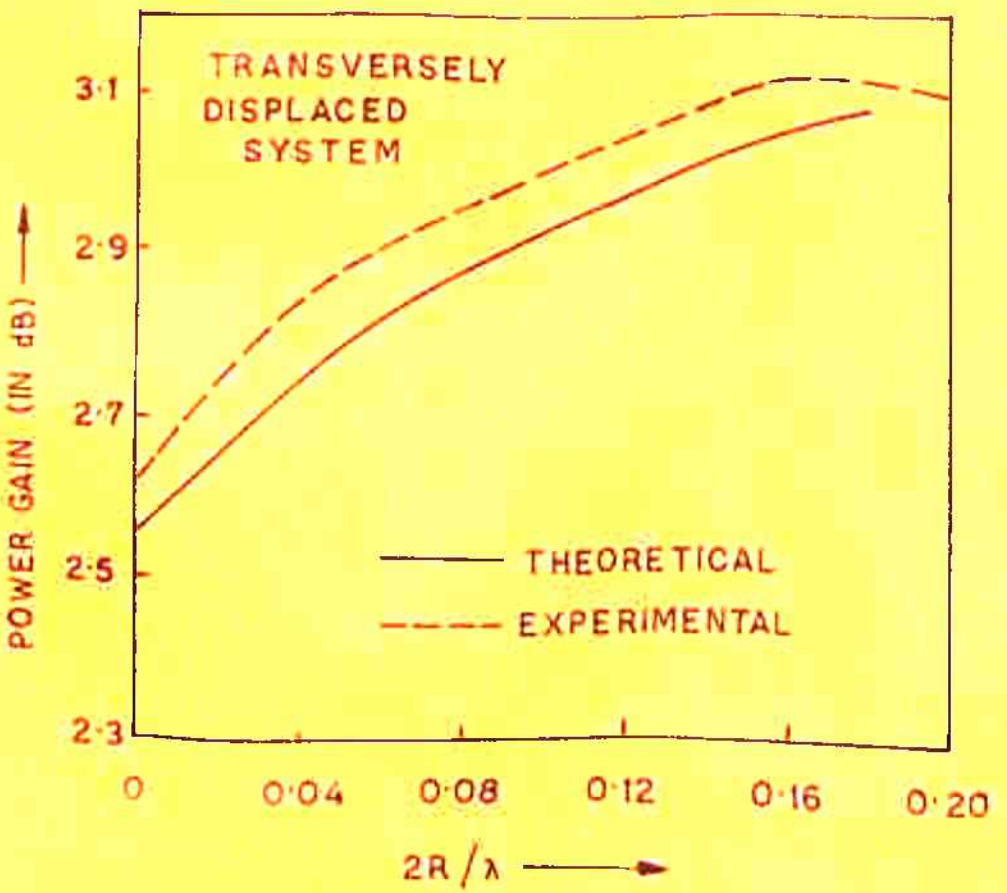

G. 2·14 POWER GAIN OF AXIALLY AND TRANSVERSELY DISPLACED ASYMMETRIC DIPOLE ANTENNAS.

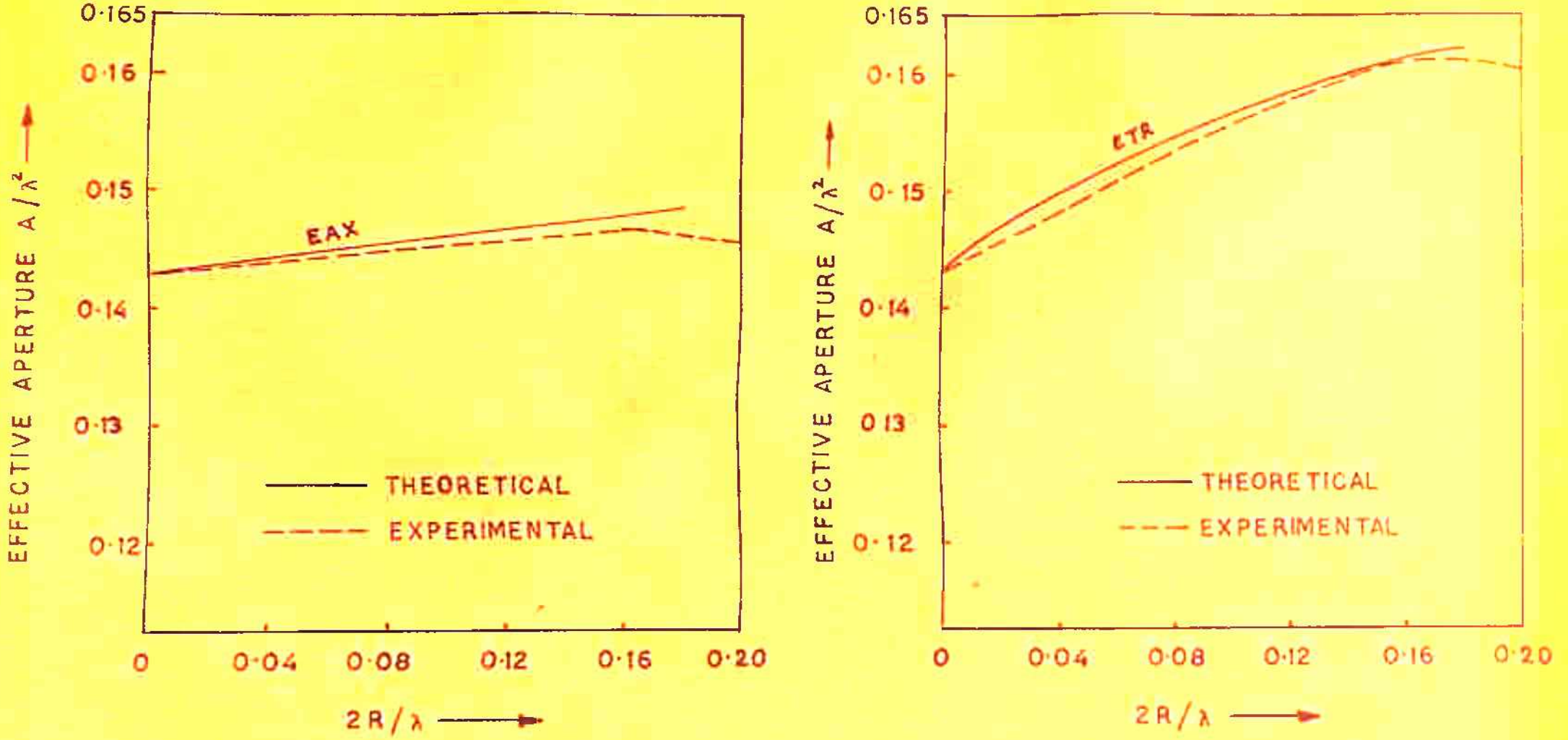

FIG. 2·15. EFFECTIVE APERTURE OF AXIALLY AND TRANSVERSELY DISPLACED ASYMMETRIC DIPOLE ANTENNA.

The pattern is 4 lobed and is symmetrical about the 0^{o}-180^{o} axis. However for the axially displaced case, direction of maximum radiation and the position of other lobes in the pattern remain unchanged with the increase in $\frac{2R}{\lambda}$ values in the range mentioned above. H-plane patterns are omnidirectional for both the cases. It is evident that the experimental results support the theoretical results with out much deviation.

2.4.2 Radiation Resistance:

From the theoretical curves shown in fig.(2.6), the radiation resistance for the axially and arbitrarily displaced cases increases upto $\frac{2R}{\lambda} = 0.11$ and then starts decreasing. However, the same for transverse displacement continuously decreases with change of $\frac{2R}{\lambda}$ in the range discussed above.

2.4.3 Power Gain and Effective Aperture:

Fig. (2.7) and fig. (2.8) show the theoretical variations of power gain and the effective aperture. Power gain for all the three configurations (axially, transversely and arbitrarily displaced configurations) increases with $2R/\lambda$ values. It first increases rapidly up to $\frac{2R}{\lambda} = 0.12$, then approaches a constant value as $\frac{2R}{\lambda}$ approaches 0.16. Effective aperture curves of fig. (2.8) also show a similar variation with $\frac{2R}{\lambda}$.

Experimental findings seem to be in good agreement with the theoretical results as is shown in figs.(2.14). Fig.(2.15) shows the variation of effective aperture along with the theoretical curves. The experimental results are found to support the theoretical results.

2.4.4 Voltage and Current Distribution:

Experimental results of the voltage and current distribution measurements for the transversely and axially displaced configurations are shown in figs.(2.10a,b) and (2.11a,b). It is seen from the voltage distribution curves for the transversely displaced case that the voltage maximum, at a point half wave from the starting point of measurement (in the fig. it is zero) shifts as $\frac{2R}{\lambda}$ value is increased from 0.04 to 0.12. For the axially displaced case, the curves become more and more flat as $\frac{2R}{\lambda}$ value is increased.

From the current distribution curves it is found that the current distribution on the displaced system is sinusoidal for both the configurations.

It can be seen from the radiation pattern plots [fig.(2.13a....2.13f)] that there are small minor side lobes appearing in the experimental curves which are unlike the theoretical predictions. This may be due to the following reasons.

(i) In deriving the theoretical expressions, the unavoidable coupling between the displaced system and the feeder line has been neglected for the sake of simplicity. This coupling becomes more and more pronounced as the feed point displacement increases.

(ii) The field in the gap region (created by the displacement) is not taken into account.

(iii) The assumed sinusodial current distribution does not hold good for larger values of the feed point displacement. However, for values of feed point displacement up to 0.12, the theoretical and experimental results show a close agreement. The validity of the assumed sinusodial distribution for smaller values of $\frac{2R}{\lambda}$ is apparent from the current distribution curves of fig.(2.11a, 2.11b).

C H A P T E R - 3

EFFECT OF TRANSVERSE FEED DISPLACEMENT ON INPUT IMPEDANCE OF ASYMMETRIC DIPOLE ANTENNA

§ 3.1 INTRODUCTION

Conventional design of log-periodic dipole arrays requires the noncollinear deployment of two dipole halves in order to realise current distributions, which produce a unidirectional backfire radiation. Design of such arrays for a prescribed radiation pattern and VSWR performance has been largely solved, but the analysis (27,28) on which they are based have been formulated for a collinear basic dipole element, whereas actually, the dipole halves have finite feed displacement. It is, therefore, essential to analyse this basic element before studying the non-planar log-periodic dipole array.

Present chapter deals with the effect of transverse feed displacement on the asymmetric dipole antenna which forms the basic element of a new log-periodic structure consisting of array of asymmetric dipoles to be discussed in chapter-5. Assuming sinusoidal current distribution, the expression for input impedance has been derived and the effect of varying the transverse feed displacement $2R/\lambda$ has been studied both theoretically and experimentally.

§ 3.2 ANALYSIS

For the upper limb of the asymmetric dipole shown in fig.(3.1b) and labelled 1, the vector potential on its surface has two components:

1) Vector potential due to scalar potential V_o maintained across its feed point and given by

$$A_{z11}(z) = \frac{\mu_o}{4\pi} \int_o^{h_1} I_{z1}(z') \frac{e^{-j\beta R_S}}{R_S} dz' \qquad (3.1)$$

where μ_o = free space permeability

$$R_S = \sqrt{(z-z')^2 + a^2}$$

2) Vector potential due to the coupling of the lower limb to the upper limb which is given by

$$A_{z12}(z) = \frac{\mu_o}{4\pi} \int_{-h_2}^{o} I_{z2}(z') \frac{e^{-j\beta R_C}}{R_C} dz' \qquad (3.2)$$

where $R_C = \sqrt{(z+z')^2 + (2R-a)^2}$

Total contribution to the vector potential due to the upper limb is

$$A_{zT1} = A_{z11} + A_{z12}$$

$$= \frac{\mu_o}{4\pi} \left[\int_o^{h_1} I_{z1}(z') \frac{e^{-j\beta R_S}}{R_S} dz' + \int_{-h_2}^{o} I_{z2}(z') \frac{e^{-j\beta R_C}}{R_C} dz' \right] \qquad (3.3)$$

Assuming the current distribution of the form

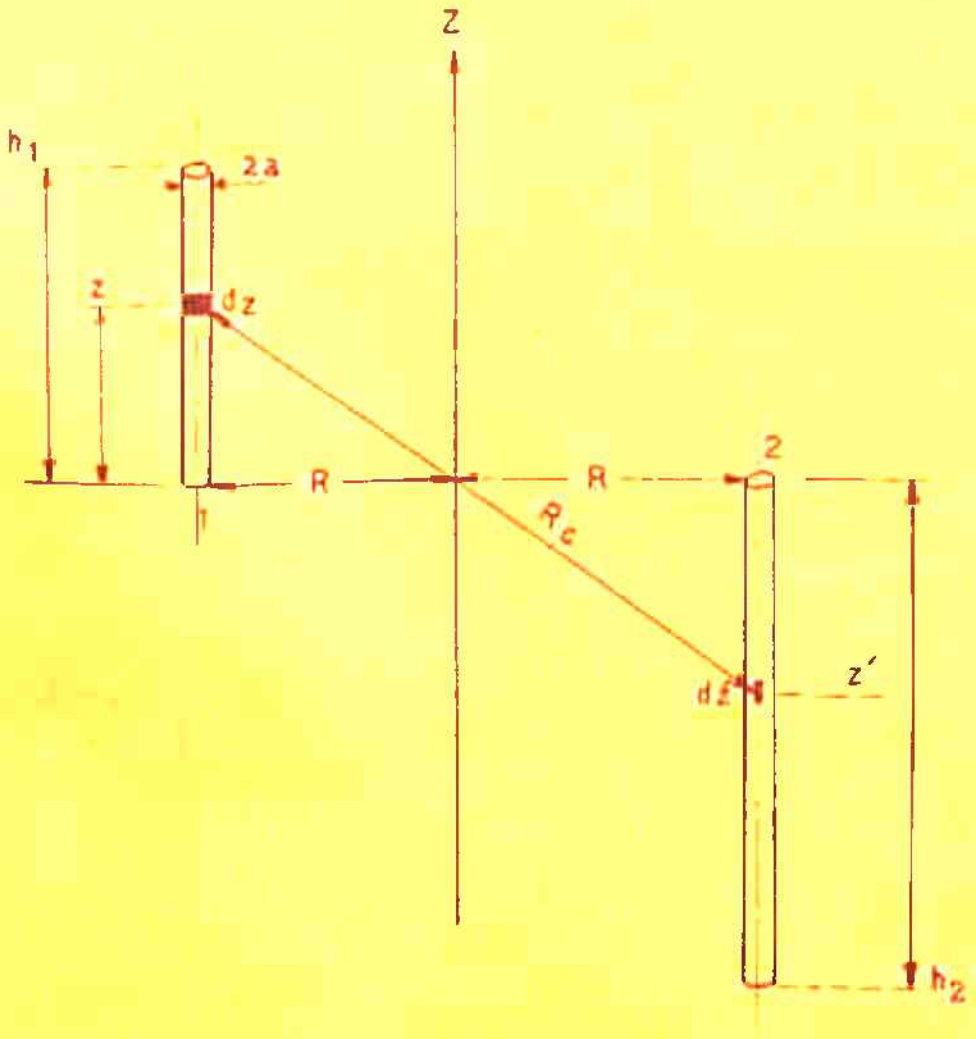

FIG. (3·1a) TRANSVERSELY DISPLACED FEED.

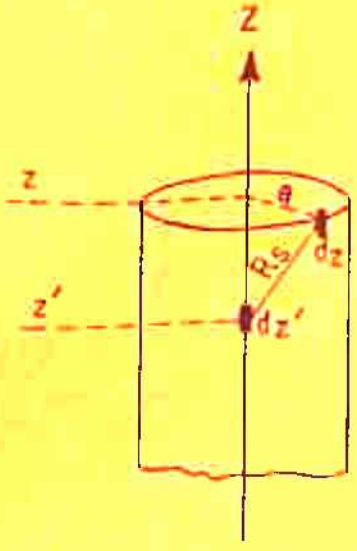

FIG. (3·1b) ELEMENTS OF INTEGRATION

$$I_{z1}(z') = I_m \sin(\beta h_2) \sin[\beta(h_1 - z')],\ 0 < z' < h_1$$

$$I_{z2}(z') = I_m \sin(\beta h_1) \sin[\beta(h_2 + z')],\ -h_2 < z' < 0$$

and substituting in equation (3.3), the vector potential is

$$A_{zT1}(z) = \frac{\mu_o I_m}{4\pi} \left[\sin(\beta h_2) \int_0^{h_1} \sin[\beta(h_1 - z')] \frac{e^{-j\beta R_S}}{R_S} dz' + \sin(\beta h_1) \int_{-h_2}^{0} \sin[\beta(h_2 + z')] \frac{e^{-j\beta R_C}}{R_C} dz'\right] \quad (3.4)$$

Also, considering only axial current distribution on the dipole, a solution to the wave equation for the surface vector potential is

$$A_{zT1}(z) = \frac{-j}{c}\left[C_1 \cos(\beta z) + \frac{V_o}{2} \sin(\beta z)\right] \quad (3.5)$$

Putting $z = h_1$ in equation (3.4), $A_{zT1}(z)$ becomes:

$$A_{zT1}(h_1) = \frac{\mu_o I_m}{4\pi} \left[\sin(\beta h_2) \int_0^{h_1} \sin[\beta(h_1 - z')] \frac{e^{-j\beta R_{S1}}}{R_{S1}} dz' + \sin(\beta h_1) \int_{-h_2}^{0} \sin[\beta(h_2 + z')] \frac{e^{-j\beta R_{C1}}}{R_{C1}} dz'\right]$$

$$= \frac{j}{c} U \quad (3.6)$$

where $R_{S1} = \sqrt{(h_1 - z')^2 + a^2}$

$$R_{C1} = \sqrt{(h_1 + z')^2 + (2R - a)^2}$$

$$U = \frac{\mu_o}{4\pi} I_m \frac{c}{j} U' \quad (3.7)$$

$$U' = \sin(\beta h_2) \int_0^{h_1} \sin[\beta(h_1 - z')] \frac{e^{-j\beta R_{S1}}}{R_{S1}} dz'$$

$$+ \sin(\beta h_1) \int_{-h_2}^{0} \sin[\beta(h_2 + z')] \frac{e^{-j\beta R_{C1}}}{R_{C1}} dz' \quad (3.8)$$

Subtracting $\frac{4\pi}{\mu_0} A_{zT1}(h_1)$ from both the sides equation (3.4) and equation (3.5),

$$A_{zT1}(z) - A_{zT1}(h_1) = I_m[\sin(\beta h_2) \int_0^{h_1} \sin[\beta(h_1 - z')]$$

$$\left[\frac{e^{-j\beta R_S}}{R_S} - \frac{e^{-j\beta R_{S1}}}{R_{S1}} \right] dz' + \sin(\beta h_1) \int_{-h_2}^{0} \sin[\beta(h_2 + z')]$$

$$\left[\frac{e^{-j\beta R_C}}{R_C} - \frac{e^{-j\beta R_{C1}}}{R_{C1}} \right] dz' = \frac{-j}{c} \left[\frac{4\pi}{\mu_0} \left[C_1 \cos(\beta z) + \frac{V_0}{2} \sin(\beta z) \right. \right.$$

$$\left. \left. + U \right] \right] \quad (3.9)$$

Putting $z = h_1$,

L.H.S. of equation (3.9) becomes zero,

$$\text{from which } C_1 = - \frac{V_0 \sin(\beta h_1) + 2U}{2 \cos(\beta h_1)}$$

Substituting the value of C_1 in equation (3.9), the equation becomes

$$I_m[\sin(\beta h_2) \int_0^{h_1} \sin[\beta(h_1 - z')] \left[\frac{e^{-j\beta R_S}}{R_S} - \frac{e^{-j\beta R_{S1}}}{R_{S1}} \right] dz'$$

$$+ \sin(\beta h_1) \int_{-h_2}^{0} \sin[\beta(h_2 + z')] \left[\frac{e^{-j\beta R_C}}{R_C} - \frac{e^{-j\beta R_{C1}}}{R_{C1}} \right] dz']$$

$$= \frac{-j}{c} \left[\frac{4\pi}{\mu_0} \left(- \frac{V_0 \sin(\beta h_1) + 2U}{2 \cos(\beta h_1)} \cos(\beta z) + \frac{V_0}{2} \sin(\beta z) + U \right) \right] \quad (3.10)$$

On substitution of U from equation (3.7) and simplifying, equation (3.10) takes the form:

$$I_m[\sin(\beta h_2)\int_o^{h_1}\sin[\beta(h_1-z')]\{\frac{e^{-j\beta R_S}}{R_S}-\frac{e^{-j\beta R_{S1}}}{R_{S1}}\}dz' +$$

$$\sin(\beta h_1)\int_{-h_2}^{o}\sin[\beta(h_2+z')]\{\frac{e^{-j\beta R_C}}{R_C}-\frac{e^{-j\beta R_{C1}}}{R_{C1}}\}dz'] = \frac{j}{c}\frac{4\pi}{\mu_o}$$

$$\frac{1}{\cos(\beta h_1)}[\frac{V_o}{2}\sin[\beta(h_1-z)] + U'\{\cos(\beta z)-\cos(\beta h_1)\}] \quad (3.11)$$

On rearranging

$$I_m[\sin(\beta h_2)\int_o^{h_1}\sin[\beta(h_1-z')]\{\frac{e^{-j\beta R_S}}{R_S}-\frac{e^{-j\beta R_{S1}}}{R_{S1}}\}dz'$$

$$+\sin(\beta h_1)\int_{-h_2}^{o}\sin[\beta(h_2+z')]\{\frac{e^{-j\beta R_C}}{R_C}-\frac{e^{-j\beta R_{C1}}}{R_{C1}}\}dz'$$

$$-U'\{\cos(\beta z)-\cos(\beta h_1)\}] = j\frac{4\pi}{\mu_o}\frac{V_o}{2}\frac{\sin[\beta(h_1-z)]}{\cos(\beta h_1)}$$

$$= \frac{1}{60}\frac{V_o\sin[\beta(h_1-z)]}{\cos(\beta h_1)} \quad (3.12)$$

Putting the value of U' from equation (3.8) in equation (3.12),

$$I_m[\sin(\beta h_2)\int_o^{h_1}\sin[\beta(h_1-z')]\,K_{dS}(z,z')dz' + \sin(\beta h_1)\int_{-h_2}^{o}$$

$$\sin[\beta(h_2+z')]\,K_{dC}(z,z')dz' - [\frac{\cos(\beta z)-\cos(\beta h_1)}{\cos(\beta h_1)}]$$

$$\{\sin(\beta h_2)\int_o^{h_1}\sin[\beta(h_1-z')K_S(h_1,z')dz' + \sin(\beta h_1)\int_{-h_2}^{o}$$

$$\sin[(h_2+z')]\,K_C(h_1,z')dz']] = \frac{jV_o}{60}\frac{\sin[\beta(h_1-z)]}{\cos(\beta h_1)} \quad (3.13)$$

where $K_{dS}(z,z') = \dfrac{e^{-j\beta R_S}}{R_S} - \dfrac{e^{-j\beta R_{Sl}}}{R_{Sl}}$

$K_{dC}(z,z') = \dfrac{e^{-j\beta R_C}}{R_C} - \dfrac{e^{-j\beta R_{Cl}}}{R_{Cl}}$

$K_S(h_1,z') = \dfrac{e^{-j\beta R_{Sl}}}{R_{Sl}}$

$K_C(h_1,z') = \dfrac{e^{-j\beta R_{Cl}}}{R_{Cl}}$ (3.14)

Input impedance is defined as

$$Z_{in} = \frac{V_o}{I_m \sin(\beta h_2)\sin[\beta(h_1 - z)]}\Bigg|_{z=0}$$

Multiplying both sides of equation (3.13) by $\dfrac{\cos(\beta h_1)}{\sin(\beta h_2)\sin^2[\beta(h_1-z)]}$ and applying the above definition of input impedance, the input impedance Z_{in} due to the upper limb is obtained as

$$Z_{in} = -\frac{j60}{\sin(\beta h_2)\sin^2(\beta h_1)}\Big[\cos(\beta h_1)[\sin(\beta h_2)\int_0^{h_1}\sin\{\beta(h_1-z')\}K_{dS}(0,z')dz' + \sin(\beta h_1)\int_{-h_2}^{0}\sin\{\beta(h_2+z')\}K_{dC}(0,z')dz'] - \{1-\cos(\beta h_1)\}[\sin(\beta h_2)\int_0^{h_1}\sin\{\beta(h_1-z')\}K_S(h_1,z')dz' + \sin(\beta h_1)\int_{-h_2}^{0}\sin\{\beta(h_2+z')\}K_C(h_1,z')dz']\Big]$$

(3.15)

where $K_{dS}(0,z')$ and $K_{dC}(0,z')$ are obtained by putting $z = 0$ in first two equations of equation (3.14).

Following the method used for the vector potential due to the upper limb, we have two parts of vector potential due to the lower limb, namely:

1) that due to the limb labelled (2) itself:

$$A_{z21} = \frac{\mu_o}{4\pi} I_m \sin(\beta h_2) \int_{-h_2}^{o} \sin[\beta(h_2 + z')] \frac{e^{-j\beta R_S}}{R_S} dz' \quad (3.16)$$

2) that due to the coupling of upper limb to the lower limb:

$$A_{z22} = \frac{\mu_o}{4\pi} I_m \sin(\beta h_1) \int_{o}^{h_1} \sin[\beta(h_1 - z')] \frac{e^{-j\beta R_C}}{R_C} dz' \quad (3.17)$$

Adding these two equations

$$A_{zT2}(z) = \frac{\mu_o I_m}{4\pi}[\sin(\beta h_2) \int_{-h_2}^{o} \sin[\beta(h_2 + z')] \frac{e^{-j\beta R_S}}{R_S} dz' + \sin(\beta h_1) \int_{o}^{h_1} \sin[\beta(h_1 - z')] \frac{e^{-j\beta R_C}}{R_C} dz'] \quad (3.18)$$

Also, by solving the wave equation for axial currents,

$$A_{zT2}(z) = \frac{-j}{c}[C_2 \cos(\beta z) + \frac{V_o}{2} \sin(\beta z)] \quad (3.19)$$

Equating this equation to equation (3.18),

$$\frac{\mu_o I_m}{4\pi}[\sin(\beta h_1) \int_{-h_2}^{o} \sin[\beta(h_2 + z')] \frac{e^{-j\beta R_S}}{R_S} dz' + \sin(\beta h_2) \int_{o}^{h_1} \sin[\beta(h_1 - z')] \frac{e^{-j\beta R_C}}{R_C} dz'] = -\frac{1}{c}[C_2 \cos(\beta z) + \frac{V_o}{2} \sin(\beta z)] \quad (3.20)$$

Putting $z = -h_2$ in equation (3.20), the equation becomes

$$A_{zT2}(-h_2) = \frac{\mu_o}{4\pi} I_m[\sin(\beta h_1) \int_{-h_2}^{o} \sin[\beta(h_2+ z')] \frac{e^{-j\beta R_{S2}}}{R_{S2}} dz' +$$

$$+ \sin(\beta h_2) \int_{o}^{h_1} \sin[\beta(h_1- z')] \frac{e^{-j\beta R_{C2}}}{R_{C2}} dz']$$

$$= \frac{j}{c} U_1 \qquad (3.21)$$

where $R_{S2} = \sqrt{(h_2+ z')^2+ a^2}$, $R_{C2} = \sqrt{(h_2- z')^2+(2R-a)^2}$

$$U_1 = \frac{\mu_o I_m}{4\pi} \frac{c}{j} U'' \qquad (3.22)$$

$$U'' = [\sin(\beta h_1) \int_{-h_2}^{o} \sin[\beta(h_2+ z')] \frac{e^{-j\beta R_{S2}}}{R_{S2}} dz' +$$

$$+ \sin(\beta h_2) \int_{o}^{h_1} \sin[\beta(h_1- z')] \frac{e^{-j\beta R_{C2}}}{R_{C2}} dz'] \qquad (3.23)$$

Subtracting $(\frac{4\pi}{\mu_o})$ $A_{zT2}(-h_2)$ from both sides of equation(3.20)

$$A_{zT2}(z) - A_{zT2}(-h_2) = I_m[\sin(\beta h_1) \int_{-h_2}^{o} \sin[\beta(h_2+ z')]$$

$$[\frac{e^{-j\beta R_S}}{R_S} - \frac{e^{-j\beta R_{S2}}}{R_{S2}}] dz' + \sin(\beta h_2) \int_{o}^{h_1} \sin[\beta(h_1- z')]$$

$$[\frac{e^{-j\beta R_C}}{R_C} - \frac{e^{-j\beta R_{C2}}}{R_{C2}}]dz'] = - \frac{j}{c} \frac{4\pi}{\mu_o}[C_2 \cos(\beta z) + \frac{V_o}{2}$$

$$\sin(\beta z) + U_1] \qquad (3.24)$$

Putting $z = -h_2$, L.H.S. = 0 ,

$$\therefore C_2 \cos(\beta h_2) - \frac{V_o}{2} \sin(\beta h_2) + U_1 = 0$$

$$\text{or} \quad C_2 = \frac{V_o \sin(\beta h_2) - 2U_1}{2\cos(\beta h_2)}$$

On substitution of this value of C_2 in equation (3.24), the equation takes the form,

$$I_m[\sin(\beta h_1) \int_{-h_2}^{o} \sin[\beta(h_2 + z')] K'_{ds}(z,z')dz' + \sin(\beta h_2) \int_{o}^{h_1} \sin[\beta(h_1 - z')]K'_{dc}(z,z')dz'] = -\frac{j}{c\cos(\beta h_2)} \frac{4\pi}{\mu_o}$$

$$[U_1[-\cos(\beta z) + \cos(\beta h_2)] + \frac{V_o}{2} \sin[\beta(h_2 + z)]] \qquad (3.25)$$

Applying the definition of input impedance as given for the upper limb, equation (3.25) transforms to

$$Z_{D2} = \frac{j60}{\sin(\beta h_1)\sin^2(\beta h_2)} [\cos(\beta h_2)[\sin(\beta h_1) \int_{-h_2}^{o} \sin[\beta(h_2 + z')]K'_{ds}(0,z')dz' + \sin(\beta h_2) \int_{o}^{h_1} \sin[\beta(h_1 - z')]$$

$$K'_{dc}(0,z')dz'] - [1 - \cos(\beta h_2)][\sin(\beta h_1) \int_{-h_2}^{o} \sin[\beta(h_2 + z')]K'_s(h_2, z')dz' + \sin(\beta h_2) \int_{o}^{h_1} \sin[\beta(h_1 - z')]$$

$$K'_c(h_2, z')dz']] \qquad (3.26)$$

where $K'_{ds}(z,z') = \frac{e^{-j\beta R_3}}{R_3} - \frac{e^{-j\beta R_{32}}}{R_{32}}$

$$K'_{dC}(z,z') = \frac{e^{-j\beta R_C}}{R_C} - \frac{e^{-j\beta R_{C2}}}{R_{C2}}$$

$$K'_S(h_2,z') = \frac{e^{-j\beta R_{S2}}}{R_{S2}}$$

$$K'_C(h_2,z') = \frac{e^{-j\beta R_{C2}}}{R_{C2}}$$

and $K'_{dS}(0,z')$, $K'_{dC}(C,z')$ are obtained by putting $z = 0$ in above equations. Total input impedance due to lower and upper limbs is given by

$$Z_{in} = Z_{D1} + Z_{D2}$$

Theoretical calculations were carried out for various values of feed point displacement $2R/\lambda$. They are given in Table 3.1.

TABLE - 3.1

Feed Point Displacement $2R/\lambda$	Resistance (in ohms)	Reactance (in ohms)	Impedance (in ohms)
0.0	120.6	121.2	171.1
0.04	116.5	82.8	144.0
0.08	105.0	94.8	137.0
0.12	100.2	88.8	133.7
0.16	97.8	92.0	133.0
0.20	96.0	90.0	131.6

§ 3.3 EXPERIMENTAL INVESTIGATIONS

Measurements of input impedance for the transverse displacement of feed points were carried out using conventional impedance measurement technique. Block diagram of the set up is shown in fig.(3.2a) and the photograph in fig.(3.2b). An asymmetric dipole antenna with design details described in section (2.3.2) given in chapter 2 was used. The output of the signal generator, comprising of G.R. unit oscillator (Type 1209-B) modulated by G.R. Audio oscillator (Type 1214-A) at 1OCC C.P.S. was fed to the transversely displaced configuration through a slotted section (Type G.R. 874-LB). The output of the slotted line is fed to the standing wave indicator (HP415-B) through a crystal detector connected to the slotted line. The position of the first voltage minimum and the VSWR were determined. Then the load was replaced by a coaxial short and again the first minimum is determined. Using this data with the help of Smith's Chart, the impedance is determined for various values of feed point displacement. Experimental values of individual components of the input impedance along with the input impedance are given in table (3.2). Results are shown graphically in fig. (3.3).

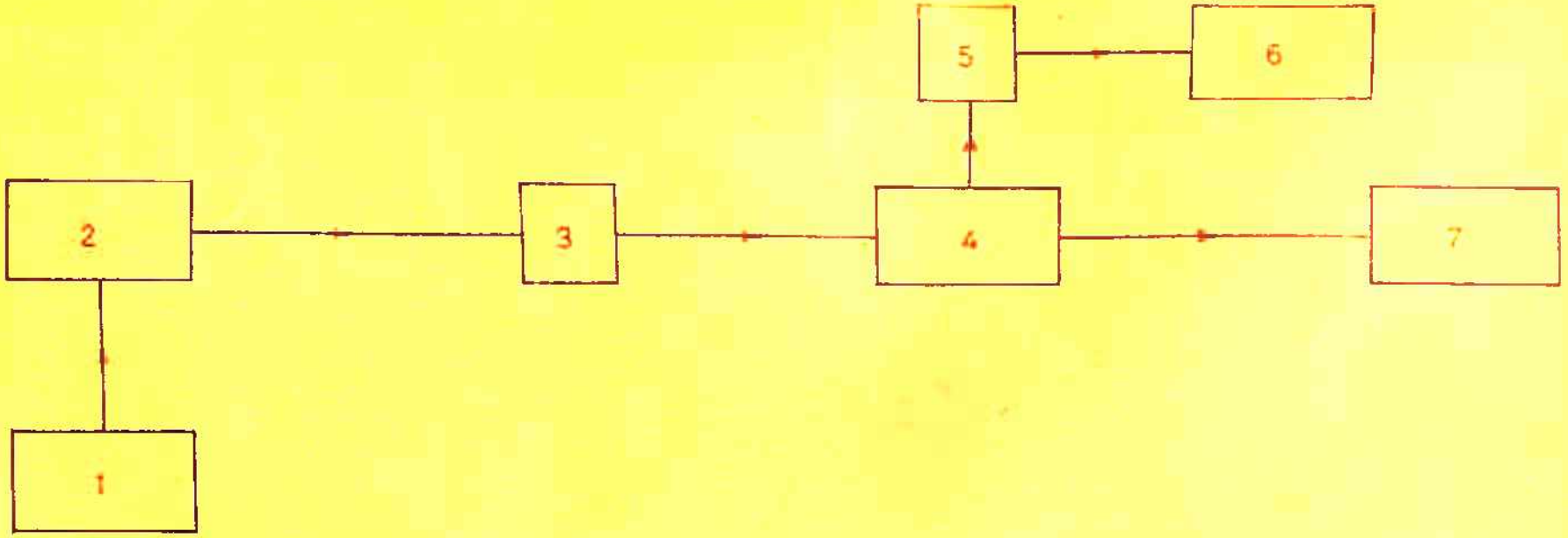

1 MODULATOR (TYPE 1214 – A)

2 G. R. UNIT OSCILLATOR (TYPE 1209 – B)

3 10 dB PAD

4 SLOTTED LINE (TYPE 874 – LB)

5 DETECTOR

6 STANDING WAVE INDICATOR (HP 415 – B)

7 ANTENNA SYSTEM

FIG. (3·2a) BLOCK DIAGRAM FOR INPUT IMPEDANCE MEASUREMENT.

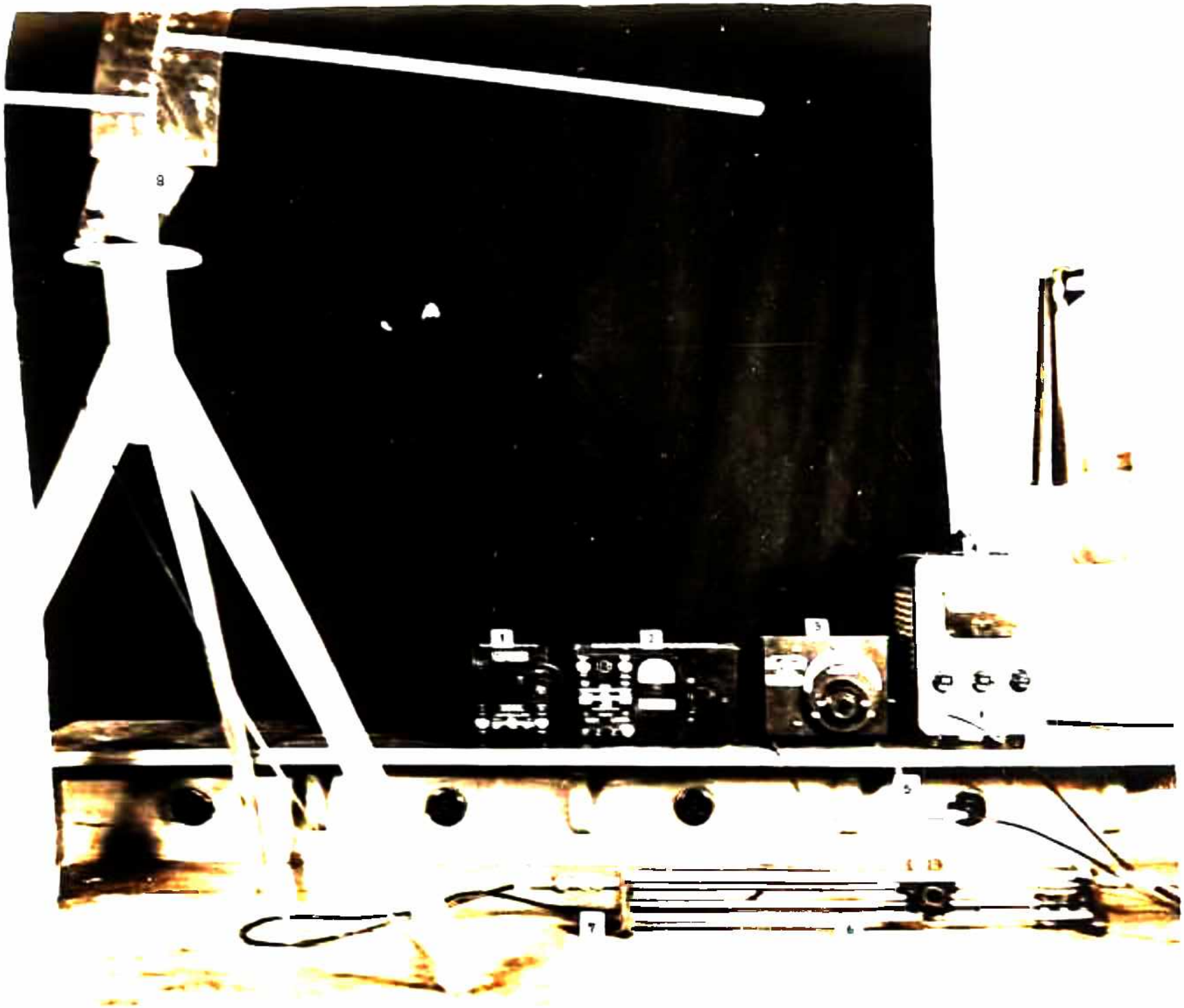

FIG.(3·2b) SETUP FOR INPUT IMPEDANCE MEASUREMENT.

1. MODULATOR 2. POWER SUPPLY 3. G. R. UNIT OSCILLATOR 4. S. W. R. METER 5 CRYSTAL DETECTOR 6. SLOTTED LINE 7. 10 dB PAD 8. DISPLACED ASY. DIPOLE ANTENNA

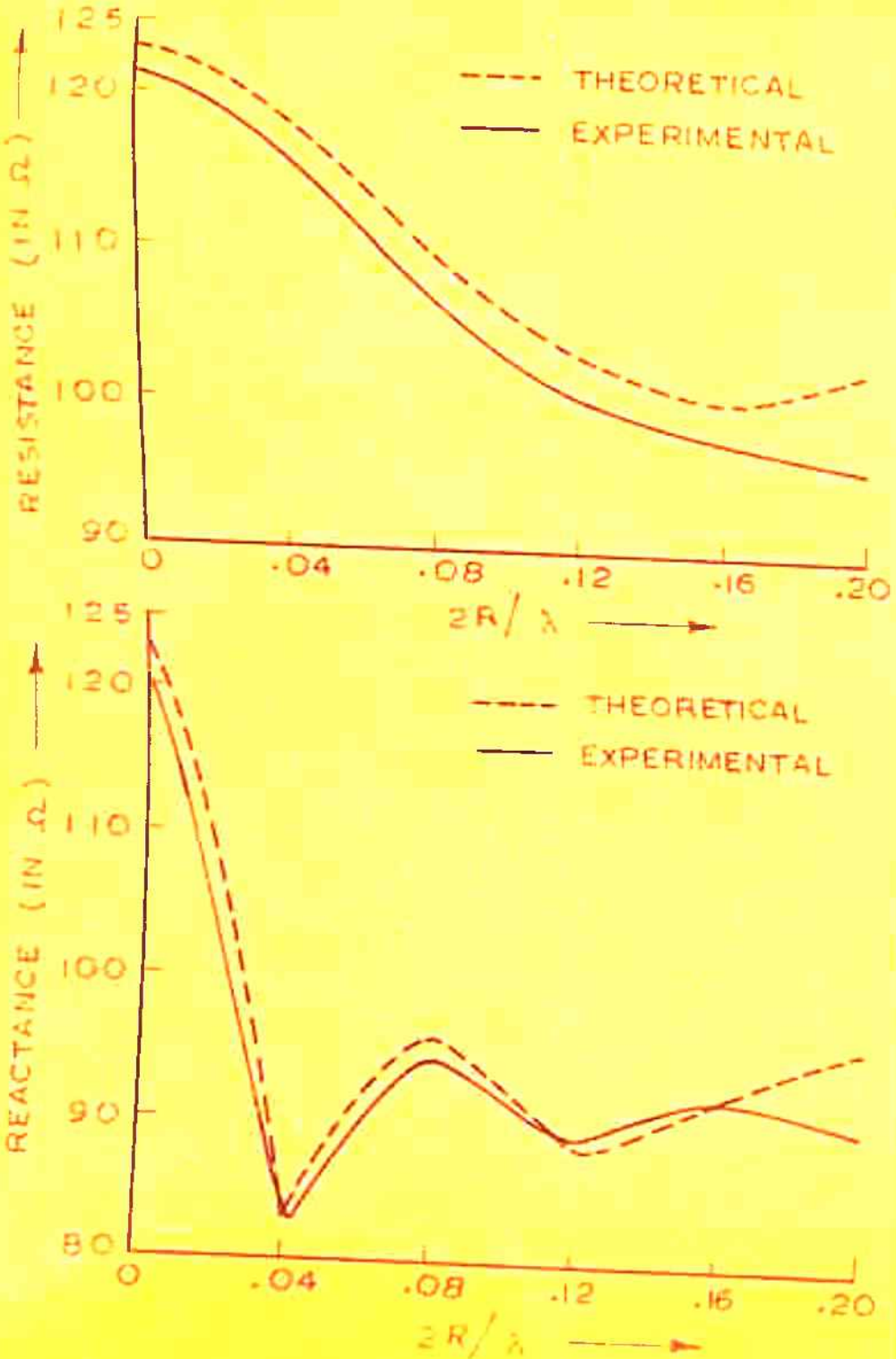
125
120
110
100
90
RESISTANCE (IN Ω)
THEORETICAL
EXPERIMENTAL
0
.04
.08
.12
.16
.20
2R/λ
125
120
110
100
90
80
REACTANCE (IN Ω)
THEORETICAL
EXPERIMENTAL
0
.04
.08
.12
.16
.20
2R/λ

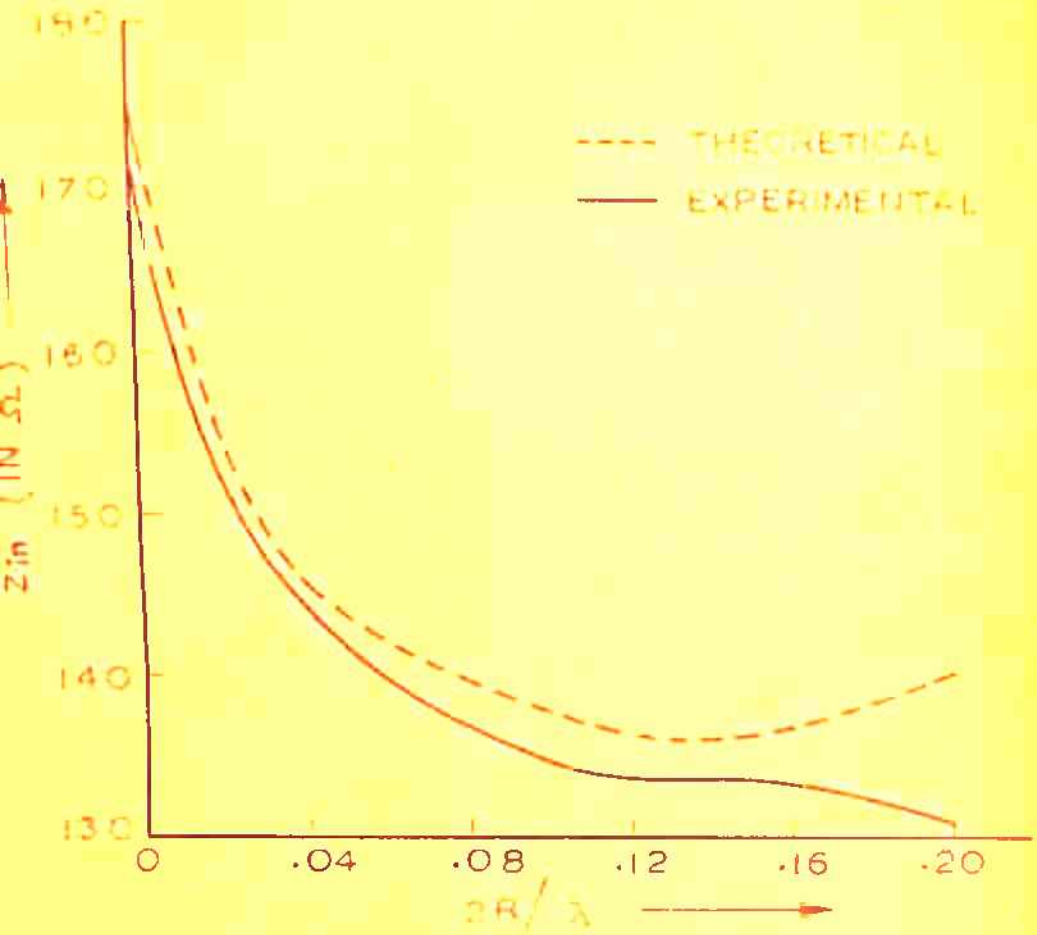

FIG. 3.3 EXPERIMENTAL AND THEORETICAL CURVES FOR TOTAL RESISTANCE, TOTAL REACTANCE AND INPUT IMPEDANCE.

TABLE - 3.2

Feed Point Displacement $2R/\lambda$	Resistance (in ohms)	Reactance (in ohms)	Impedance (in ohms)
0.0	123.0	123.0	174.1
0.04	119.0	83.0	145.5
0.08	110.0	96.0	140.0
0.12	103.5	88.5	136.5
0.16	100.5	92.0	136.7
0.20	102.5	95.5	140.5

§ 3.4 DISCUSSION AND CONCLUSION

It can be seen from the theoretical and experimental curves given in fig.(3.3) that the discrepancy between theoretical and experimental results starts after $\frac{2R}{\lambda} = 0.16$. It may be due to the fact that the constant C_1 in the solution of the wave equation is determined assuming the scalar potential V_o maintained across the gap to be constant along the line and δ function generator is applied to describe this potential. However, when the displacement of the feed points is considered, the scalar potential ϕ, there, is no more a continuous function and

one has to consider the proper distribution of the scalar potential. Nevertheless, the theoretical and experimental results agree reasonably good upto $\frac{2R}{\lambda} = 0.16$. Beyond this value of displacement, the more accurate results could be obtained by determining the actual form of the field distribution at the feed gap.

C H A P T E R - 4

INPUT IMPEDANCE, RADIATION RESISTANCE AND GAIN OF LOG-PERIODIC DIPOLE ANTENNA

§ 4.1 INTRODUCTION

Monser (23) reported some experimental results for the radiation pattern, input impedance and gain of the log-periodic dipole antenna with separation angle ϕ [fig.(1.3)] between the two halves not equal to zero. It was shown that the input impedance and gain increase with the increase in separation angle ϕ and radiation resistance decreases with the increase of ϕ. However, no theoretical explanation was given to accout for these observed variations in gain, radiation resistance and input impedance. Kosta (18) put forward the theory of log-periodic dipole antenna with $\phi \neq 0^{\circ}$ to explain Monser's experimental results. LPDA was analysed by him applying linear antenna array concept. In this chapter his results for radiation pattern have been used to explain theoretically few more parameters like input impedance, radiation resistance and gain of non-planar ($\phi \neq 0^{\circ}$) log-periodic dipole antenna. Theoretical results have been given which explain successfully the experimentally observed variations. In addition, experimental measurements have also been carried out for input impedance and gain of this antenna.

§ 4.2 ANALYSIS

4.2.1 Radiation Resistance: An approximate expression for the far field radiation pattern of the log periodic dipole

antenna with $\phi \neq 0^{\circ}$ has been given by Kosta (18) as

$$E(\theta, \phi) = \frac{j\,120\, I_m\, e^{j(\omega t - \frac{r_o}{c})}}{r_o}$$

$$\left[\cos\left\{ \frac{\pi}{2} \cos\theta + \beta R_n \sin\frac{\psi}{2} \sin\theta \sin\phi \right\} \right.$$

$$\left. + \cos\theta \sin\left\{\beta R_n \sin\frac{\psi}{2} \sin\theta \sin\phi\right\}\right] / \sin\theta$$

$$\left[\frac{\cos\left\{ \frac{N \pi R_n}{\lambda} \cos\frac{\psi}{2} (1 - \tau)(\sin\theta \cos\phi - 1)\right\}}{\cos\left\{ \frac{\pi R_n}{\lambda} \cos(\frac{\psi}{2})(1 - \tau)(\sin\theta \cos\phi - 1)\right\}} \right]$$

$$\sin\left\{ \frac{\pi R_n}{\lambda} \cos\frac{\psi}{2} \left(\frac{1}{\tau} - 1 \right) \sin\theta \cos\phi \right\} \qquad (4.1)$$

where τ = scaling factor

N = total number of dipoles in the active region

R_n = distance of the Nth dipole from the apex of the LPD antenna

In Kraus (25), the expression for the total radiated power is given by

$$W = \frac{1}{2} \sqrt{(\mu_o/\epsilon_o)} \int_0^{2\pi} \int_0^{\pi} |H_\phi|^2 r_o^2 \sin\theta \, d\theta \, d\phi \qquad (4.2)$$

where μ_o = free space permeability

ϵ_o = free space permittivity

$|H_\phi|$ = absolute value of magnetic field

r_o = distance of the far point from the dipole centre.

Using the relation

$$|H_\phi| = |E(\theta , \phi)|/\eta_o , \quad \eta_o = 120\pi$$

in equation (4.2), total power radiated becomes

$$W = \frac{60\, I_m^2}{\pi} \int_0^{2\pi} \int_0^{\pi} |f(\theta , \phi)|^2 \sin\theta \, d\theta \, d\phi \qquad (4.3)$$

where $|E(\theta , \phi)| = \frac{120\, I_m}{r_o} |f(\theta , \phi)|$

Equating equation (4.3) to $\frac{I_m^2 R_o}{2}$, the expression for radiation resistance is obtained as

$$R_o = \frac{120}{\pi} \int_0^{2\pi} \int_0^{\pi} |f(\theta , \phi)|^2 \sin\theta \, d\theta \, d\phi \qquad (4.4)$$

The integral involved in equation (4.4) has been solved by the method of Numerical Integration. Theoretical calculations were carried out for the following data:

α = 35°

r = 0.888

N = 3

λ = 30 cms.

ϕ = 0°, 10°, 20°, 30° and 40°

Results are given in table (4.1) and shown graphically in fig.(4.1).

FIG. 4.1. RADIATION RESISTANCE AS FUNCTION OF SEPERATION ANGLE Ψ

TABLE - 4.1

Angle ϕ	Radiation Resistance R_o (in ohms)
0^o	29.35
10^o	27.71
20^o	24.56
30^o	20.46
40^o	16.54

4.2.2 Input Impedance: From the periodically loaded line analysis (2.9) the phase shift constant β of the loaded line is given as

$$\cos \beta d = \cos Kd \mp \frac{Z_o}{2X} \sin Kd \qquad (4.5)$$

where

$K = \frac{2\pi}{\lambda}$ = phase shift constant of the unloaded line

λ = free space wavelength

X = reactance of the dipole

d = period between two successive dipoles

$Z_o = 276 \log(\frac{D}{r})$

= characteristic impedance of the unloaded transmission line

D = centre to centre spacing of the transmission line

r = radius of the line.

The short dipole region of the log-periodic dipole antenna (LPDA), fig.(4.2a), can be considered, to a first order approximation, as a periodically loaded transmission line loaded with dipoles shown in fig.(4.2b). Now, if $Z_A = jX_A$, $Z_B = jX_B = jX$ and X_A is negligible in comparison to X, then using the approximations for sine and cosine functions and treating the short dipole region (dipole lengths $< \lambda/2$) as a slow wave structure, equation (4.5) transforms into

$$\beta = K\sqrt{(1 + \frac{Z_o}{KXd})} \qquad (4.6)$$

Following Carrel's (28) method, the characteristic impedance of the loaded line (also the input impedance) is obtained as

$$Z_{in} = \frac{Z_o}{\sqrt{(1 + \frac{Z_o}{KXd})}} \qquad (4.7)$$

From the figures (4.2a) and (4.2b), the average feed point displacement of the first two dipoles is

$$D = \frac{2(R_1 + R_2)\sin\frac{\phi}{2}}{2} \qquad (4.8)$$

Corresponding period d is given by

$$d = (R_2 - R_1)\cos\frac{\phi}{2} \qquad (4.9)$$

Z_o can be calculated from equation

$$Z_o = 276 \log\frac{D}{r}$$

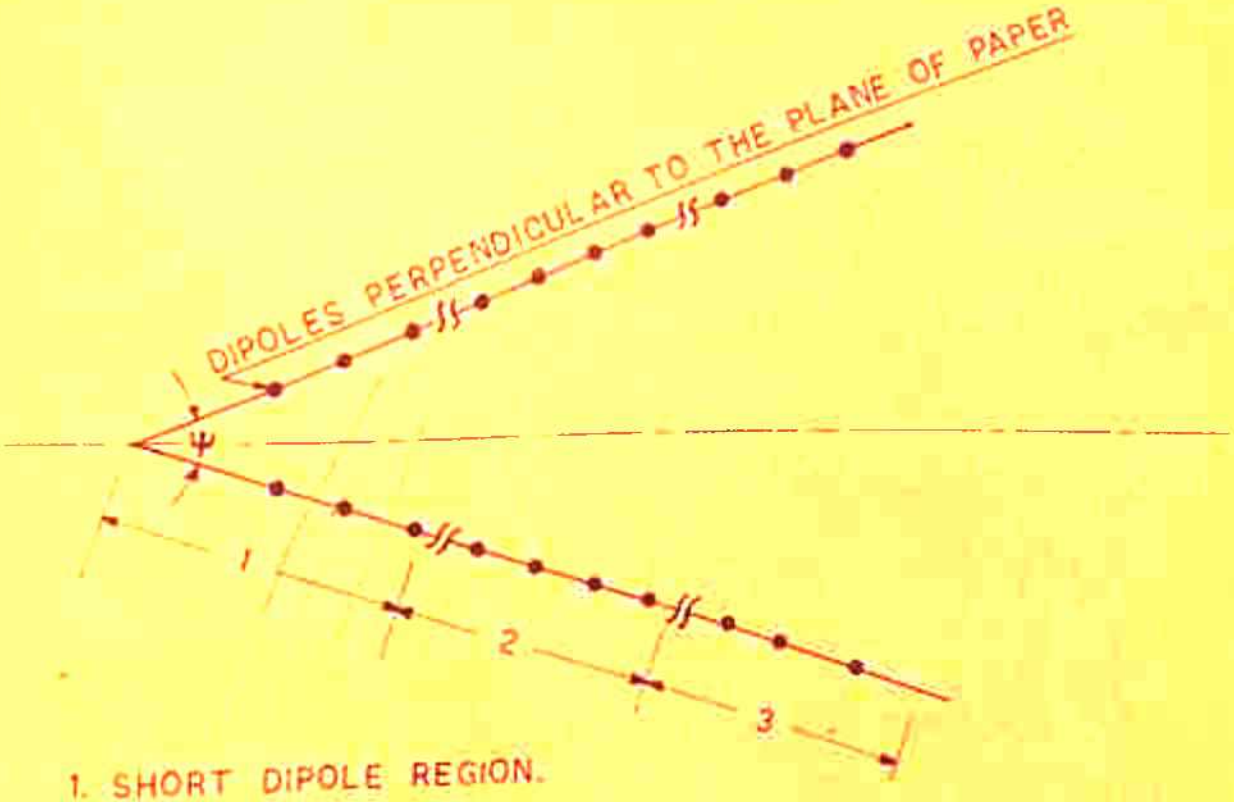

1. SHORT DIPOLE REGION.
2. ACTIVE REGION
3. UNEXCITED LONG DIPOLE REGION

FIG. (4·2a) TWO HALVES OF THE LPD ANTENNA

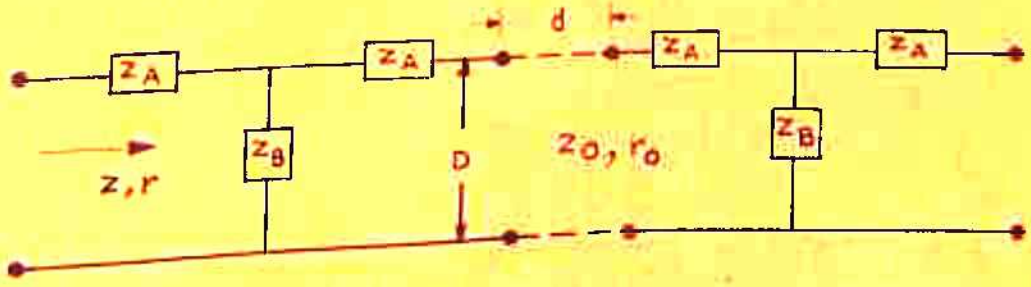

FIG. (4·2b) EQUIVALENT PERIODICALLY LOADED TRANSMISSION LINE.

Using the value of D from equation (4.8) Z_{in} can be obtained from equation (4.7) by using the value Z_o so calculated.

Theoretical calculations were carried out using the following data:

$\alpha = 35^o$, $r = 0.888$

$\lambda = 30$ cms , $\phi = 10^o, 20^o, 30^o, 40^o, 50^o$ and 60^o

$R_1 = 7.534$ cms, $R_2 = 8.559$ cms.

Average dipole lengths of two short dipoles = 2.55 cms.

Radius of the feeder line wire r = 0.3 cm.

The value of X for the average length of the first two dipoles was found from the curves given in Jorden (30). Results are given in table (4.2). Variation of Z_{in} with ϕ is shown graphically in fig.(4.3)

Table - 4.2

Angle ϕ	Input Impedance Z_{in} (in ohms)
10^o	116.1
20^o	148.3
30^o	163.7
40^o	172.6
50^o	178.1
60^o	180.2

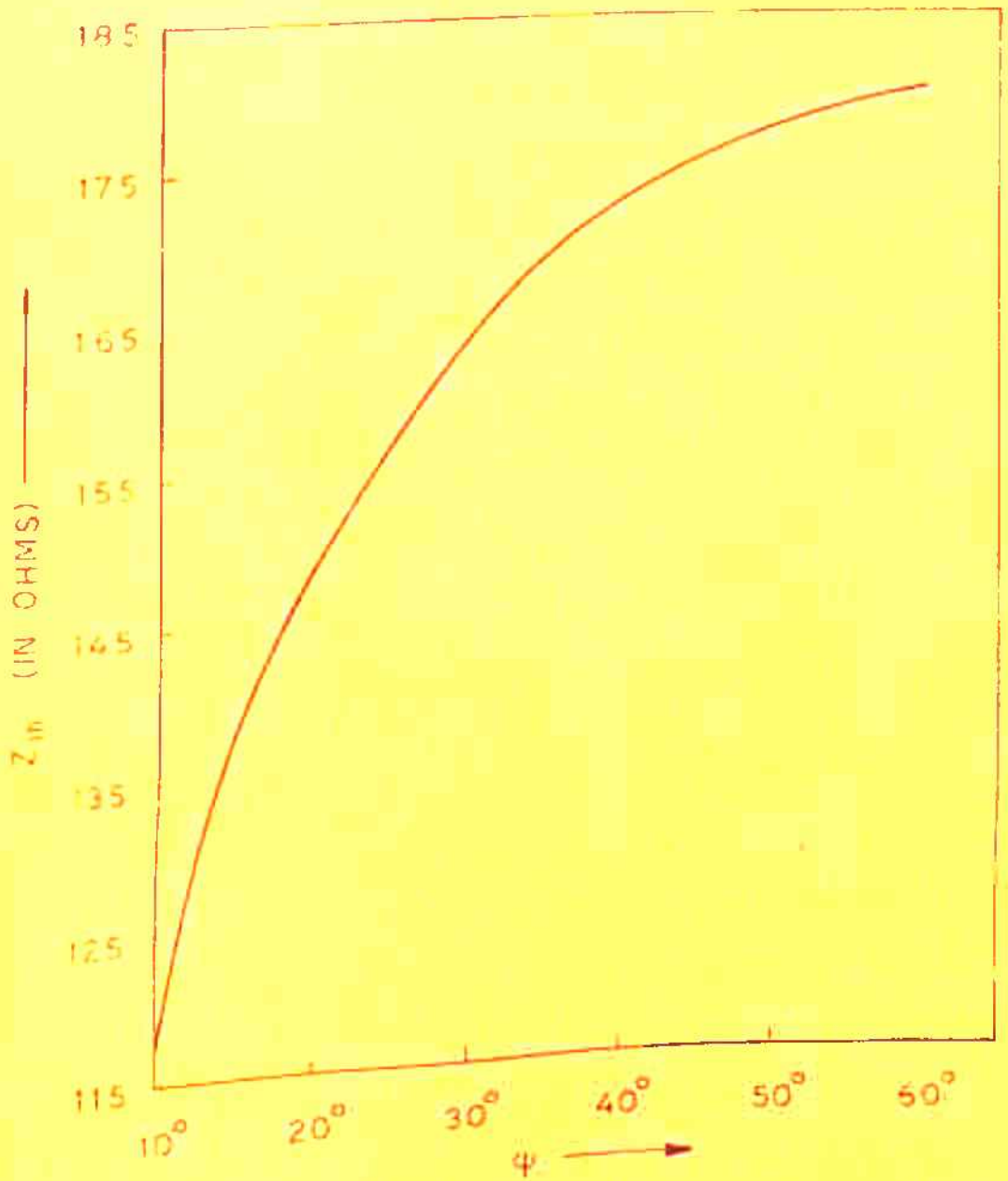

FIG. 4·3. INPUT IMPEDANCE (Z_{in}) AS FUNCTION OF SEPERATION ANGLE Ψ

4.2.3 Power Gain and Effective Aperture:- Directivity D is defined as

$$D = kG \qquad (4.10)$$

where k is the efficiency factor (coming due to losses in the antenna system) and G is the gain. The relation given by equation (4.10) also holds good for power gain if the losses in the antenna system are negligible, i.e. k = 1. However, most of the broad band antennas are designed to have very small loss as compared to the other antennas. Hence neglecting the losses, power gain is given by

$$G = D \qquad (4.11)$$

An approximate formula for directivity is

$$D = 10 \log\left(\frac{41253}{\theta_E \, \theta_H}\right) \qquad (4.12)$$

where θ_E = 3 dB beam width of E-plane pattern.

θ_H = 3 dB beam width of H-plane pattern.

Hence power gain is also given by equation (4.12)

θ_E and θ_H can be obtained from the E and H-plane patterns. Calculations were carried out for the parameters given in section (4.1). Table - 4.3 shows the E and H-plane 3dB beam widths and also the power gain results calculated from these values of θ_E and θ_H for various values of ϕ. A graphical representation of the results of power gain tabulated in table 4.3 is shown in fig.(4.4).

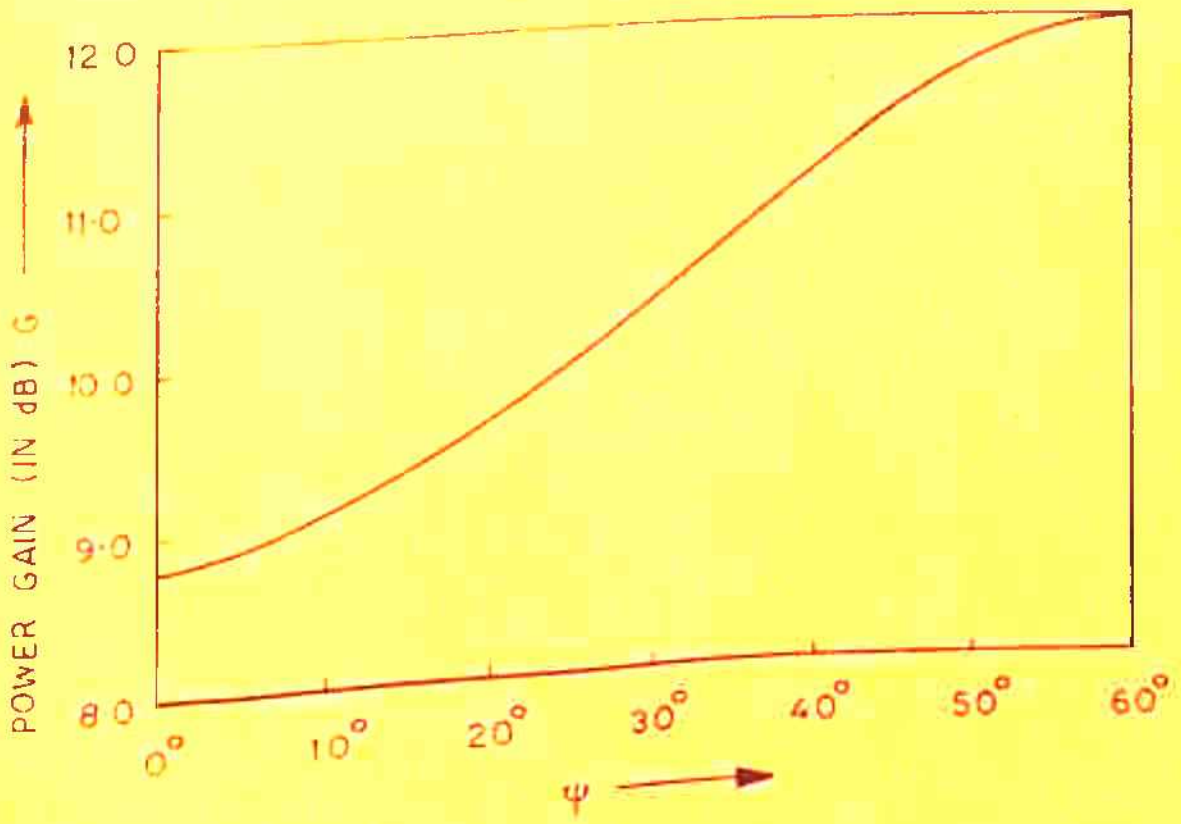

FIG. 4·4. POWER GAIN VS SEPERATION ANGLE Ψ

Effective aperture can be calculated from the power gain values given by equation (4.12). Results so calculated are given in table - 4.4 and shown graphically in fig.(4.5).

TABLE - 4.3

Separation Angle ϕ	3 dB Beam Width		Power Gain G (in dB)
	E - Plane	H - Plane	
0^o	60^o	90^o	8.83
10^o	60^o	84^o	9.13
20^o	60^o	74^o	9.68
30^o	60^o	66^o	10.18
40^o	60^o	54^o	11.05
50^o	60^o	50^o	11.75
60^o	60^o	47^o	12.0

§ 4.3 EXPERIMENTAL VERIFICATION

4.3.1 Design Considerations for the LPD Antenna: There is no theoretical formulation upon which the design of LPDA is based. The design has to be carried out on logical experimental methods. The design data for fabrication of the antenna system used for experimental study in this chapter is taken from the investigations of Carrel (28). Carrel in his investigations has shown

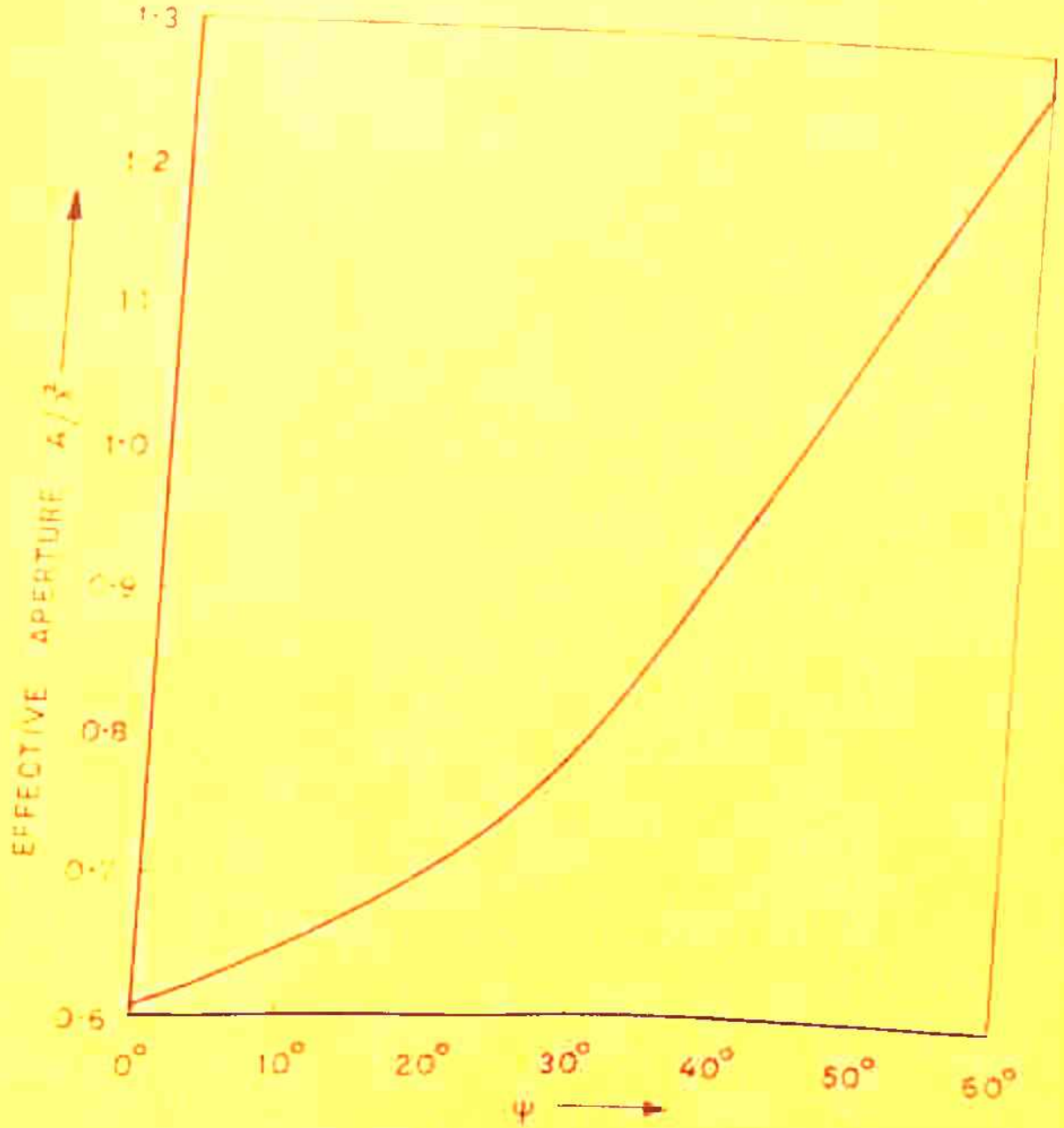

FIG. 4·5. EFFECTIVE APERTURE VS SEPERATION ANGLE Ψ

TABLE - 4.4

Seperation Angle ϕ	Effective Aperture A/λ^2
0^0	0.611
10^0	0.647
20^0	0.7006
30^0	0.7962
40^0	0.9469
50^0	1.125
60^0	1.262

the variation of electrical parameters of the antenna under consideration with various important design parameters like, τ , α and σ . After a careful examination of these curves a suitable set of parameters were chosen for fabrication. Details of the design procedure is given in appendix - 1. A pyramidal LPD antenna [fig.(4.6)] was designed to meet the following requirements:

Directive gain = ~~7.5~~ dB

Band width ratio = 1.5 between the lowest and the highest frequency

Input impedance = 75 ohms

λ_{max} = 100 cms

τ = 0.9

α = 25^0

N = 19

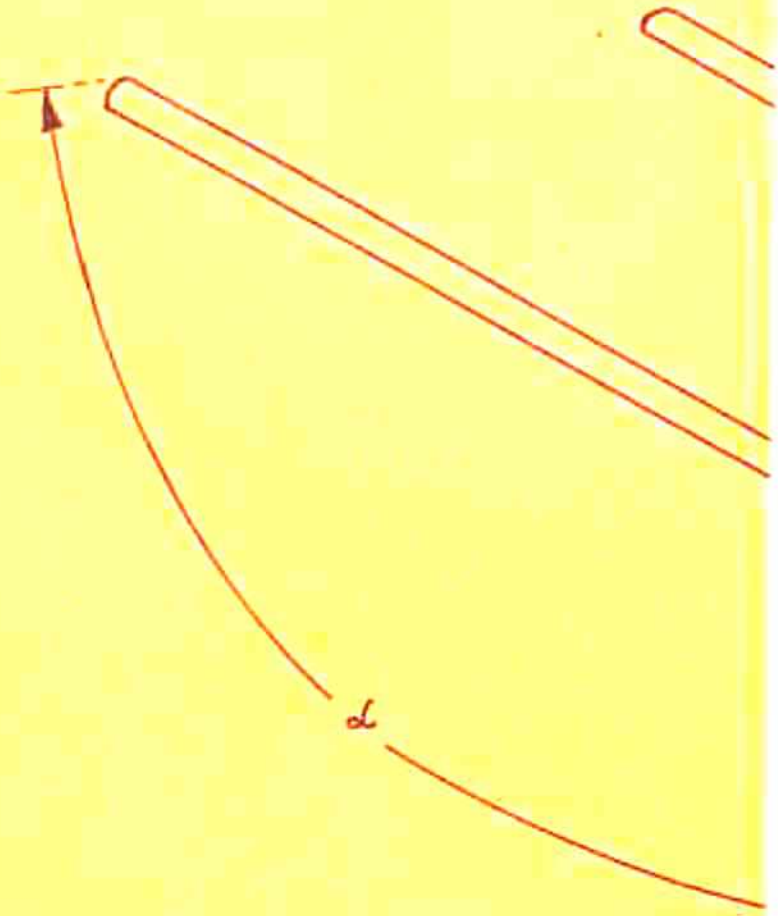

FIG. 4.6.ONE

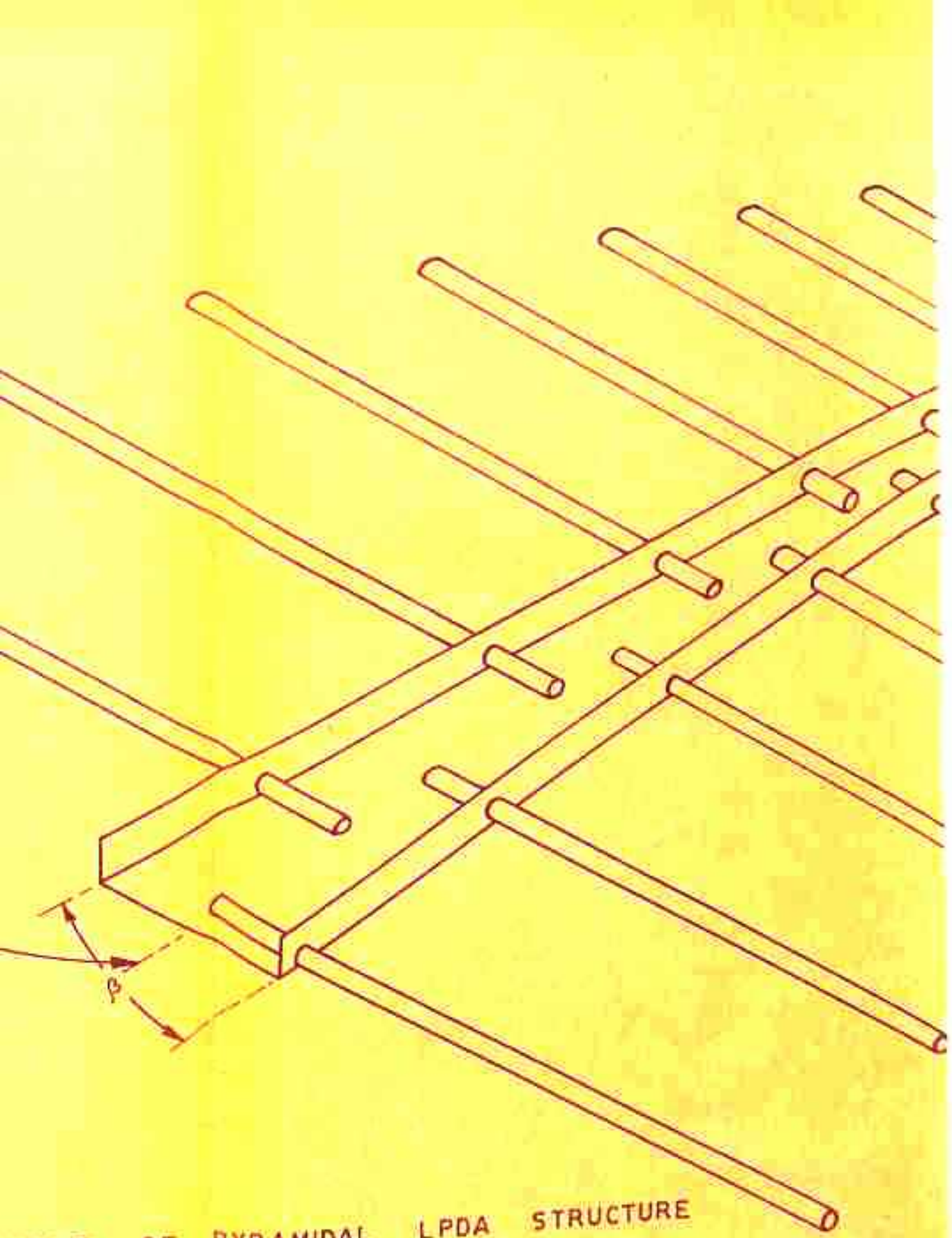

HALF OF PYRAMIDAL LPDA STRUCTURE

Relative boom length = 0.46

First element on low frequency side = $\frac{\lambda_{max}}{4}$

4.3.2 Measurements

(i) Input Impedance: The method employed for the measurement of input impedance has been described in chapter - 3 (section 3.3). The set up remains the same. However, the displaced dipole configuration is now replaced by the LPDA under investigation. Plots for VSWR and the input impedance have been shown in fig.(4.7) and given in table (4.5).

TABLE - 4.5

Separation Angle ϕ	VSWR	Input Impedance Z_{in} (in ohms)
0^o	1.5	-
10^o	2.4	80.1
20^o	2.6	110.05
30^o	2.3	123.3
40^o	2.6	132.2
50^o	2.7	137.5
60^o	2.3	140.0
70^o	2.0	135.1

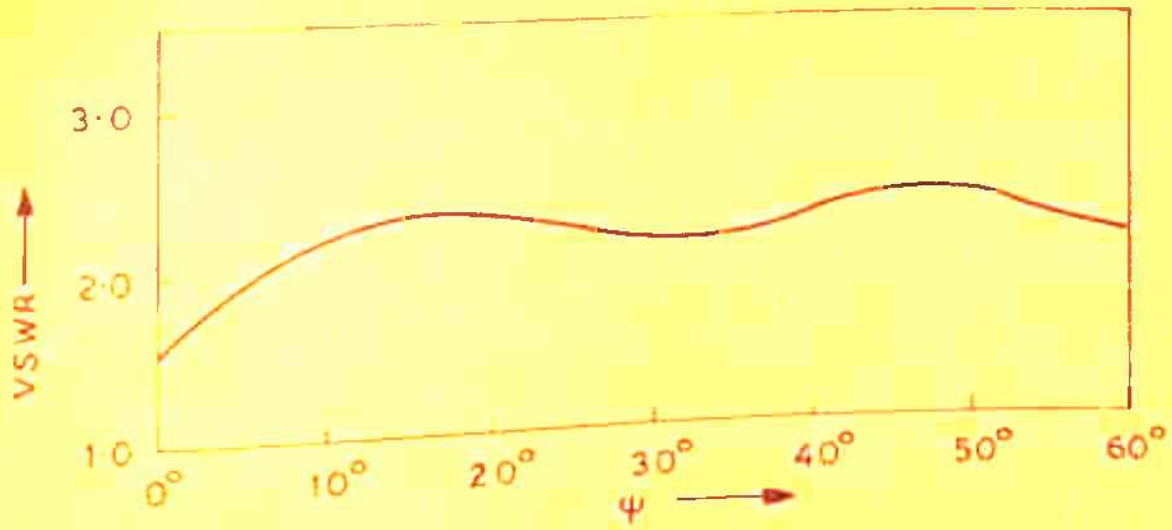

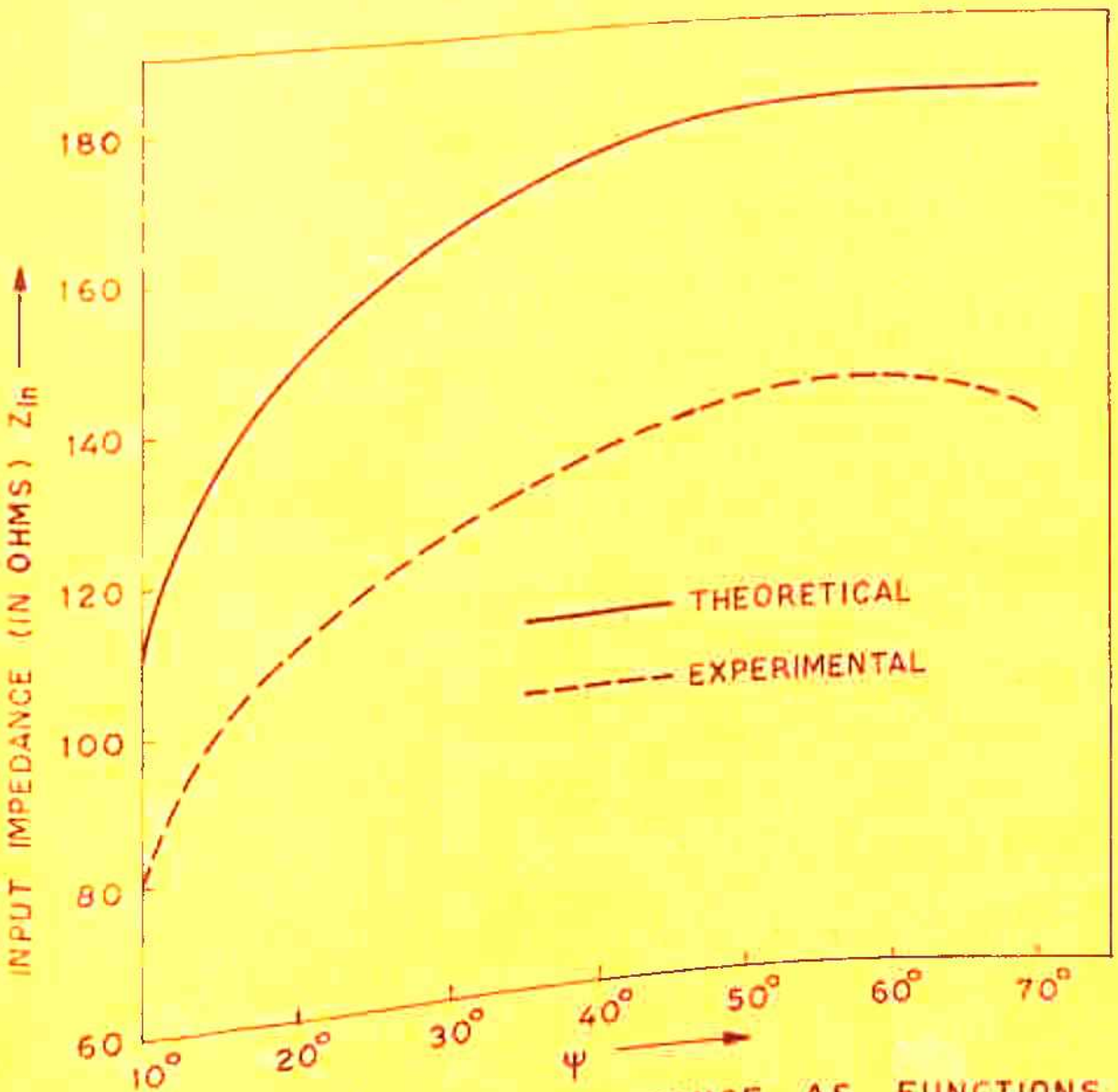

FIG. 4-7. VSWR AND INPUT IMPEDANCE AS FUNCTIONS OF SEPERATION ANGLE Ψ

(ii) Gain: The gain of an antenna is generally defined as the ratio of the maximum radiation intensity in a given direction to the maximum radiation intensity produced in the same direction by an isotropic antenna radiating the same total power. If this gain is defined in the direction of maximum radiation, then a measurement of this quantity gives a measure of directivity. It is well known that

$$D = KG \qquad G = KD \qquad (4.13)$$

where the symbols carry the usual meaning.

Usually the very sophisticated and the careful design of the most of the broad band antennas provides a basis to neglect the losses (which are actually very small).

To measure the gain of an antenna, a reference antenna whose gain is known, is used in place of an isotropic radiator. In the present investigation, a dipole antenna was used as the reference antenna. The set up is shown schematically in fig.(4.8). The LPD antenna was connected to the detector and oriented so that the indicator showed a maximum output P_m. Then this antenna was replaced by the reference dipole and was again oriented so that the indicator gives the maximum reading P_S. The power gain of the LPD antenna was then given by

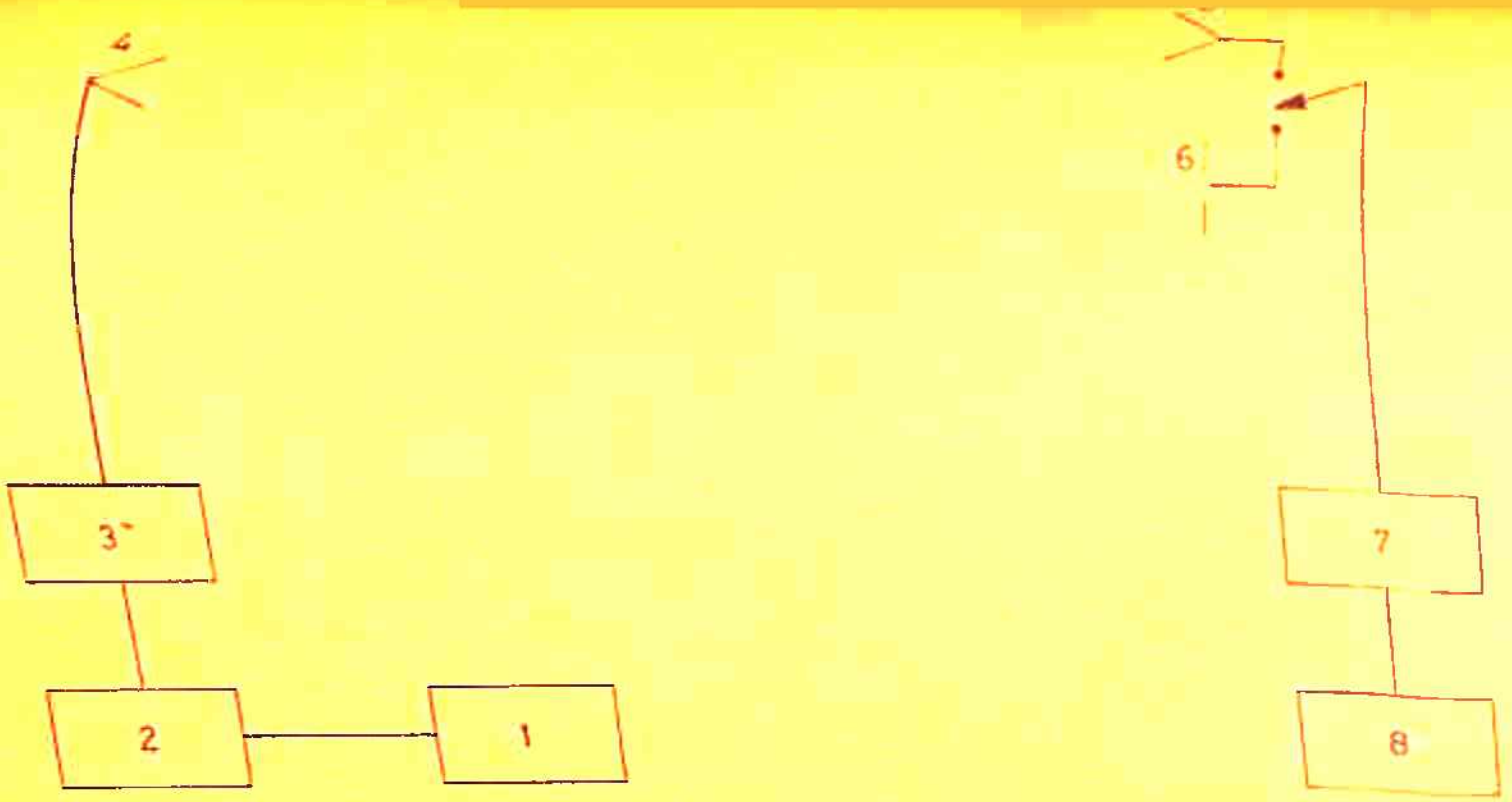

1 MODULATOR (TYPE 1214 – A)

2 G. R. UNIT OSCILLATOR (TYPE 1209 – B)

3 FILTER

4 TRANSMITTING ANTENNA

5 TEST ANTENNA

6 REFERENCE DIPOLE

7 DETECTOR

8 SWR METER (TYPE HP 415 – B)

FIG. 4·8. BLOCK DIAGRAM FOR GAIN MEASUREMENT.

$$G = \left(\frac{P_m}{P_S}\right) G_S \qquad (4.14)$$

where G_S is the gain of the standard dipole.

Above procedure was repeated for various values of separation angle ϕ. Results are given in table (4.6) and shown graphically in fig.(4.9). Measurements were taken at 600 Mc/S. Also, by equation (4.11), the directivity is same as the power gain.

TABLE - 4.6

Angle ϕ	Power Gain (in dB)
0^o	8.85
10^o	9.10
20^o	9.45
30^o	10.0
40^o	10.75
50^o	11.5
60^o	12.0

(iii) Effective Aperture: From the experimental values of power gain given in table (4.6) values of effective aperature were calculated using the expression given in equation (2.28). Results have been given in table (4.7) and plotted in figure (4.10).

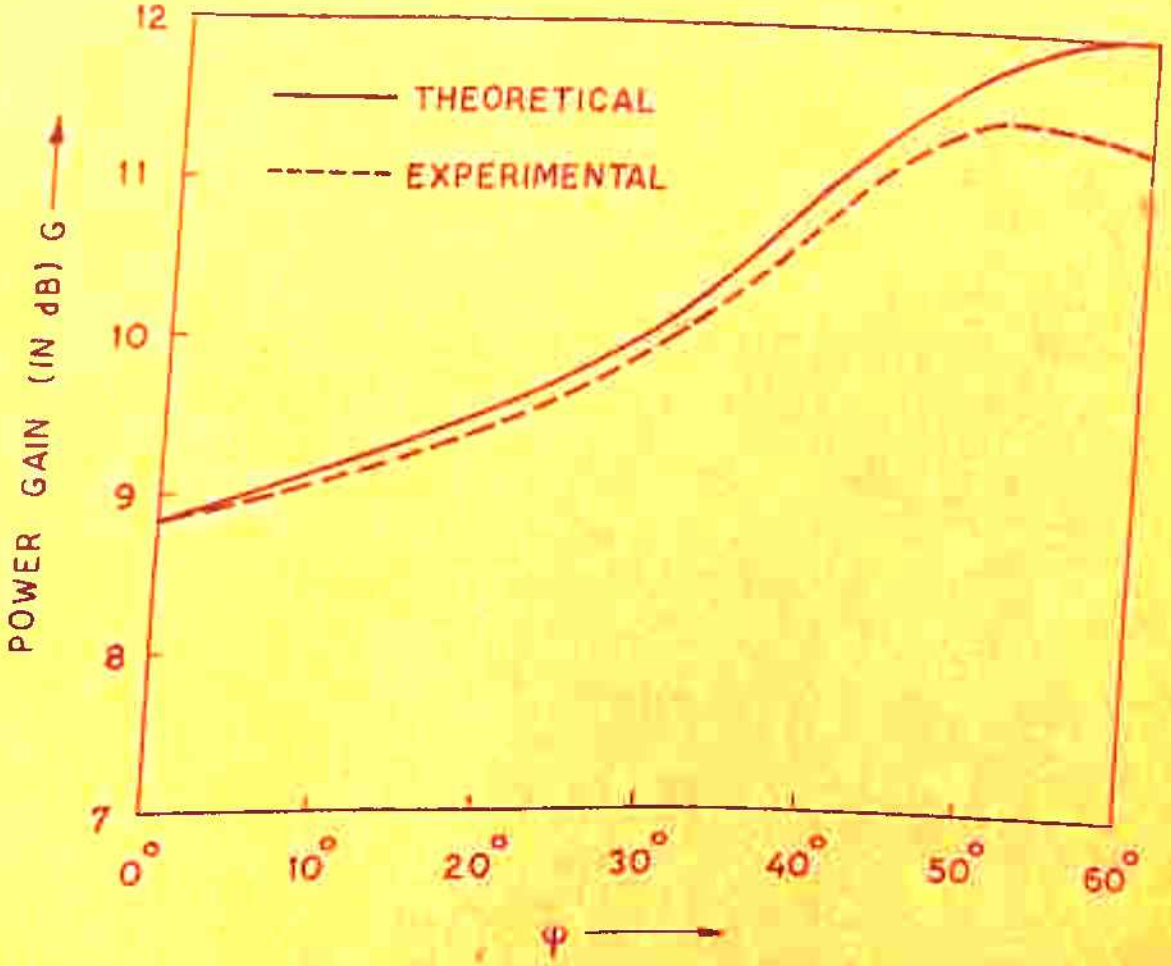

FIG. 4·9. POWER GAIN AS FUNCTION OF SEPERATION ANGLE ψ

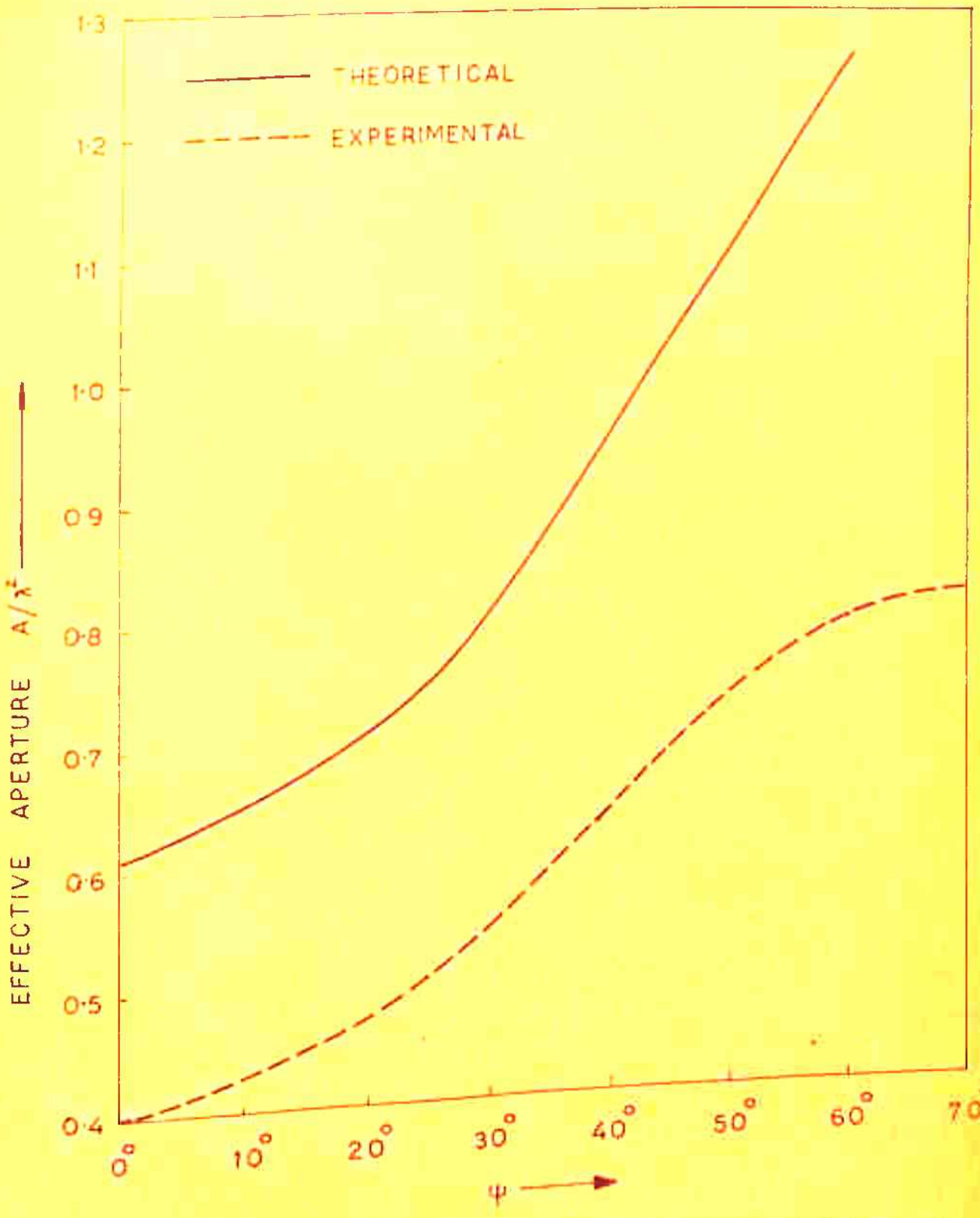

FIG. 4·10. EFFECTIVE APERTURE VS SEPERATION ANGLE Ψ

TABLE - 4.7

Seperation Angle ϕ	Effective Aperture A/λ^2
0^o	0.4
10^o	0.425
20^o	0.47
30^o	0.54
40^o	0.635
50^o	0.725
60^o	0.79
70^o	0.81

§ 4.4 CONCLUSIONS AND DISCUSSIONS

From fig.(4.1) it can be seen that the radiation resistance decreases as the separation angle ϕ increases which is a well known fact. Also fig.(4.4) shows similar sort of variation in power gain. However, the power gain measurements shown in fig.(4.9) shows some discrepancy between the theoretical and experimental results.

A theoretical variation of input impedance as a function of ϕ has been shown in fig.(4.3). Z_{in} gradually

increases with the increase in ϕ and becomes constant as ϕ approaches 60°. However, as shown by fig.(4.7), as ϕ is increased beyond 60°, Z_{in} starts decreasing. Thus it can be seen that the theoretical predictions contradict the experimental observations. The reason for such discrepancies could be that the far field expression given in equation (4.1) has been developed using the far field expression for an asymmetric dipole antenna with its feed points displaced transverse to its axis (first quantity in square brackets of equation 4.1). For larger displacements in feed points ($\frac{2R}{\lambda}$) the field in the gap becomes appreciable. However, for the sake of simplicity in analysis this field has been neglected as the consideration of this field in the gap requires complicated functions. Nevertheless, for smaller displacements, the results are in good agreement with the theoretical predictions. The LPD array consists of such displaced dipoles as its elements. The displacements in the feed points (displacement = $R_n \sin \frac{\psi}{2}$) becomes appreciable if ψ is increased beyond 60°. The theory, then ceases to be valid for the values of ϕ as large as above and consequently the results obtained in this way are very inaccurate.

Since both the radiation resistance and the gain have been calculated by using ($R_n \sin \frac{\psi}{2}$) as one of the

factors, hence the results obtained for these parameters will be inaccurate for values of ϕ beyond 60°. Hence the values of ϕ as high as 60° are usually avoided.

As may be seen from the figures (4.2a) and (4.2b), the LPD array has been considered as a periodically loaded tapered transmission line. For the sake of simplicity the tapered structure has been transformed to the equivalent periodically loaded transmission line with equivalent period d and the spacing between the lines D . These two quantities reach far from the actual values (the actual values mean the values of these quantities in tapered configuration) for larger values of ϕ and hence give inaccurate results.

C H A P T E R - 5

A NEW LOG PERIODIC STRUCTURE WITH ASYMMETRIC DIPOLE ELEMENTS

§ 5.1 INTRODUCTION

In chapter - 2 a generalised analysis was given for an asymmetric dipole antenna with arbitrary displacement of feed points. It was pointed out there that one of the configurations, namely, the transversely displaced system has got an important use in constructing a new log periodic structure [fig.(5.1)]. Present chapter has been devoted to the analysis of such a structure. Theoretical expressions for the far-field radiation pattern, radiation resistance, power gain and effective aperture have been developed. An expression has been derived to show the variation of input impedance with the seperation angle ϕ using the concept of periodically loaded line theory. In many applications where the conventional LPD antenna made of symmetric dipoles do not find its use, the structure suggested in this chapter will have its immense use. Specially, in aircraft tails, where the shape of this part requires the asymmetric nature of the antenna system, the LPD antenna made of asymmetric dipoles will be useful. The experimental verification of theoretical results have also been given in this chapter.

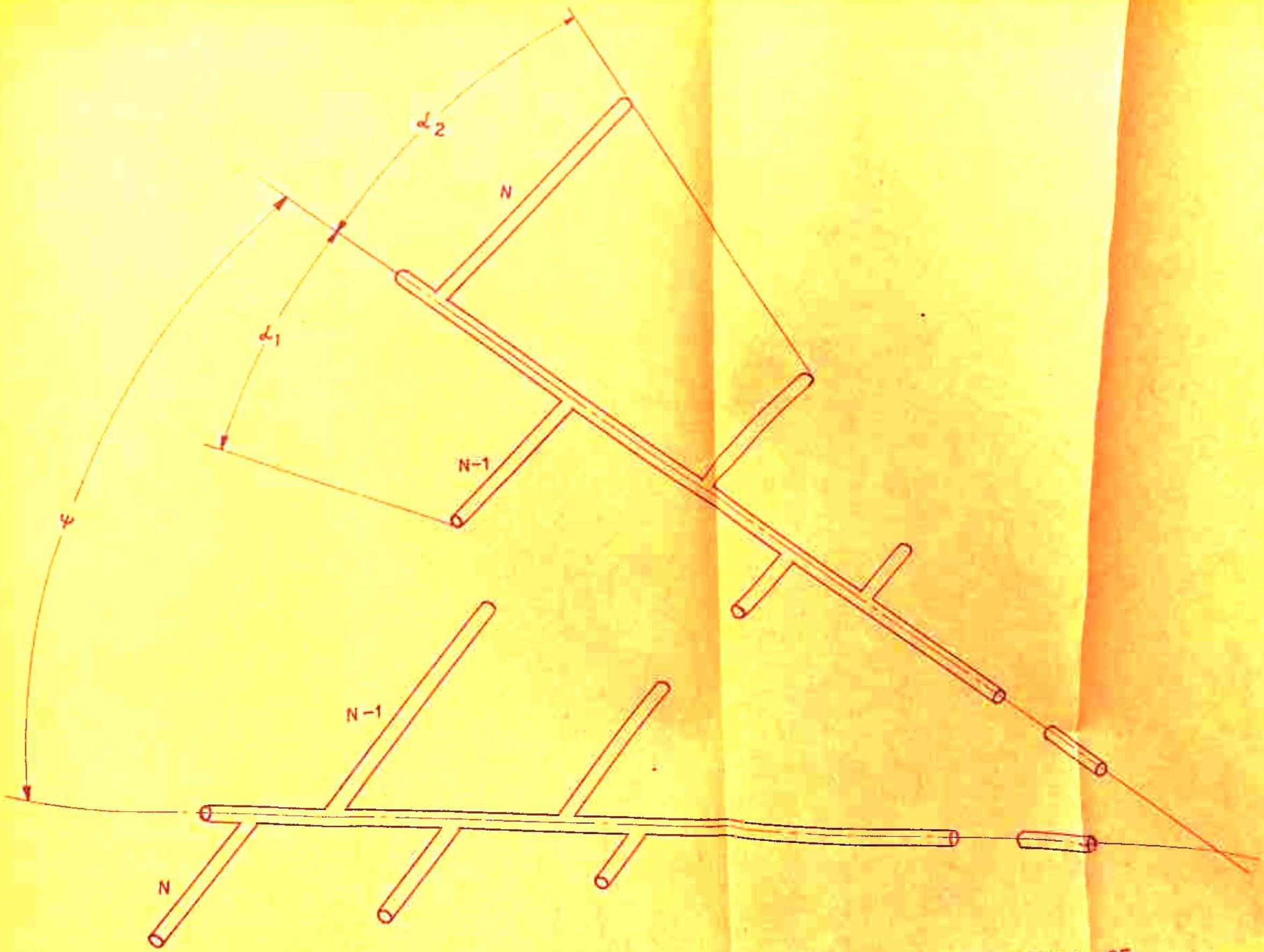

FIG.5·1. PARAMETER AND COORDINATE SYSTEM OF L P D STRUCTURE CONSISTING OF ASYMMETRIC DIPOLE ELEMENTS.

§ 5.2 MATHEMATICAL ANALYSIS

5.2.1 Far field Radiation Pattern: The expression for the far-field radiation pattern of the LPD antenna consisting of half wave centre fed dipoles with $\phi \neq 0^{\circ}$ is given by (18)

$$E(\theta, \phi) = \frac{j\,120\, I_m\, e^{j(\omega t - r_o/c)}}{r_o \sin\theta} \left[\cos\left\{\frac{\pi}{2}\cos\theta + \beta R_n \sin\frac{\psi}{2}\sin\theta\sin\phi\right\} + \cos\theta \sin\left\{\beta R_n \sin\frac{\psi}{2}\sin\theta\sin\phi\right\}\right] \times \left[\frac{\cos\left\{\frac{N\pi R_n}{\lambda}(1-\tau)\cos\frac{\psi}{2}(\sin\theta\cos\phi - 1)\right\}}{\cos\left\{\frac{\pi R_n}{\lambda}(1-\tau)\cos\frac{\psi}{2}(\sin\theta\cos\phi - 1)\right\}}\right] \times \left[\sin\left\{\frac{\pi R_n}{\lambda}\left(\frac{1}{\tau} - 1\right)\sin\theta\cos\phi\cos\frac{\psi}{2}\right\}\right] \qquad (5.1)$$

where N = total No. of dipoles in active region

τ = scaling factor

R_n = distance of Nth dipole from the apex of the LPD antenna

$= \frac{\lambda}{4}\cot\left(\frac{\alpha}{2}\right)$

α = angle subtended by the tips of the dipoles at the apex

ψ = separation angle between the two halves

β = phase shift constant

In equation (5.1), the first term in square brackets is the far-field pattern of a half wave symmetric dipole antenna with feed points displaced transverse to the axis of the dipole. The new configuration results when this term is replaced by the far-field pattern expression of the asymmetrically driven dipole with its feed points displaced transverse to its axis. The far-field expression for such a displaced configuration of the asymmetrically driven dipole is given by (equation 2.17, chapter - 2);

$$E_{TR}(\theta,\phi) = \frac{j30[I]}{r_o \sin\theta}\Bigg[\sin(\beta h_2)\{e^{j\beta(R_n \sin\frac{\phi}{2} U_1 + h_1\cos\theta)} - e^{j\beta R_n \sin\frac{\phi}{2} U_1}[j\cos\theta\sin(\beta h_1) + \cos(\beta h_1)]\} + \sin(\beta h_1)\{e^{-j\beta(R_n \sin\frac{\phi}{2} U_1 + h_2\cos\theta)} - e^{-j\beta R_n \sin\frac{\phi}{2}}[j\cos\theta\sin(\beta h_2) - \cos(\beta h_2)]\}\Bigg] \qquad (5.2)$$

where $[I] = I_m e^{j(\omega t - r_o/c)}$.

The expression in equation (5.2) has been derived by putting $U_1 = U_2 = U_1$ and $R_1 = R_2 = R_n \sin\frac{\phi}{2}$ which are appropriate to the case of an LPD antenna with $\phi \neq 0^o$.

In this case $R_n = \frac{\lambda}{4} \cot\left(\frac{\alpha_1}{2}\right)$ as one of the arms (the upper limb of the asymmetric dipole) has been assigned a constant value of $\lambda/4$ for convenience and the length of the lower half has been varied to get the effect of varying the asymmetry ratio AR. However, the expression is general and R_n may be asigned any value.

Since the 2nd term in square brackets of equation (5.1) has been derived assuming an array of point sources, this term is applicable to the new structure as well. Also, the last term remains unchanged, as this term represents the effect of the unexcited longer dipoles which act as parasitic reflector. Taking into consideration above facts, the final expression for the LPD antenna consisting of asymmetric dipoles is given by

$$E(\theta, \phi) = 2[P] \cdot [Q] \cdot [S] \qquad (5.3)$$

where $P = E_{TR}$

$$Q = \frac{\cos\left[\frac{\pi R_n}{\lambda}(1-\tau)\cos\frac{\phi}{2}(\sin\theta\cos\phi - 1)\right]}{\cos\left[\frac{\pi R_n}{\lambda}(1-\tau)\cos\frac{\phi}{2}(\sin\theta\cos\phi - 1)\right]}$$

$$S = \sin\left[\frac{\pi R_n}{\lambda}\left(\frac{1}{\tau} - 1\right)\sin\theta\cos\phi\cos\frac{\phi}{2}\right]$$

The factor 2 appears in equation (5.3) in deriving S. The factor P for the application to the asymmetric LPD antenna is obtained by putting $U_1 = \sin\theta$ in the general expression for U_1 (equation 2.4, chapter - 2,

sec. 2.2.1). It should be noted here that the expression (5.3) is valid for the active region of the LPD antenna.

Theoretical calculations for the far-field radiation pattern have been carried out using the following data:

$\alpha_1 = 17.5^\circ$

$r = 0.888$

$\phi = 0^\circ, 20^\circ, 30^\circ, 40^\circ$ and 60°.

Plots of the E and H-plane patterns have been shown in figs.(5.2a - 5.2g) for various values of ϕ and asymmetry ratio $AR = h_1/h_2$. Results have been given in table - 5.1 .

TABLE - 5.1

Asymmetry Ratio AR	Separation Angle ϕ	3 dB Beam width	
		E-Plane	H-Plane
0.694	0°	60°	90°
0.616	20°	60°	72°
	40°	60°	52°
	60°	60°	38°
0.50	0°	60°	88°
	20°	60°	88°
	40°	60°	88°
	60°	60°	88°
0.42	0°	93°	88°
	20°	93°	115°
	30°	96°	117°
	40°	113.5°	120°

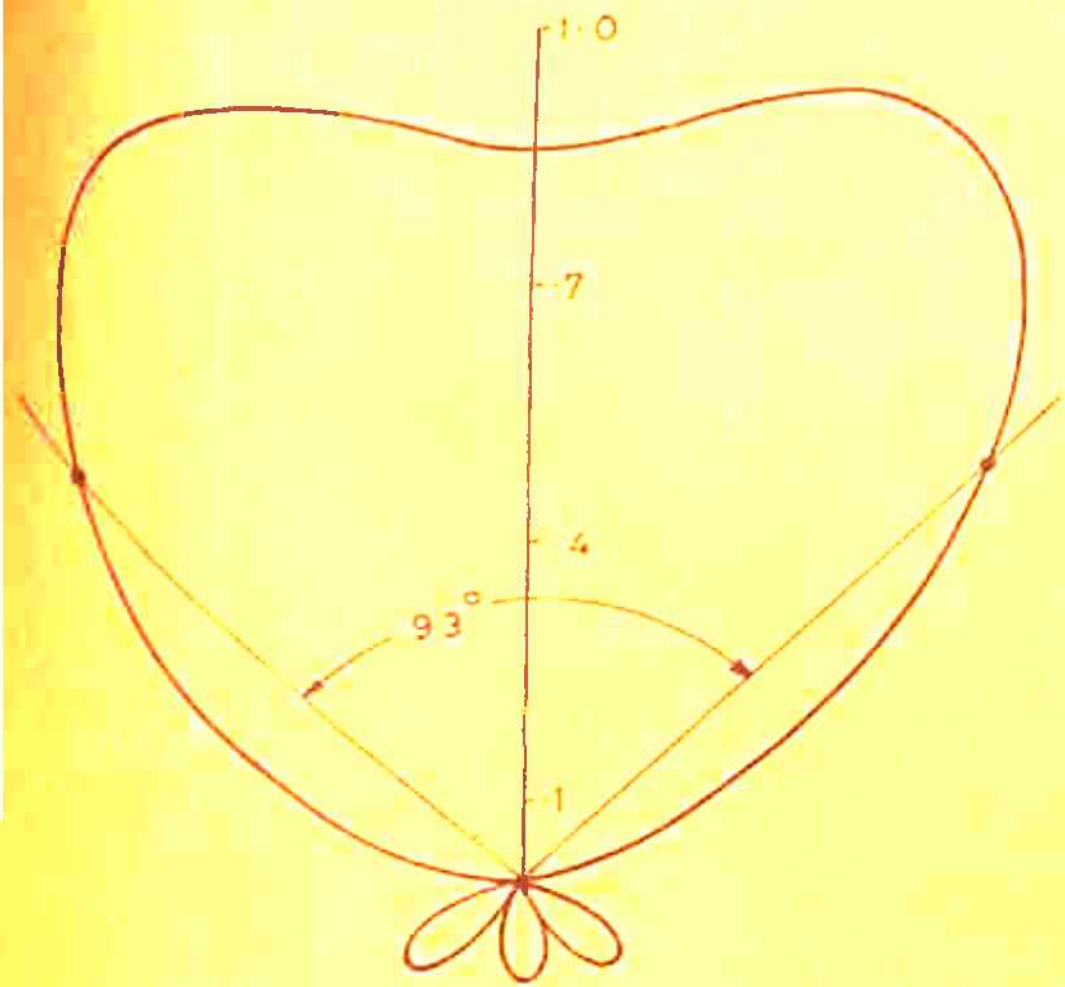

$(\psi = 0°, 20°)$

FIG. (5·2 a)

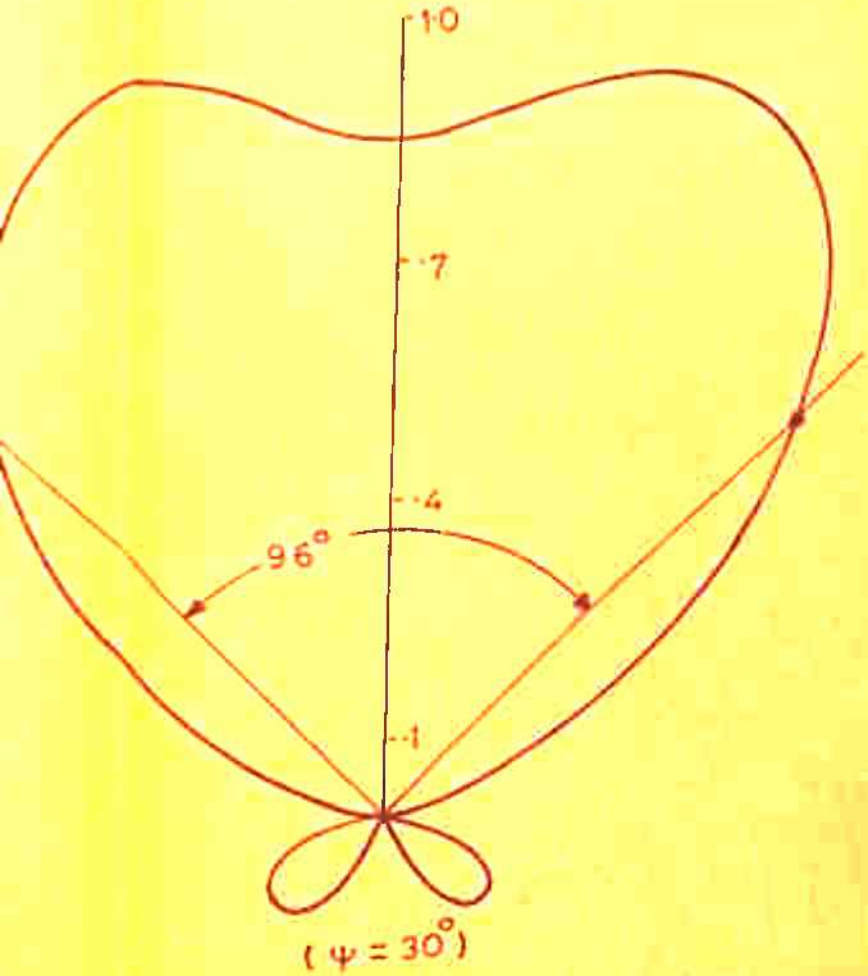

E — PLANE PATTERN FOR ASYMMETRY RATIO

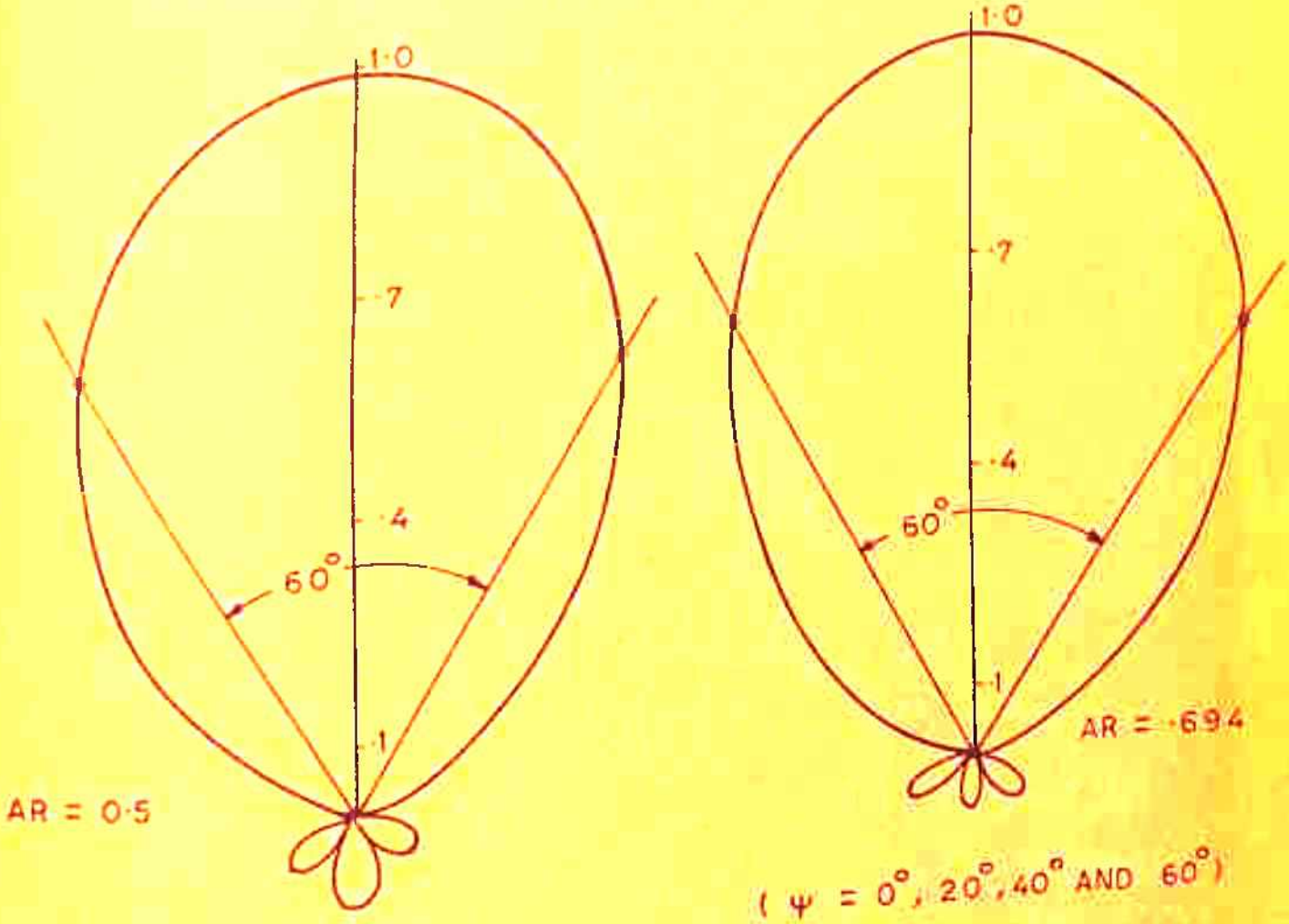

FIG. (5·2b) E – PLANE PATTERN FOR ASYMMETRY RATIO ·5 AND ·694.

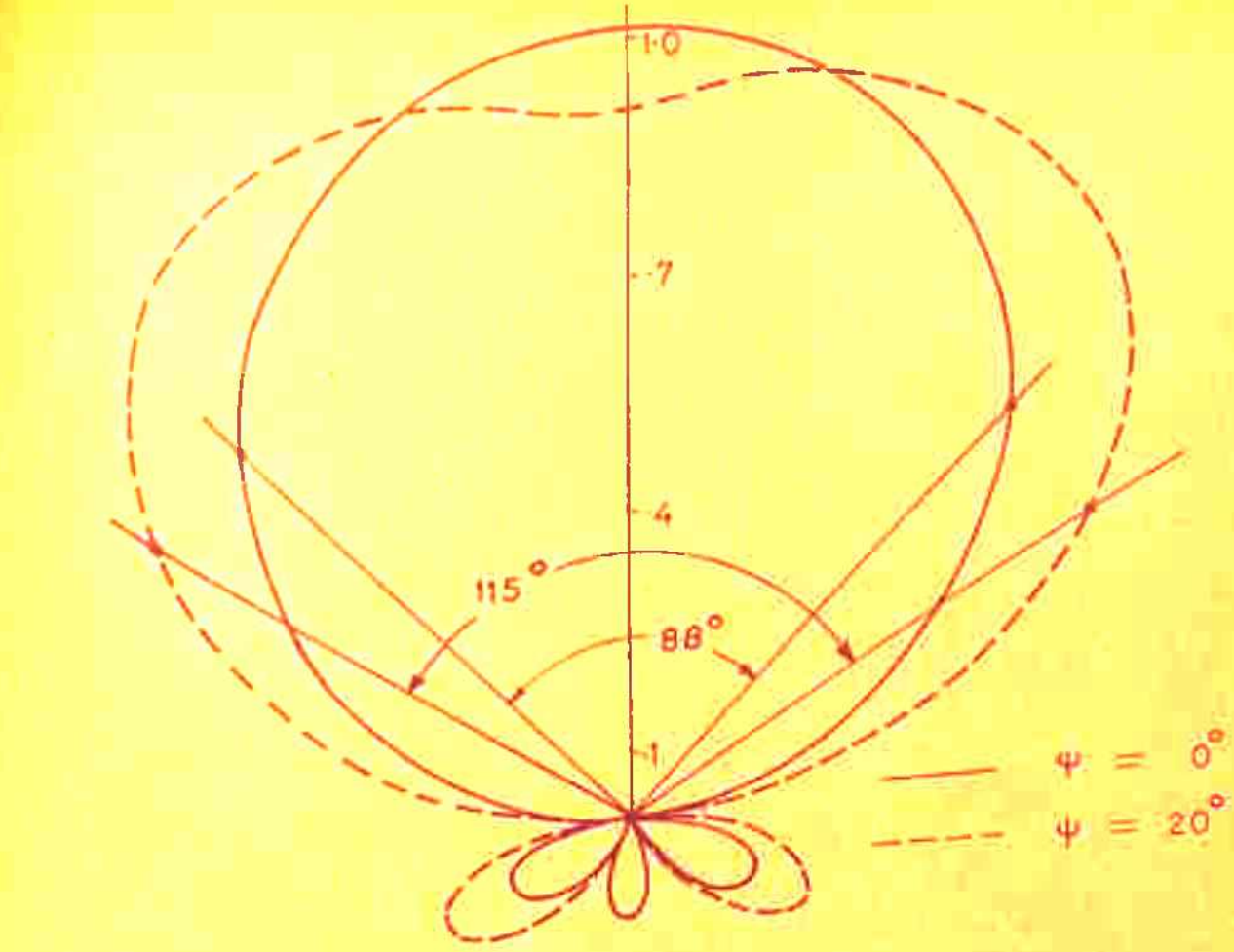

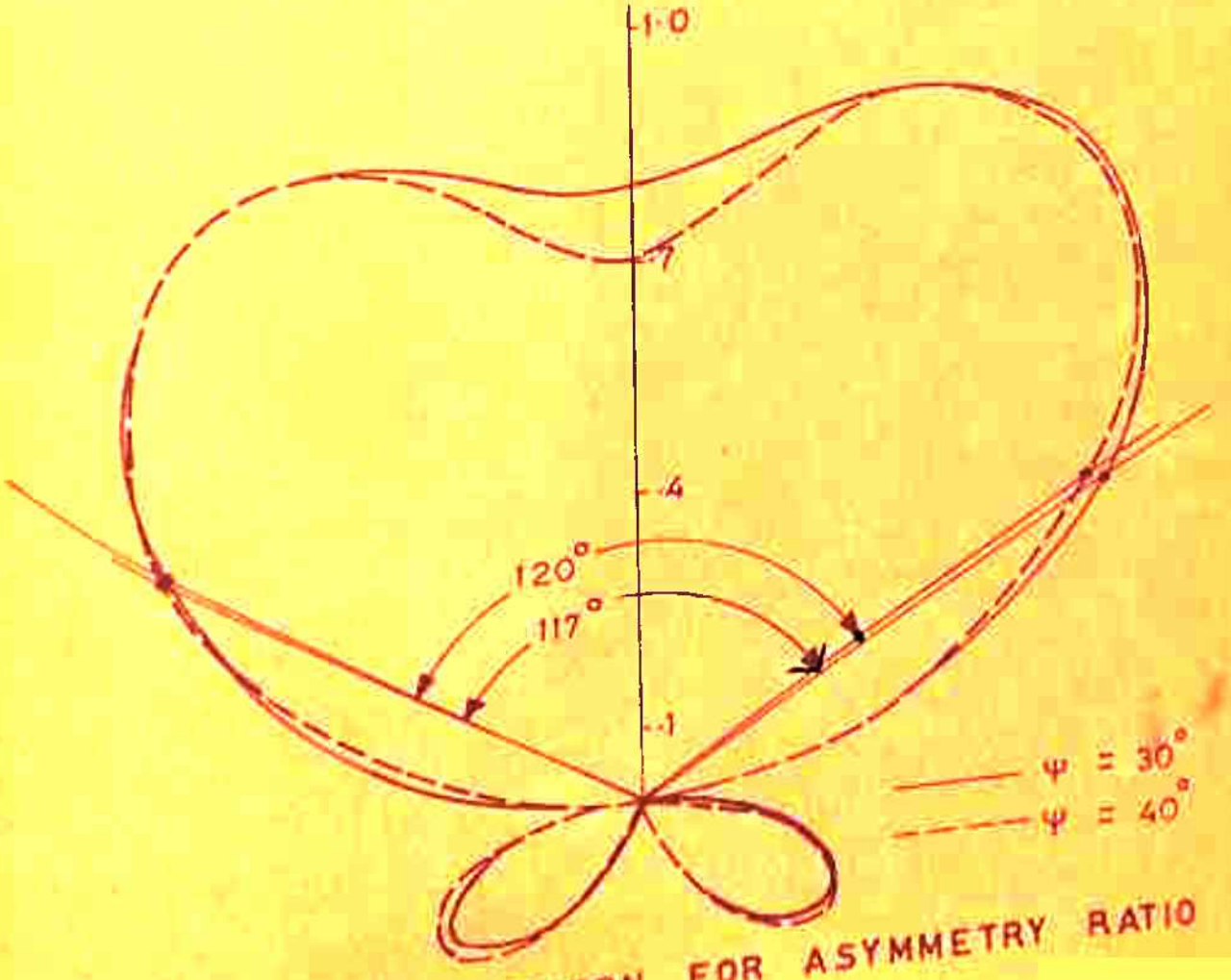

FIG. (5·2c) H-PLANE PATTERN FOR ASYMMETRY RATIO ·42·

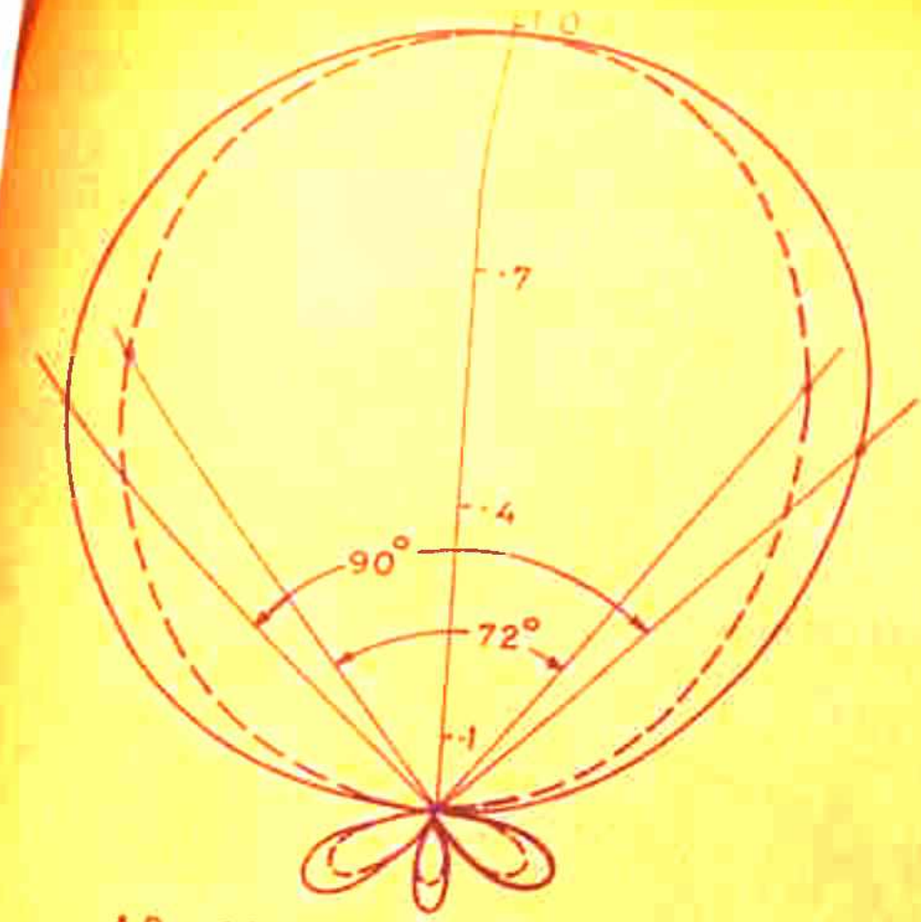

AR = ·694

— Ψ = 0°

---Ψ = 20°

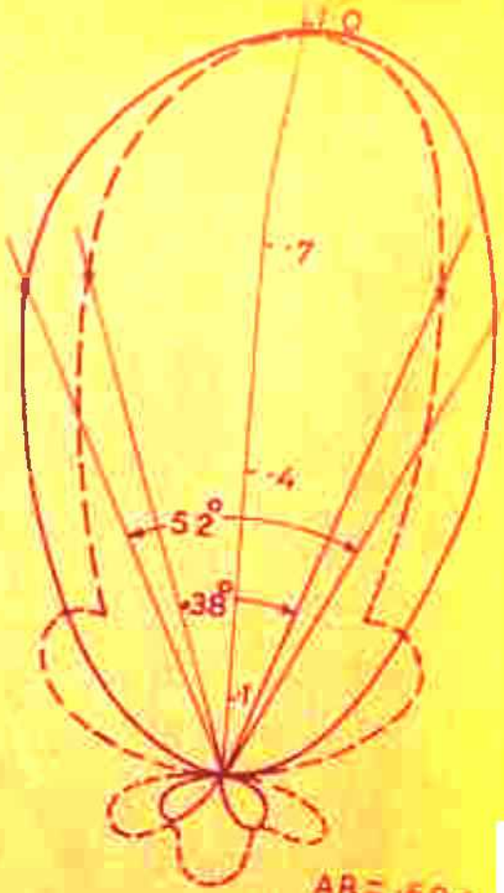

AR = ·694

— Ψ = 40°

---Ψ = 60°

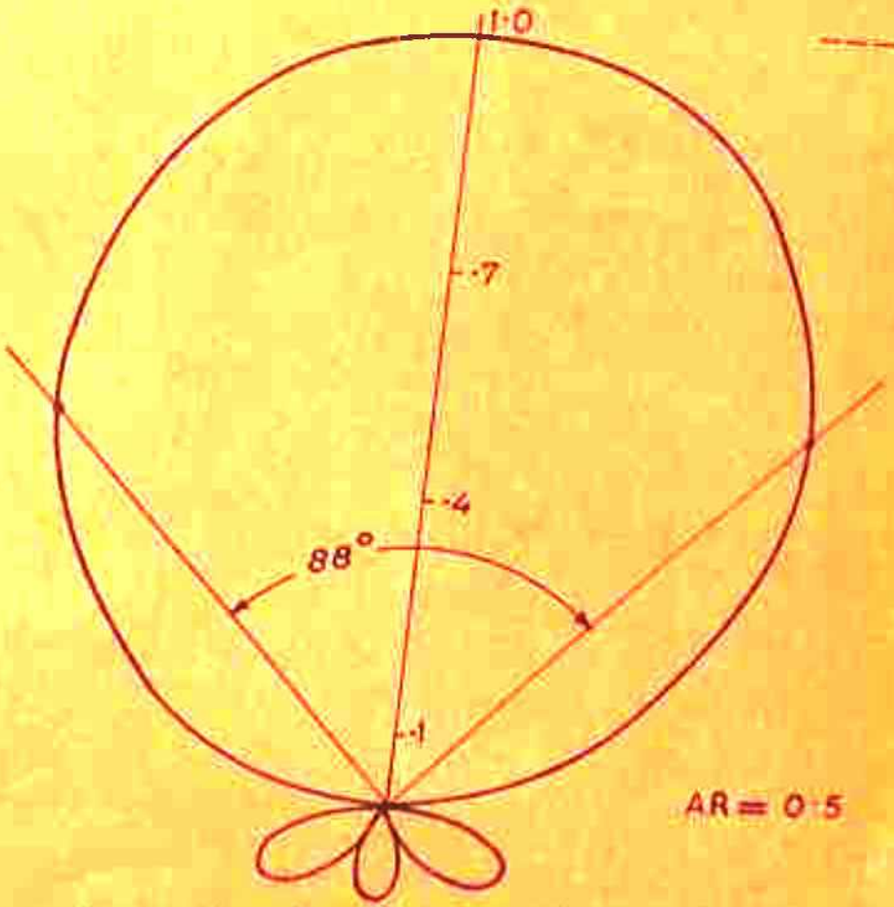

AR = 0·5

(Ψ = 0°, 20°, 40° AND 60°)

FIG. (5-2d). H — PLANE PATTERN FOR ASYMMETRY RATIO 0·5 AND 0·694.

5.2.2 Radiation Resistance: The expression for the total power radiated is given by (25)

$$W = \frac{1}{2\eta_o}\int_0^{2\pi}\int_0^{\pi} |E(\theta, \phi)|^2 r_o^2 \sin\theta \, d\theta \, d\phi \quad (5.4)$$

where $\eta_o = \sqrt{(\mu_o/\varepsilon_o)}$, the intrinsic impedance of free space

μ_o = permeability of free space

ε_o = permittivity of free space.

Substitution of equation (5.3) in equation (5.4) gives

$$W = \frac{15}{\pi}\int_0^{2\pi}\int_0^{\pi} [P \cdot Q \cdot S]^2 \sin\theta \, d\theta \, d\phi \quad (5.5)$$

Equating equation (5.5) to $I_m^2 R_o/2$, the expression for radiation resistance becomes

$$R_o = \frac{30}{\pi}\int_0^{2\pi}\int_0^{\pi} [P \cdot Q \cdot S]^2 \sin\theta \, d\theta \, d\phi \quad (5.6)$$

Computations were done for the following data:

$\alpha_1 = 17.5^\circ$

$r = 0.888$

$N = 3$

$\lambda = 30$ cms.

$\psi = 0^\circ, 10^\circ, 20^\circ, 30^\circ, 40^\circ, 50^\circ$ and 60°.

Results have been tabulated in table-5.2.

TABLE - 5.2

Separation Angle ψ	Radiation Resistance R_o (in ohms)
0^o	35.56
10^o	34.28
20^o	30.90
30^o	26.50
40^o	22.28
50^o	19.03
60^o	16.93

5.2.3 Input Impedance: From the periodically loaded line analysis (29), the phase shift constant β of the loaded line is given by

$$\cos \beta d = \cos Kd + \frac{Z_o}{2X} \sin Kd \qquad (5.7)$$

where $K = \frac{2\pi}{\lambda}$ = free space phase shift constant,

$X = X_1 + X_2$, total reactance due to the lower and upper limbs of the asymmetric dipole,

d = period between two consecutive elements,

$Z_o = 276 \log\left(\frac{D}{r}\right)$, characteristic impedance of the unloaded transmission line,

r (r_o) = radius of the line,

D = centre to centre spacing of the transmission line (also the feed point displacement).

The short dipole region of the LPD antenna can be considered (to a first order approximation) as a periodically loaded transmission line shown in fig.(5.3a and 5.3b). If, now, $Z_A = jX_A$, $Z_B = jX_B = jX$ and X_A is negligible in comparison to X, then using the approximations for sin and cos functions and treating the short dipole region (dipole lengths < $\lambda/2$) as a slow wave structure, equation (5.7) can be transformed to

$$\beta = K\sqrt{\left[1 + \frac{Z_o}{KXd}\right]} \qquad (5.8)$$

The characteristic impedance of the loaded line (28), also the input impedance, is obtained as:

$$Z_c = \frac{Z_o}{\sqrt{\left[1 + \frac{Z_o}{KXd}\right]}} \qquad (5.9)$$

Taking average feed point displacement of the first two dipoles as

$$D = \frac{2(R_1 + R_2)\sin\frac{\pi}{2}}{2} \qquad (5.10)$$

and period $d = (R_2 - R_1)\cos\frac{\pi}{2}$ [fig.(5.3b)] calculations were made for the input impedance of the LPD antenna under consideration using equation (5.9). Following parameters were used:

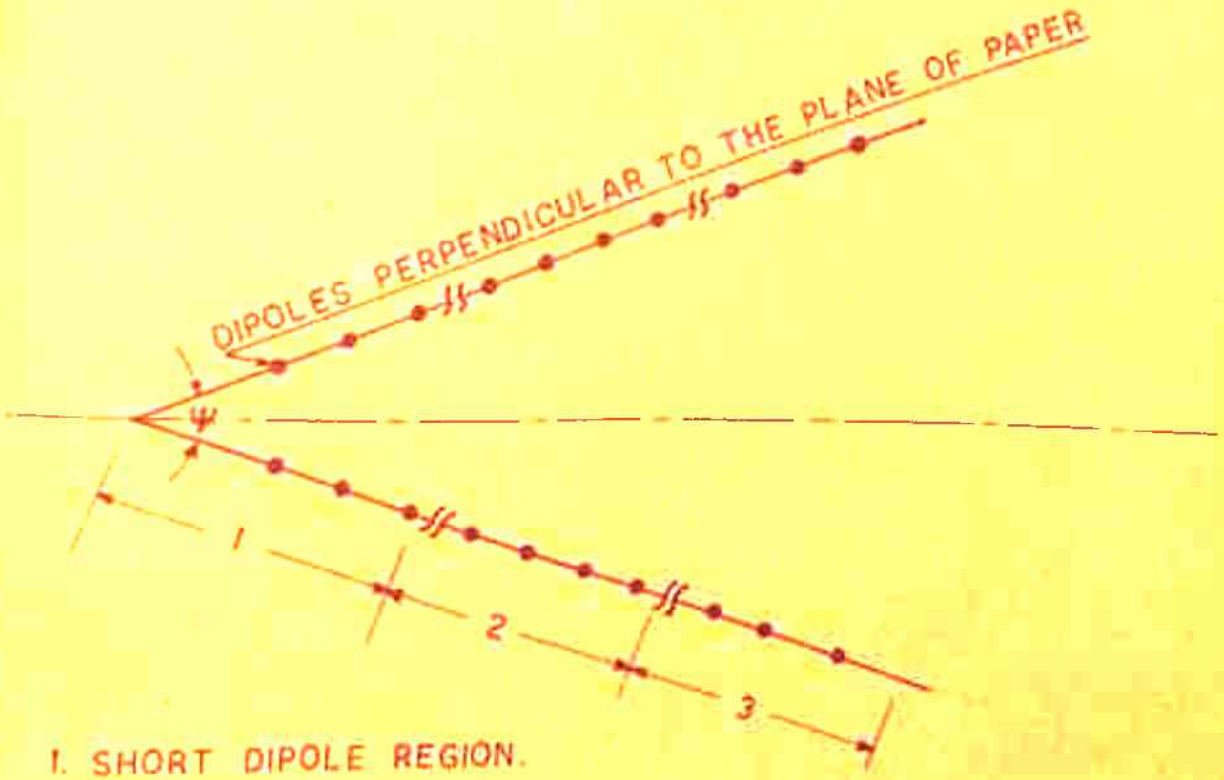

1. SHORT DIPOLE REGION.
2. ACTIVE REGION
3. UNEXCITED LONG DIPOLE REGION

FIG.(5.3a) TWO HALVES OF THE LPD ANTENNA

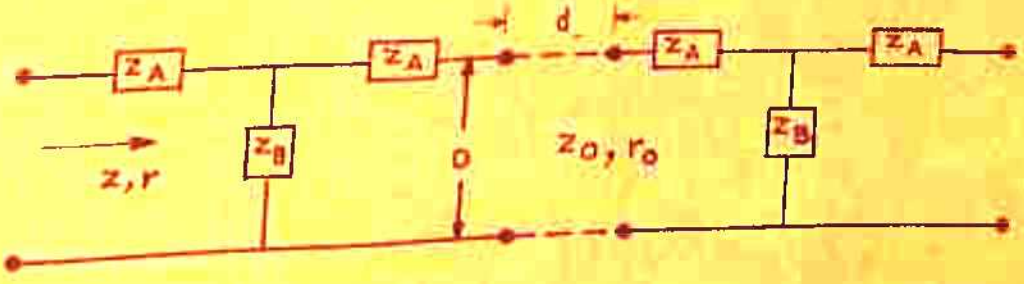

FIG.(5.3b) EQUIVALENT PERIODICALLY LOADED TRANSMISSION LINE.

$\alpha_1 = 17.5^\circ$

$\tau = 0.9$

$\lambda = 30$ cms.

$R_1 = 6.1$ cms.

$R_2 = 6.78$ cms.

$\phi = 10^\circ, 20^\circ, 30^\circ, 40^\circ, 50^\circ$ and 60°

average lengths of the last and last but one upper limbs of the asymmetric dipoles = 2.035 cms.

average length for the lower limbs of these two dipoles = 2.9 cms.

radius of the dipole a = 0.05 cms.

Radius of the feeder line wire r = 0.03 cms.

Values of X_1 and X_2 for the above mentioned average lengths of the asymmetric dipoles were found from the curves given in Jordan (30). Table (5.3) shows the various values of input impedance Z_{in} as function of seperation angle ϕ.

5.2.4 Power Gain and Effective Aperture: As mentioned in chapter - 4, sec. 4.2.3, the power gain for an antenna system with no loss is given by

$$G = 10 \log\left(\frac{41253}{\theta_E \theta_H}\right) \qquad (5.11)$$

where θ_E = half power beam width of E-plane pattern

θ_H = half power beam width of H-plane pattern.

TABLE - 5.3

Separation Angle ϕ	Input Impedance Z_{in}
10^o	91.45
20^o	119.4
30^o	132.47
40^o	139.9
50^o	144.2
60^o	146.2

Once the power gain is computed from equation (5.11), effective aperture may also be calculated using the following relation

$$A/\lambda^2 = \frac{G}{4\pi} \qquad (5.12)$$

Theoretical calculations carried out using the data given in sec. 5.2.1 have been given in table 5.4 .

§ 5.3 EXPERIMENTAL INVESTIGATIONS

5.3.1 Design of Asymmetric LPD Antenna: As stated in chapter-4, the design procedure given by Carrel (28) has been used. From table 5.1, it is obvious that asymmetry ratio AR = 0.694 will be a suitable choice as in this set the beam compression is maximum. It has been already stated

TABLE - 5.4

Separation Angle ϕ	Power Gain G(in dB)	Effective Aperture A/λ^2
0^o	8.8	0.6039
10^o	9.1	0.6471
20^o	9.8	0.7603
30^o	10.6	0.9108
40^o	11.2	1.049
50^o	11.22	1.054
60^o	11.3	1.074

that if one limb isassigned a constant length $\lambda/4$, then one can vary the length of the lower limb to study the effect of asymmetry ratio on the different parameters of the antenna system. For present investigation, following set of data has been used for fabrication:

Gain = 9 dB

$\alpha_1 = 17.5^o$

Input Impedance = 75 ohms

Ratio of lowest to highest frequency is 1 : 5

$\lambda_{max} = 100$ cms.

$r = 0.9$

height of the upper limb of the first dipole in low frequency side = λ_{max} / 4

height of the lower limb of the first dipole in low frequency side = (λ_{max} / 4)// 0.694

where 0.694 is the asymmetry ratio.

The lower limb of each dipole present in the symmetric LPD antenna has been replaced by the length calculated using the asymmetry ratio AR and design ratio τ to convert the structure into an asymmetric LPD antenna.

5.3.2 Measurements

(i) Radiation Pattern: Two masts for mounting the receiving and the transmitting antennas were fabricated as described in chapter - 2, sec. 2.3.2. The set up for the measurement remains the same except that, now, the displaced asymmetric dipole antenna is replaced by the asymmetric LPD antenna. The details of the equipments used have been given in chapter - 2, sec. 2.3.2. The procedure is repeated for various values of frequencies and ϕ. E and H-plane theoretical and experimental patterns have been shown figs.(5.4a - 5.4e).

(ii) Power Gain and Effective Aperture: Method employed for the measurement of power gain is the same as described in chapter - 4. From power gain measurements, the effective aperture may easily be calculated using equation (5.12).

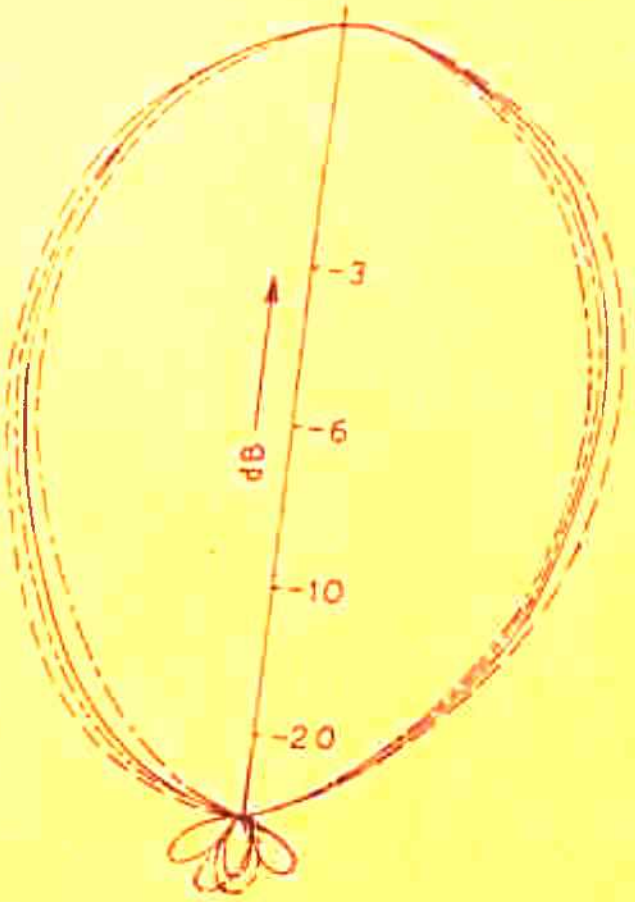

THEORETICAL —— 1 GH_z , 3 dB BEAM WIDTH = 60°

EXPERIMENTAL
- - - - 300 M_c/S , 3 dB BEAM WIDTH = 63°
- - - - 600 M_c/S , 3 dB BEAM WIDTH = 58°
- - - - 900 M_c/S , 3 dB BEAM WIDTH = 61°

FIG. (5·4a). E – PLANE PATTERN FOR $\Psi = 0°, 20°, 40°$ & $60°$

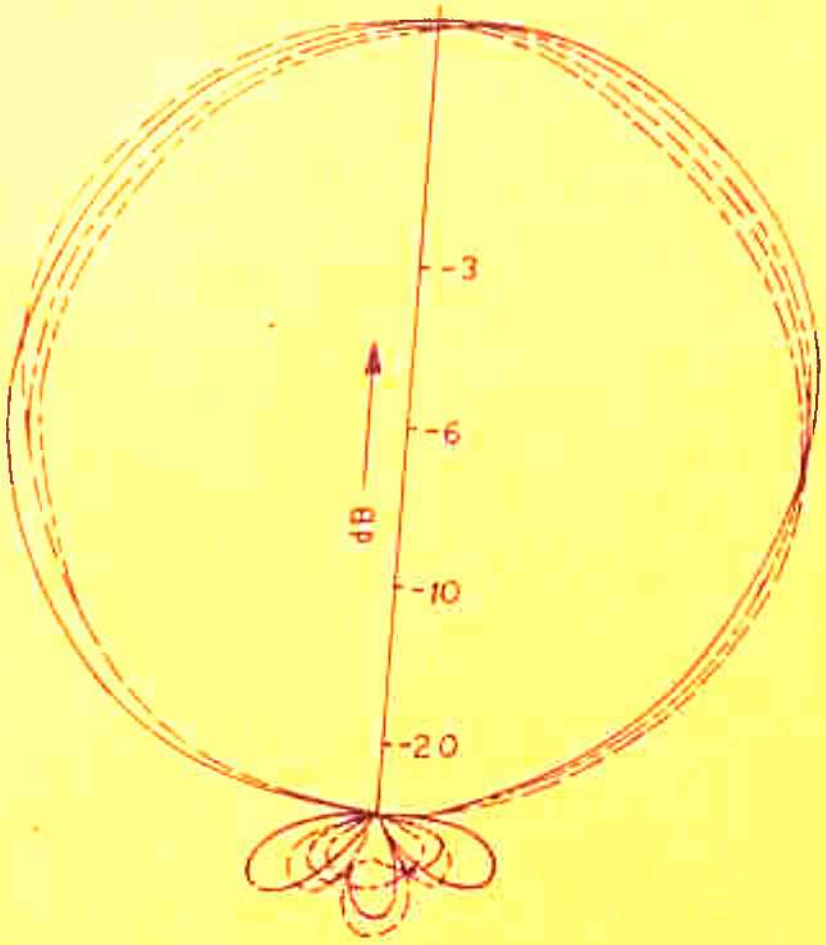

THEORETICAL —— 1 GH_z, 3 dB BEAM WIDTH = 90°

EXPERIMENTAL
- - - - 300 M_c/S, 3 dB BEAM WIDTH = 88·5°
- - - 600 M_c/S, 3 dB BEAM WIDTH = 88°
-·-· 900 M_c/S, 3 dB BEAM WIDTH = 87°

FIG. (5-4b) H-PLANE PATTERN FOR $\Psi = 0°$

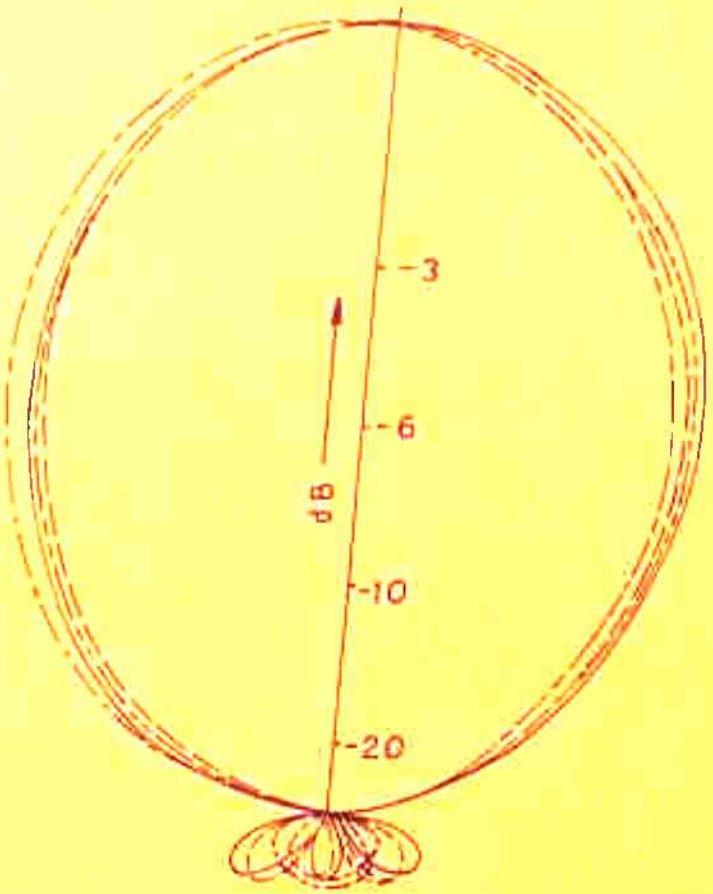

THEORETICAL —— 1 GHz, 3 dB BEAM WIDTH = 72°

EXPERIMENTAL
- — — — 300 Mc/S, 3 dB BEAM WIDTH = 70°
- — — — 600 Mc/S, 3 dB BEAM WIDTH = 72°
- — — — 900 Mc/S, 3 dB BEAM WIDTH = 70°

FIG. (5·4c) H-PLANE PATTERN FOR $\Psi = 20^{\circ}$

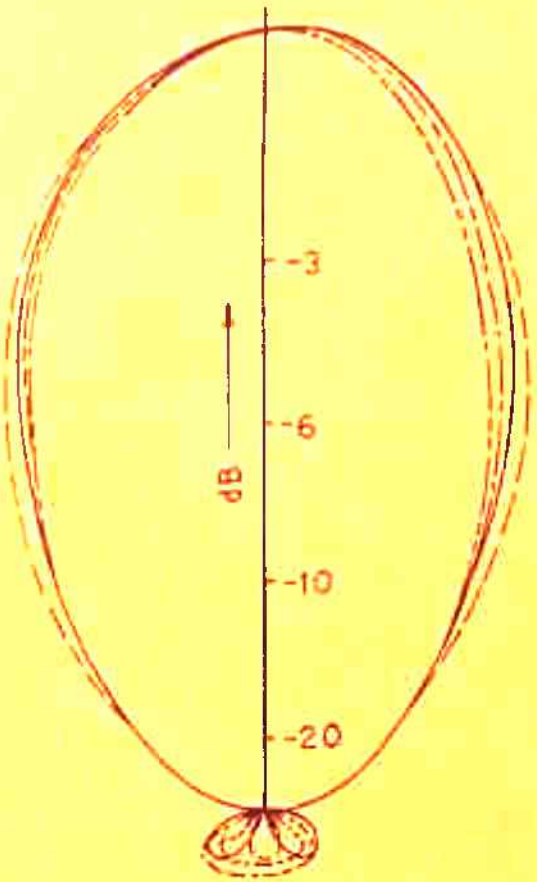

THEORETICAL —— 1 GHz , 3 dB BEAM WIDTH = 52°

EXPERIMENTAL
- - - - 300 Mc / S , 3 dB BEAM WIDTH = 55°
—— 600 Mc /S , 3 dB BEAM WIDTH = 49°
—·—· 900 Mc/S , 3 dB BEAM WIDTH = 48°

FIG. (5·4d) H-PLANE PATTERN FOR $\Psi = 40^{\circ}$

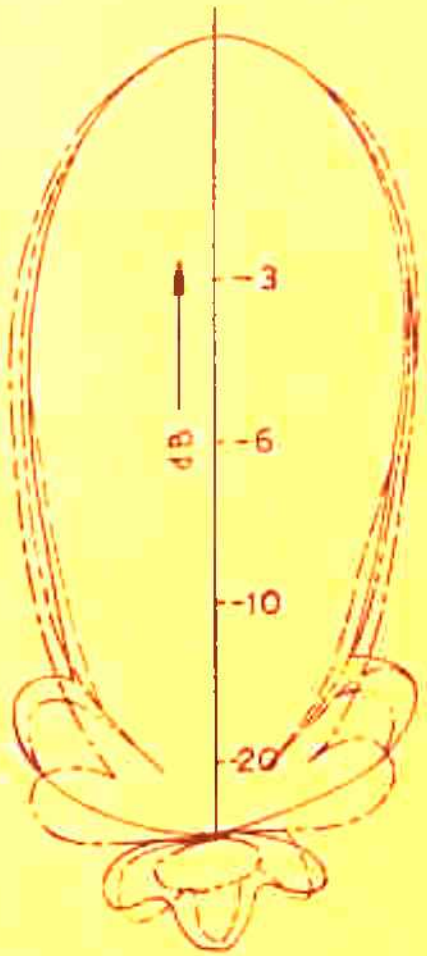

THEORETICAL ——— 1 GHz, 3dB BEAM WIDTH = 38°

EXPERIMENTAL
- - - - - 300 Mc/S, 3dB BEAM WIDTH = 40°
— · — · — 600 Mc/S, 3dB BEAM WIDTH = 39°
— · · — · · — 900 Mc/S, 3dB BEAM WIDTH = 36°

FIG. (5·4e) H — PLANE PATTERN FOR $\Psi = 60^{\circ}$

The experimental results have been given in table - 5.5 and a plot of the same along with the theoretical results is shown in figs.(5.5a, 5.5b).

TABLE - 5.5

Separation Angle ϕ	Power Gain G(in dB)	Effective Aperture A/λ^2
0^o	9.0	0.61
10^o	9.4	0.67
20^o	10.15	0.795
30^o	11.0	0.935
40^o	11.55	1.04
50^o	11.80	1.04
60^o	11.70	1.03
70^o	11.20	-

(iii) Input Impedance: The experimental set up described in chapter - 3, sec. 3.3, for the measurement of input impedance is used. The displaced configuration is now replaced by the asymmetric LPD antenna. Table 5.6 shows the values of VSWR and input impedance measurements as function of ϕ, the separation angle between the two halves. A plot of VSWR and the input impedance have been shown in figs. (5.6a, 5.6b).

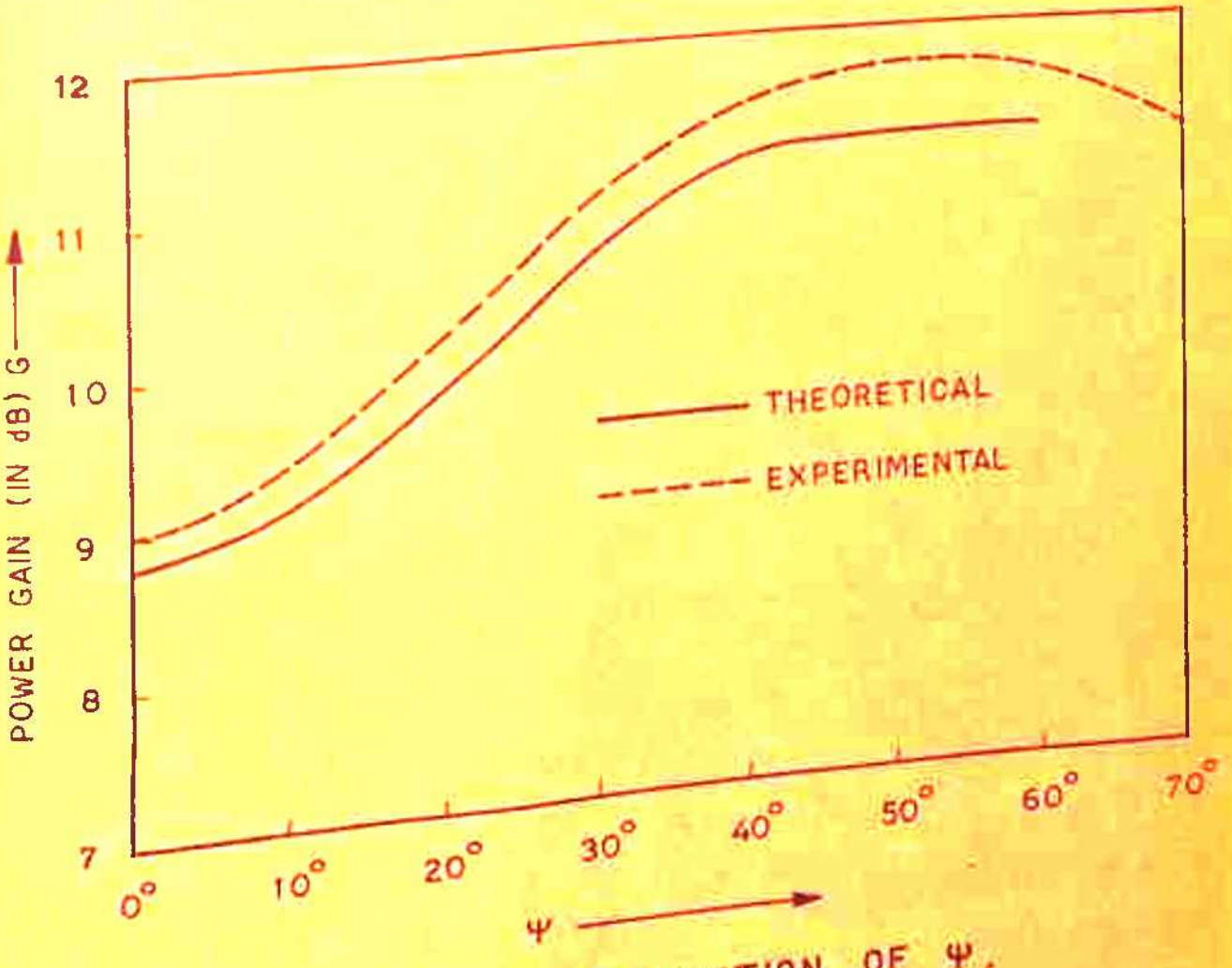

FIG. (5·5a) POWER GAIN AS FUNCTION OF Ψ.

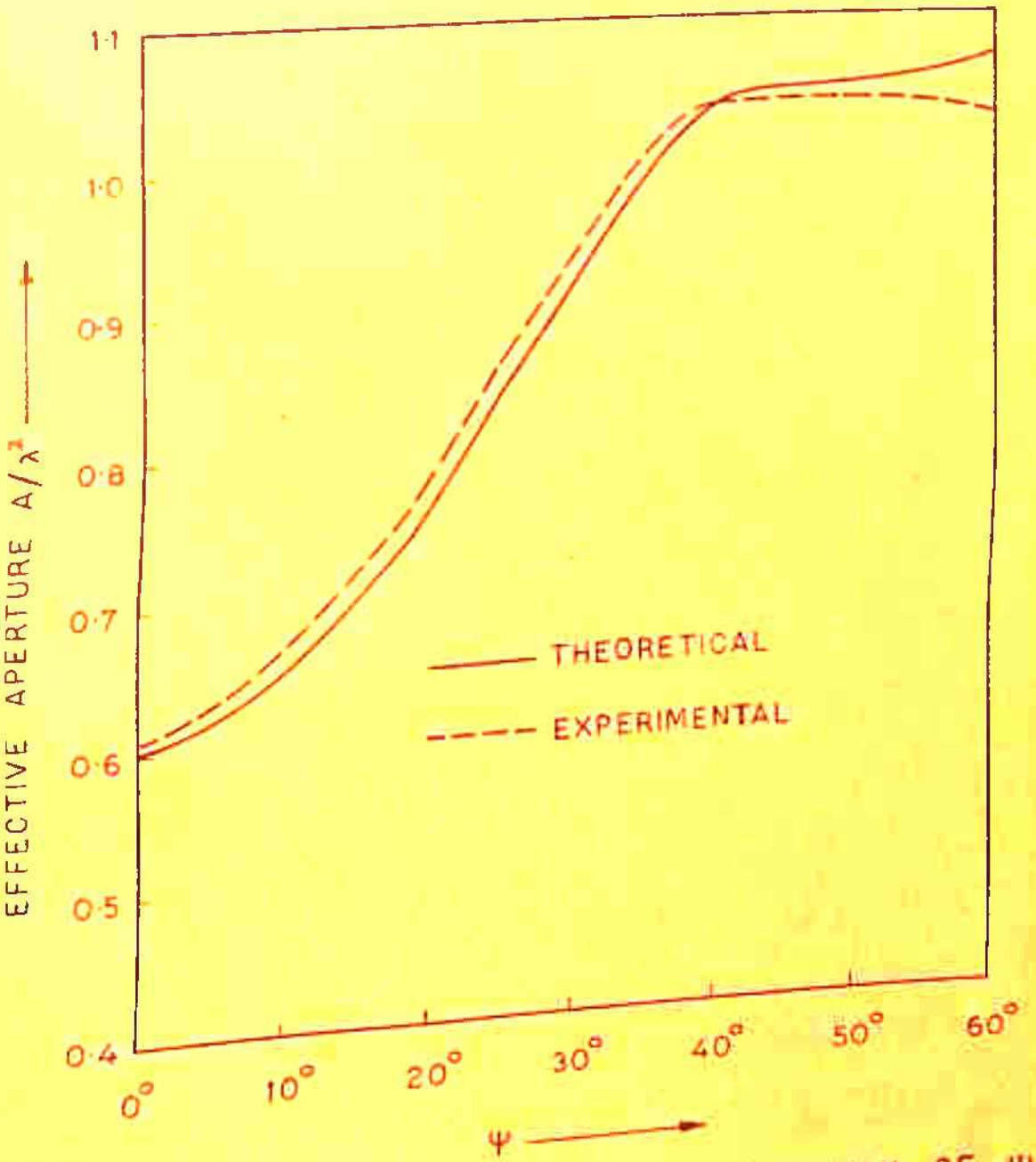

FIG. (5·5b) EFFECTIVE APERTURE AS FUNCTION OF Ψ.

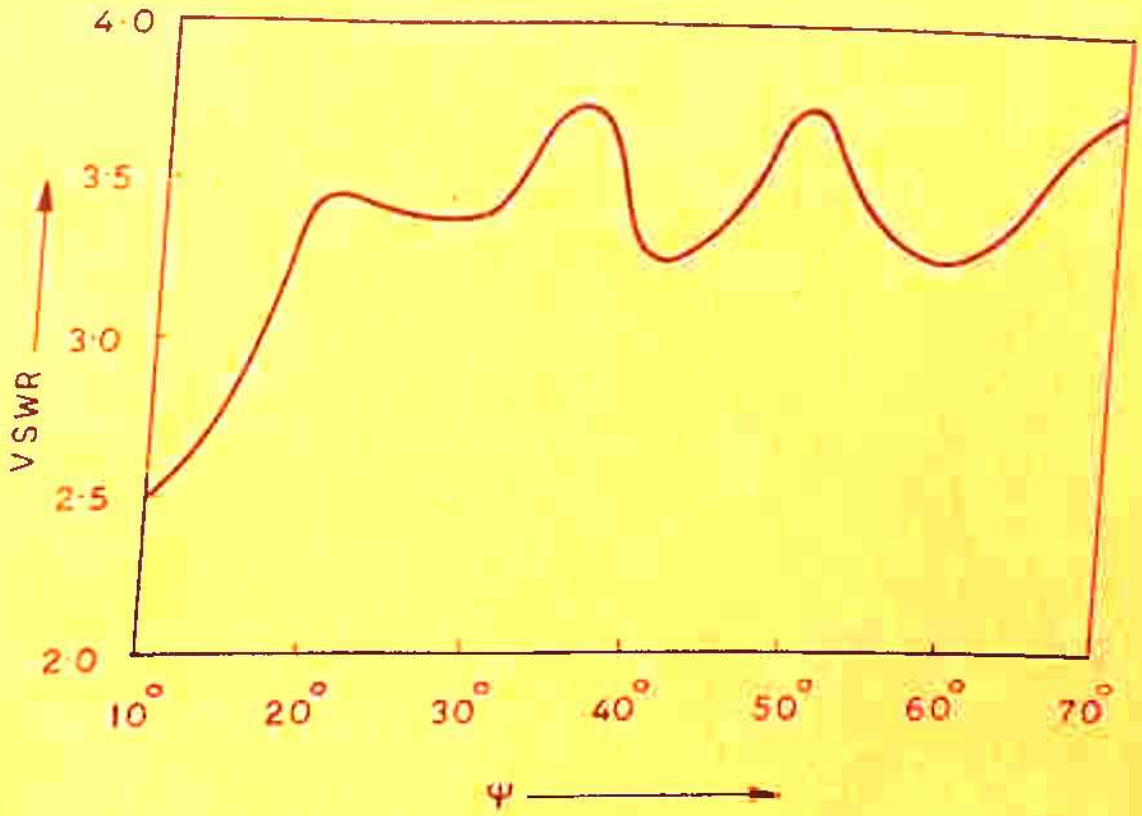

FIG. (5·6a) VSWR AS FUNCTION OF Ψ.

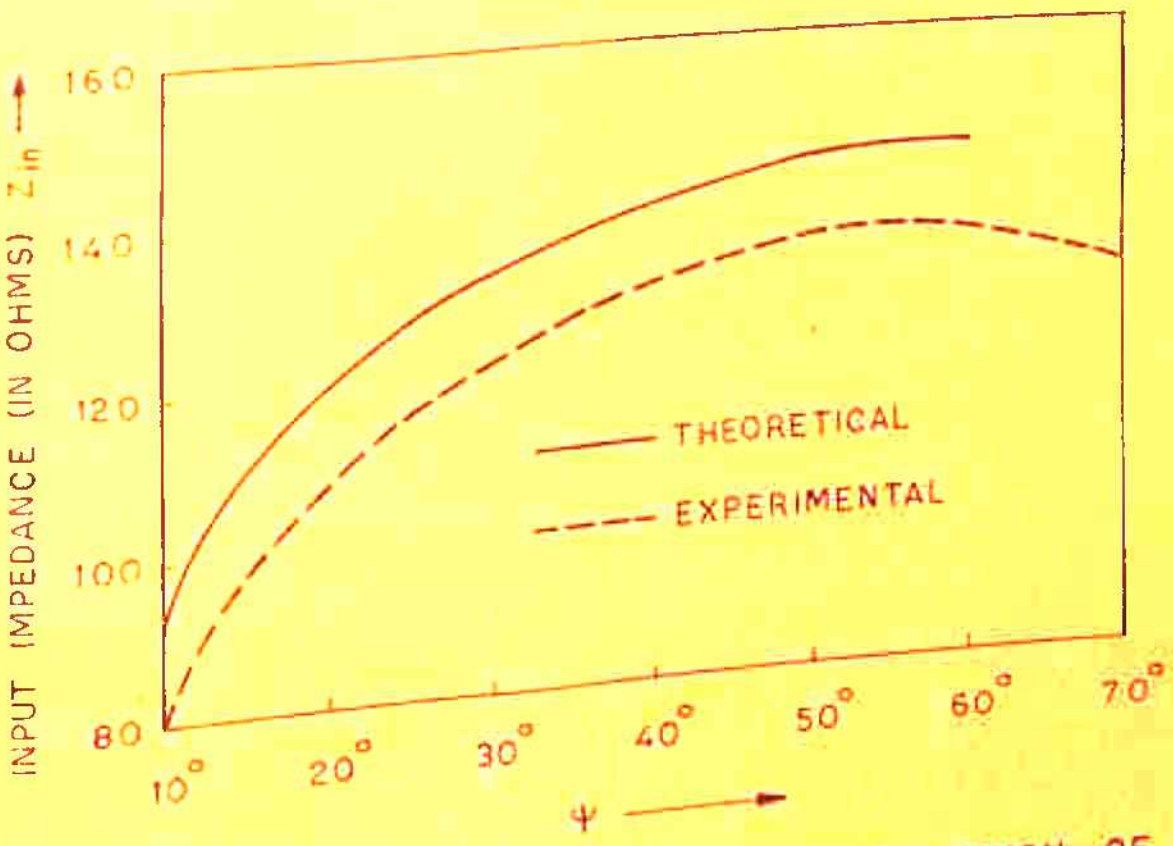

FIG. (5·6b) INPUT IMPEDANCE (Z_{in}) AS FUNCTION OF Ψ.

TABLE - 5.6

Separation Angle ϕ	VSWR	Input Impedance Z_{in} (in ohms)
10^{o}	2.5	80.0
20^{o}	3.5	108.0
30^{o}	3.4	122.0
40^{o}	3.25	130.0
50^{o}	3.75	135.0
60^{o}	3.25	134.0
70^{o}	3.75	129.0

§ 5.4 CONCLUSIONS AND DISCUSSIONS

In all results for various parameters shown graphically in figs.(5.5a, 5.5b, 5.6a and 5.6b) it is seen that the descrepancy between the theoretical and experimental results becomes prominent beyond $\phi = 60^{o}$. Possible reasons for such descrepancies are expected to be the same as explained in chapter - 4, sec. 4.4. Because of laboratory limitations, fabrication could not be carried out using the design parameters mentioned in theoretical calculations. However, the nature of various curves is evidently the same as predicted by theoretical calculations.

C H A P T E R - 6

SOME STUDIES OF ASYMMETRIC DIPOLE ANTENNA WITH ARBITRARILY DISPLACED FEED POINTS IMMERSED IN A WEAKLY IONIZED PLASMA

§ 6.1 INTRODUCTION

The effect of feed point displacement has been treated in detail in chapter - 2. There, the effect of feed point displacement has been studied on the radiation pattern, radiation resistance and gain of the antenna system. Present study is taken up with a view to investigate the effect of plasma medium on the displaced system. A theoretical study of electromagnetic and electroacoustic waves from an asymmetric dipole antenna with arbitrarily displaced feed points immersed in an infinite lossy compressible weakly ionized plasma has been made. A linearized theory has been used such that the isotropic electron plasma is regarded as a single fluid continuum. A general propagation constant is assumed on the antenna system which is taken to be complex in plasma for both electromagnetic and electroacoustic waves. The effect of electron - neutral particle collision is taken into account wherever it is effective. It is shown that the propagation is almost uneffected by the presence of plasma medium for source frequencies much higher than the plasma frequency, the plasma

medium is found to have its profound effect on the radiation. General expressions for the far-field radiation pattern, both for the electromagnetic and the plasma mode or electroacoustic modes, have been developed. The arbitrarily displaced system has been studied under three different configurations, namely arbitrary displacement, transverse displacement and the axial displacement for various values of feed point displacement $2h/\lambda$. Theoretical radiation patterns for the above mentioned configurations have been obtained for the source frequency much greater than the plasma frequency (for the electromagnetic mode). The study for the source frequency equal to and lower than the plasma frequency has not been dealt as they are not of much practical use.

§ 6.2 ANALYSIS FOR FAR ZONE ELECTROMAGNETIC (EM) AND PLASMA (P) FIELDS

6.2.1 Far Zone EM Field: System under consideration is shown in fig.(2.2), chapter - 2. Let SQ and S'Q' be the lower and the upper limbs of the asymmetric dipole antenna respectively. The entire antenna may be considered to be consisting of a number of small elements ds' each having a constant current I(s'). The magnetic vector potential of an element for the above system is given by

$$\delta_A = \frac{\mu_o}{4\pi} I(z')dz' \frac{e^{-\gamma_e r'}}{r'} \qquad (6.1)$$

where μ_o = free space permeability

γ_e = complex propagation constant

$= \alpha_e + j\beta_e$

$= j\beta\sqrt{\epsilon_e}$

$$\epsilon_e = \left(1 - \frac{\omega_p^2}{\omega^2 + \nu^2}\right) - \frac{j\,\omega_p^2\,\nu}{\omega(\omega^2 + \nu^2)}$$

$$\omega_p^2 = \frac{n_o e^2}{m\,\epsilon_o}$$

ϵ_o = free space permittivity

ν = collision frequency

ω = source frequency

n_o = ambient electron population density

m = electron mass

From equation (6.1), the magnetic and electric far zone fields are:

$$\delta H_e(\phi) = \frac{I(z')dz' \sin\theta}{4\pi} \frac{\gamma_e}{r'} e^{-\gamma_e r'} \qquad (6.2)$$

$$\delta E_e(\theta) = \frac{\eta\, I(z')dz' \sin\theta}{4\pi} \frac{\gamma_e}{r'} e^{-\gamma_e r'} \qquad (6.3)$$

where η is the intrinsic impedance of plasma medium.

due to the upper limb is

$$H_e(\phi) = \frac{I_m \gamma_e \, e^{-\gamma_e r_o}}{4\pi \, r_o} \sin\theta \sin(\beta h_2) \, e^{\gamma_e R_1 U_1} \int_0^{h_1} \sin[\beta(h_1 - z')] \, e^{\gamma_e z' \cos\theta} \, dz' \qquad (6.10)$$

Using the formula

$$\int e^{ax} \sin(c+bx)dx = \frac{e^{ax}}{a^2 + b^2} [a \sin(c+bx) - b \cos(c+bx)],$$

equation (6.10) reduces to

$$H_e(\phi) = \frac{M' \sin(\beta h_2)}{\beta^2 + \gamma_e^2 \cos^2\theta} [\beta \, e^{\gamma_e (R_1 U_1 + h_1 \cos\theta)} - e^{\gamma_e R_1 U_1} [\gamma_e \cos\theta \sin(\beta h_1) + \beta \cos(\beta h_1)]] \qquad (6.11)$$

where $M' = M \sin\theta$

$$M = \frac{I_m}{4\pi} \frac{\gamma_e}{r_o} e^{-\gamma_e r_o}$$

Substituting the current distribution and r'' from equation (6.8) and (6.5) for the lower limb S'Q' in equation (6.2) and proceeding as earlier, the field due to the lower limb is obtained as:

$$H_e(\phi) = \frac{M' \sin(\beta h_1)}{\beta^2 + \gamma_e^2 \cos^2\theta} [e^{-\gamma_e R_2 U_2} [\gamma_e \cos\theta \sin(\beta h_2) - \beta \cos(\beta h_2)] + \beta e^{-\gamma_e [R_2 U_2 + h_2 \cos\theta]}] \qquad (6.12)$$

Adding equation (6.11) and (6.12), the far zone magnetic field due to the entire antenna becomes:

$$H_\theta(\phi) = \frac{M \sin\theta}{\beta^2 + \gamma_e^2 \cos^2\theta} \Big[\sin(\beta h_2)[\beta\, e^{\gamma_e[R_1U_1 + h_1\cos\theta]} - e^{\gamma_e R_1 U_1}[\gamma_e \cos\theta \sin(\beta h_1) + \beta \cos(\beta h_1)]] + \sin(\beta h_1)[\beta\, e^{-\gamma_e[R_2U_2 + h_2\cos\theta]} + e^{-\gamma_e R_2 U_2}[\gamma_e \cos\theta \sin(\beta h_2) - \beta \cos(\beta h_2)]] \Big] \quad (6.13)$$

The corresponding magnetic field is given by

$$E_\theta(\theta) = \eta\, H_\theta(\phi) \quad (6.14)$$

where $\eta = \dfrac{\gamma_e(j\omega + \nu)}{\varepsilon_0[(\omega^2 - \omega_p^2) + j\omega\nu]^{1/2}}$

and ω_p is plasma frequency.

The study can be made in three possible cases mentioned below.

Case I Source frequency far-far greater than the plasma frequency $(\omega >> \omega_p) >> \nu$. In this case

$$\xi = \left(1 - \frac{\omega_p^2}{\omega^2 + \nu^2}\right) - \frac{j\,\omega_p^2\,\nu}{\omega(\omega^2 + \nu^2)}$$

becomes $\epsilon = 1 - \frac{\omega_p^2}{\omega^2}$

and

$$\gamma_e = j\beta\sqrt{\epsilon}$$

$$= j\beta\sqrt{(1 - \frac{\omega_p^2}{\omega^2})}$$

$$\eta = \frac{\eta_o}{\sqrt{(1 - \frac{\omega_p^2}{\omega^2})}} \quad , \quad \eta_o = 377 \ \Omega \qquad (6.15)$$

Case II Source frequency comparable to plasma frequency but both far-far greater than the collision frequency $(\omega \simeq \omega_p) >> \nu$.

In this case γ_e is given by

$$\gamma_e = \sqrt{(\frac{\omega\nu}{2c^2})}\,(1 + j) \qquad (6.16)$$

Case III Source frequency far-far less than the plasma frequency, but both greater than collision frequency $(\omega_p >> \omega) >> \nu$.

γ_e now becomes

$$\gamma_e = -\frac{\omega_p}{c}(1 + \frac{j\nu}{\omega}) \qquad (6.17)$$

However, since in most of the practical applications, source is operated at frequency higher than the plasma frequency, hence the results have been given for the first case only.

The far-field radiation pattern for the first case can be obtained by substituting the values of η and ξ from equation (6.15) into equation (6.14).

6.2.2 Far-Zone Plasma (P) Field: For the linear asymmetric dipole antenna, the scalar field n_1 is given by

$$n_1 = \frac{j\omega_p^2}{4\pi e v_o^2 \omega}\left[\int_o^{h_1}\left(\frac{\nabla\cdot I(z')}{r'}\right) e^{-\gamma_p r'} dz' + \int_{-h_2}^{o}\left(\frac{\nabla\cdot I(z')}{r''}\right) e^{-\gamma_p r''} dz'\right] \qquad (6.18)$$

where v_o is the r.m.s. thermal velocity of electrons. For the upper limb, the current distribution is

$$I(z') = I_m \sin(\beta h_2)\sin[\beta(h_1 - z')]$$

Taking the divergence of I(z')

$$[\nabla\cdot I(z')]_z = -\beta I_m \sin(\beta h_2)\sin[\beta(h_1 - z')]$$

and substituting this value of $\nabla\cdot I(z')$ and r' from equation (6.4) in the first term of equation (6.18), the scalar field n_1 due to the upper limb becomes

$$n_{1SQ} = -\frac{j\omega_p^2 \beta I_m \sin(\beta h_2)}{4\pi e v_o^2 \omega r_o} e^{-\gamma_p r_o} e^{\gamma_p R_1 U_1} \int_o^{h_1} \cos[\beta(h_1 - z')] e^{\gamma_p z' \cos\theta} dz'$$

$$\text{or} \quad \Pi_{1SQ} = - A\, e^{\gamma_p R_1 U_1} \int_0^{h_1} \cos[\beta(h_1 - z')]\, e^{\gamma_p z' \cos\theta}\, dz' \qquad (6.19)$$

$$\text{where} \quad A = \frac{j\,\omega_p^2\,\beta\, I_m \sin(\beta h_2)}{4\pi\, e\, v_o^2\, \omega\, r_o}\, e^{-\gamma_p r_o}$$

Applying the formula

$$\int e^{ax} \cos(c+bx)\,dx = \frac{e^{ax}}{a^2+b^2}\,[\, a\cos(c+bx) + b\sin(c+bx)\,]$$

equation (6.19) transforms to

$$\Pi_{1SQ} = \frac{A}{\beta^2 + \gamma_p^2 \cos^2\theta} \Big[-\sin(\beta h_2)[\gamma_p \cos\theta\; e^{\gamma_p(R_1U_1 + h_1\cos\theta)} - e^{\gamma_p R_1 U_1}\{\gamma_p \cos\theta \cos(\beta h_1) - \beta \sin(\beta h_1)\}] \Big] \qquad (6.20)$$

Taking the current distribution for the lower limb and r'' from (6.8) and (6.5) respectively and proceeding as above, the scalar field due to the lower limb is obtained as:

$$n_{1S'Q'} = \frac{A}{\beta^2 + \gamma_p^2 \cos^2\theta} \left[\sin(\beta h_1)[\gamma_p \cos\theta\, e^{-\gamma_p(R_2U_2 + h_2\cos\theta)} - e^{-\gamma_p R_2 U_2}\,[\gamma_p \cos\theta \cos(\beta h_2) + \beta \sin(\beta h_2)]] \right] \quad (6.21)$$

The total field due to the entire antenna is obtained by adding equation (6.20) and (6.21), i.e.

$$n_1 = n_{1SQ} + n_{1S'Q'}$$

$$n_1 = \frac{A}{\beta^2 + \gamma_p^2 \cos^2\theta} \left[\sin(\beta h_2)[\gamma_p \cos\theta\, e^{\gamma_p(R_1U_1 + h_1\cos\theta)} - e^{\gamma_p R_1 U_1}\,[\gamma_p \cos\theta \cos(\beta h_1) - \beta \sin(\beta h_1)]] + \sin(\beta h_1)\,[\gamma_p \cos\theta\, e^{-\gamma_p(R_2U_2 + h_2\cos\theta)} - e^{-\gamma_p R_2 U_2}\,[\gamma_p \cos\theta \cos(\beta h_2) + \beta \sin(\beta h_2)]] \right] \quad (6.22)$$

The vector field V_p of the P mode is obtained by taking the gradient of the scalar field and is given by

$$V_p(r) = \frac{j\omega_p}{\gamma_p} \frac{n_1}{n_o} \quad (6.23)$$

As has been said in sec.(6.2.1), the scalar field may also be studied in three cases.

Case I $\quad [\omega >> \omega_p] >> \nu$

In general $\gamma_p = \frac{j}{v_o} [(\omega^2 - \omega_p^2) - j\omega\nu]^{1/2}$

For the above case, this reduces to

$$\gamma_p = \frac{j\omega}{v_o} \sqrt{(1 - \frac{\omega_p^2}{\omega^2})}$$

$$= \frac{j\omega}{v_o} \sqrt{\epsilon} \qquad (6.24)$$

Case II $\quad [\omega \simeq \omega_p] >> \nu$

γ_p , now, is given by

$$\gamma_p = \sqrt{(\frac{\omega\nu}{2v_o^2})} [1 + j] \qquad (6.25)$$

Case III $\quad [\omega << \omega_p] >> \nu$

In this case γ_p is given by

$$\gamma_p = \frac{\omega_p}{r} (1 + \frac{1}{2} \frac{\nu\omega}{\omega_p^2}) \qquad (6.26)$$

Theoretical plots for the electromagnetic mode for three configurations of displacements and for three special cases of the general propagation constant β(namely, $\beta = \beta_o$, free space propagation constant, $\beta = \beta_e$, electromagnetic mode propagation constant and $\beta = \beta_p$, plasma mode propagation constant) have been shown in figures (6.1a to 6.11) for various values of feed point displacement $\frac{2R}{\lambda}$.

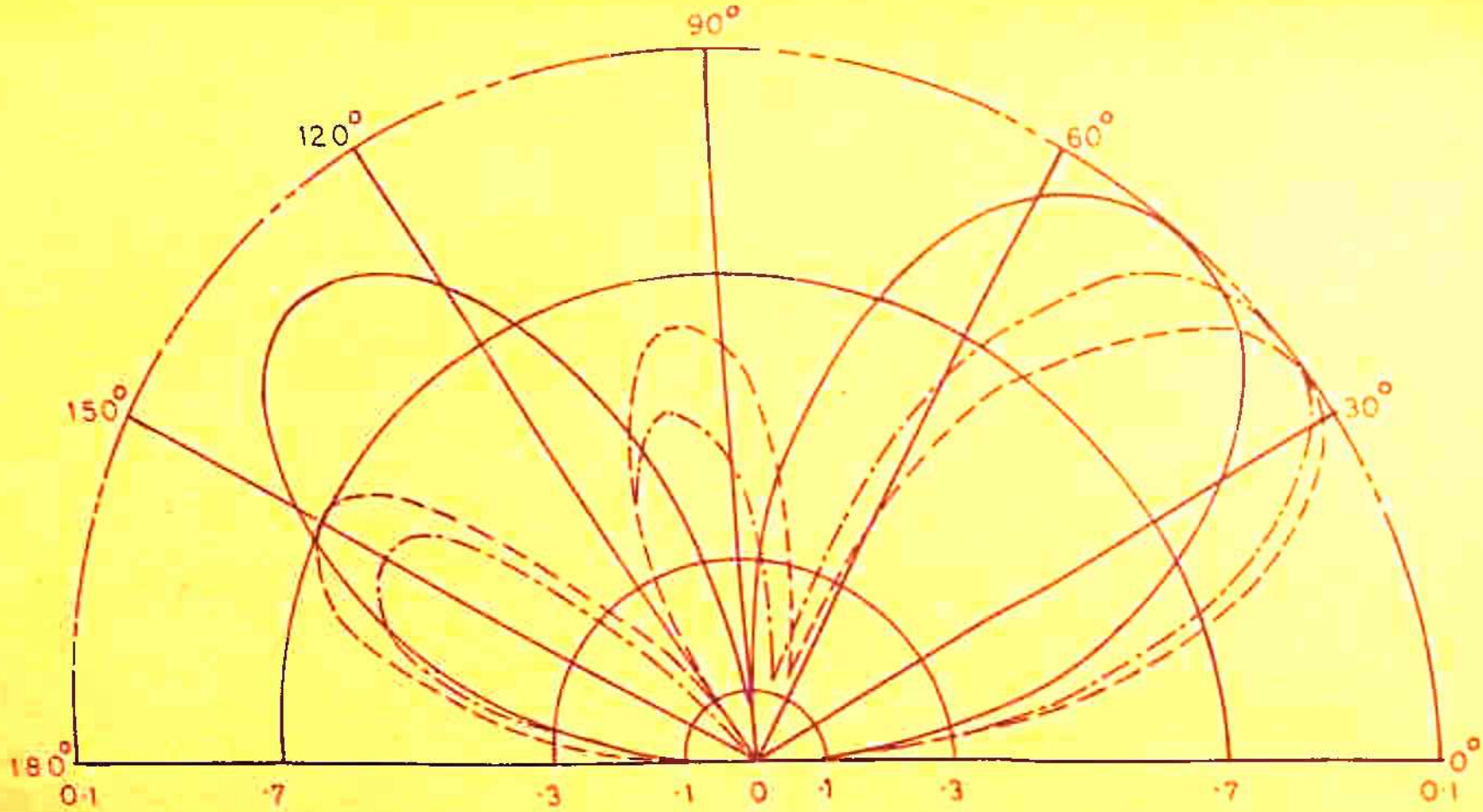

FIG. (6.1a) E AND H-PLANE PATTERNS (ELECTROMAGNETIC MODE) FOR ARBITRARILY DISPLACED ASYMMETRIC DIPOLE ANTENNA FOR $\beta = \beta_0$

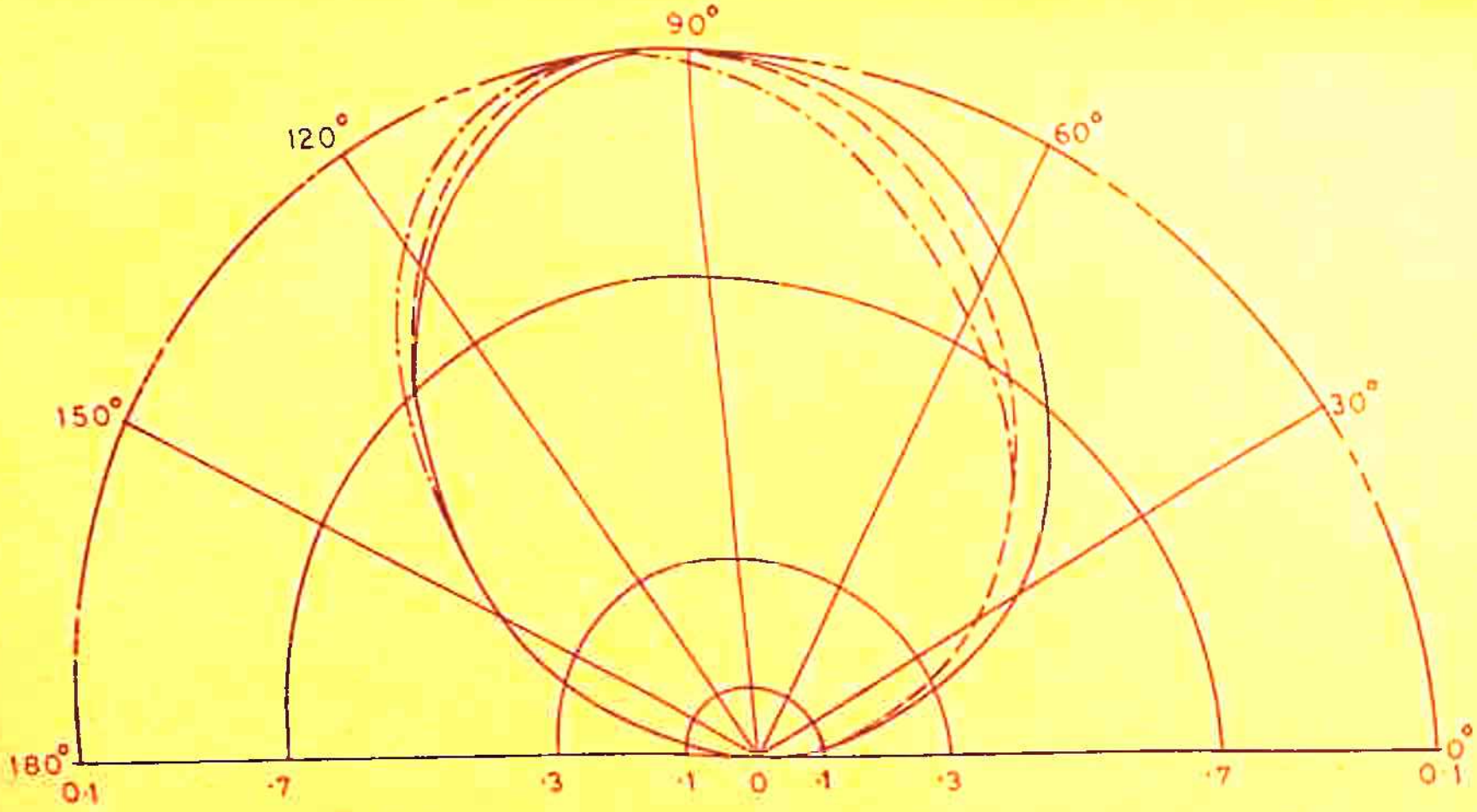

FIG. (6·16) E AND H-PLANE PATTERNS (ELECTROMAGNETIC MODE) FOR ARBITRARILY DISPLACED ASYMMETRIC DIPOLE ANTENNA FOR $\beta = \beta_e$

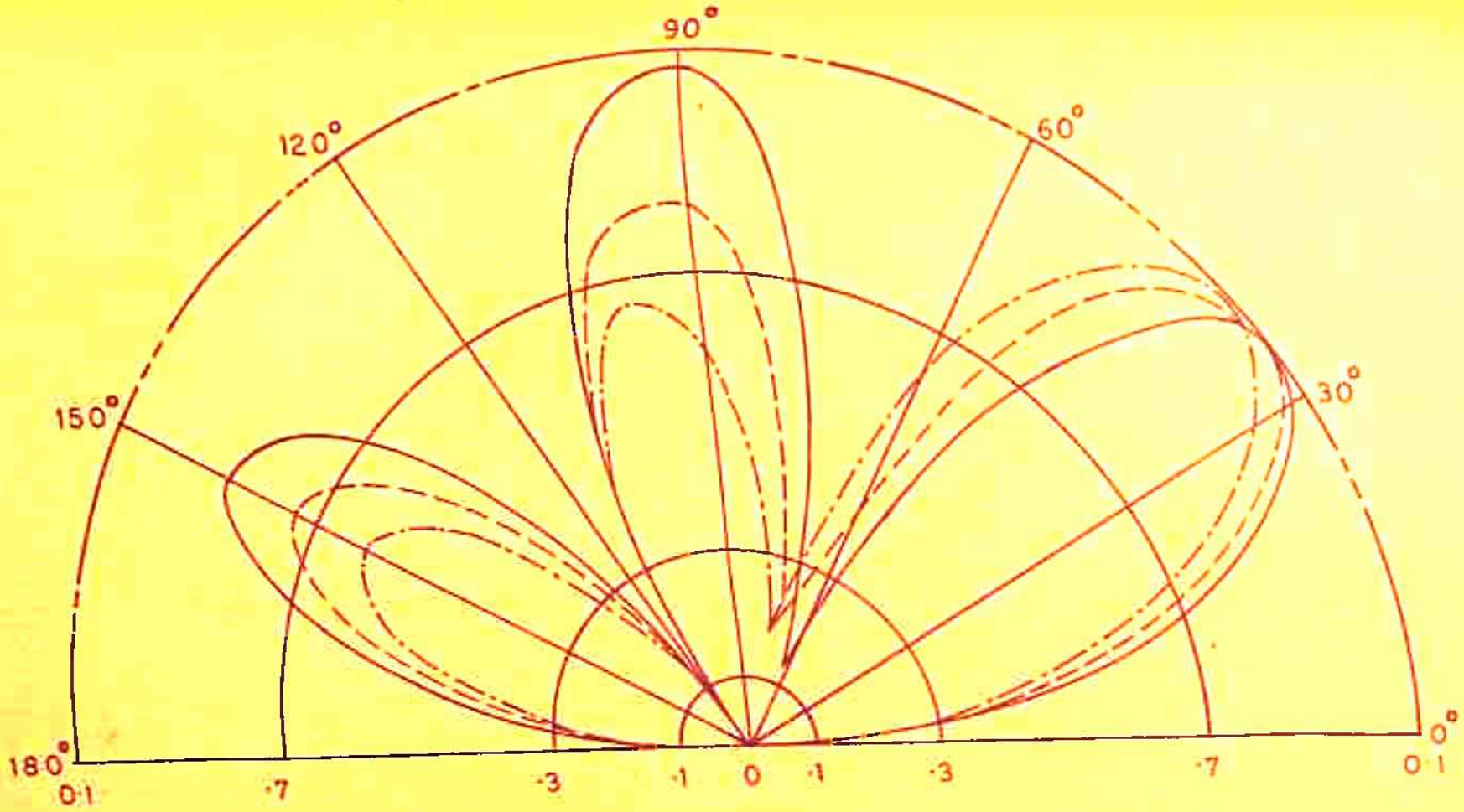

FIG. (6·1c) E AND H-PLANE PATTERNS (ELECTROMAGNETIC MODE) FOR ARBITRARILY DISPLACED ASYMMETRIC DIPOLE ANTENNA FOR $\beta = \beta_p$

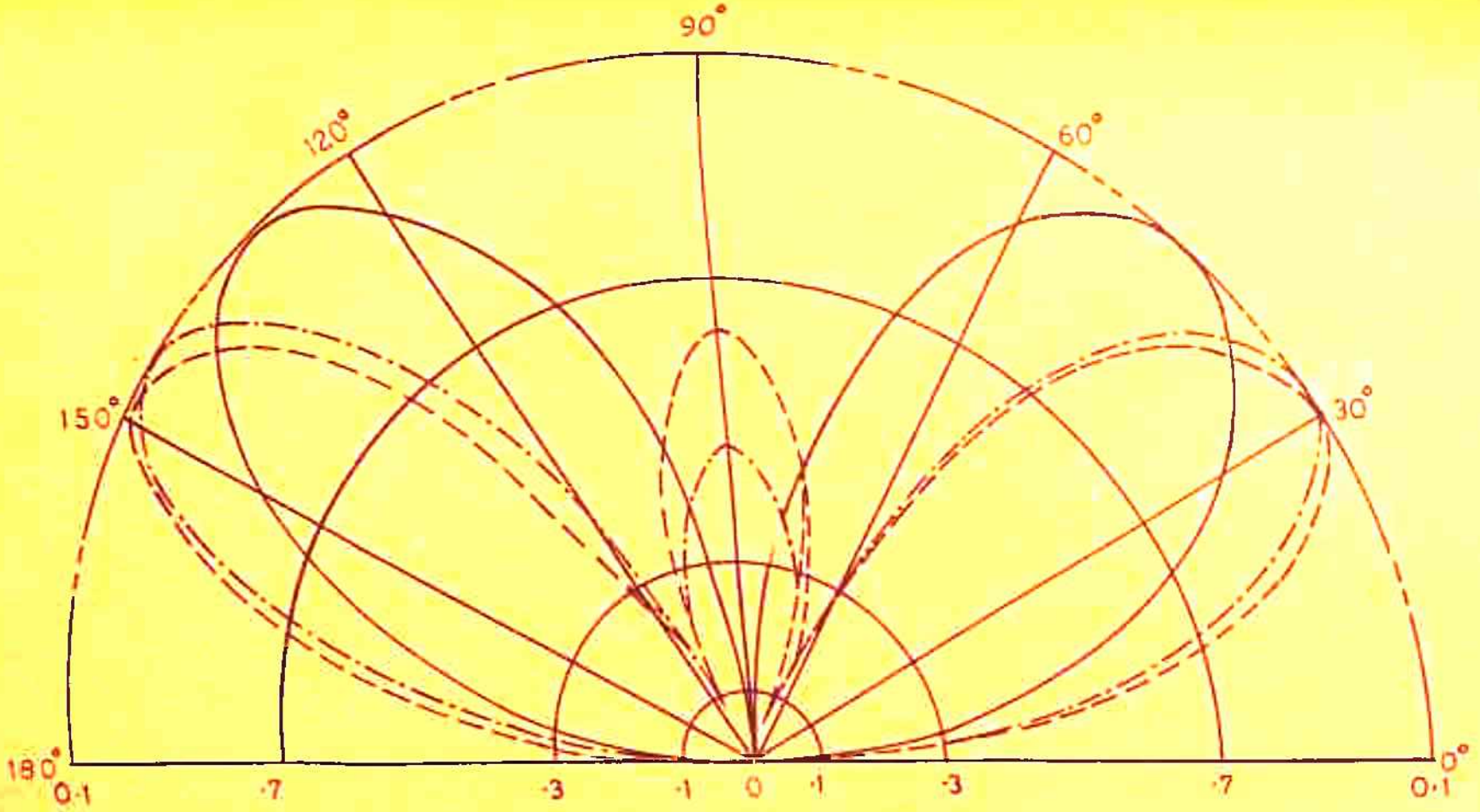

FIG. (6·1d) E AND H-PLANE PATTERNS (ELECTROMAGNETIC MODE) FOR AXIALLY DISPLACED ASYMMETRIC DIPOLE ANTENNA FOR $\beta = \beta_0$

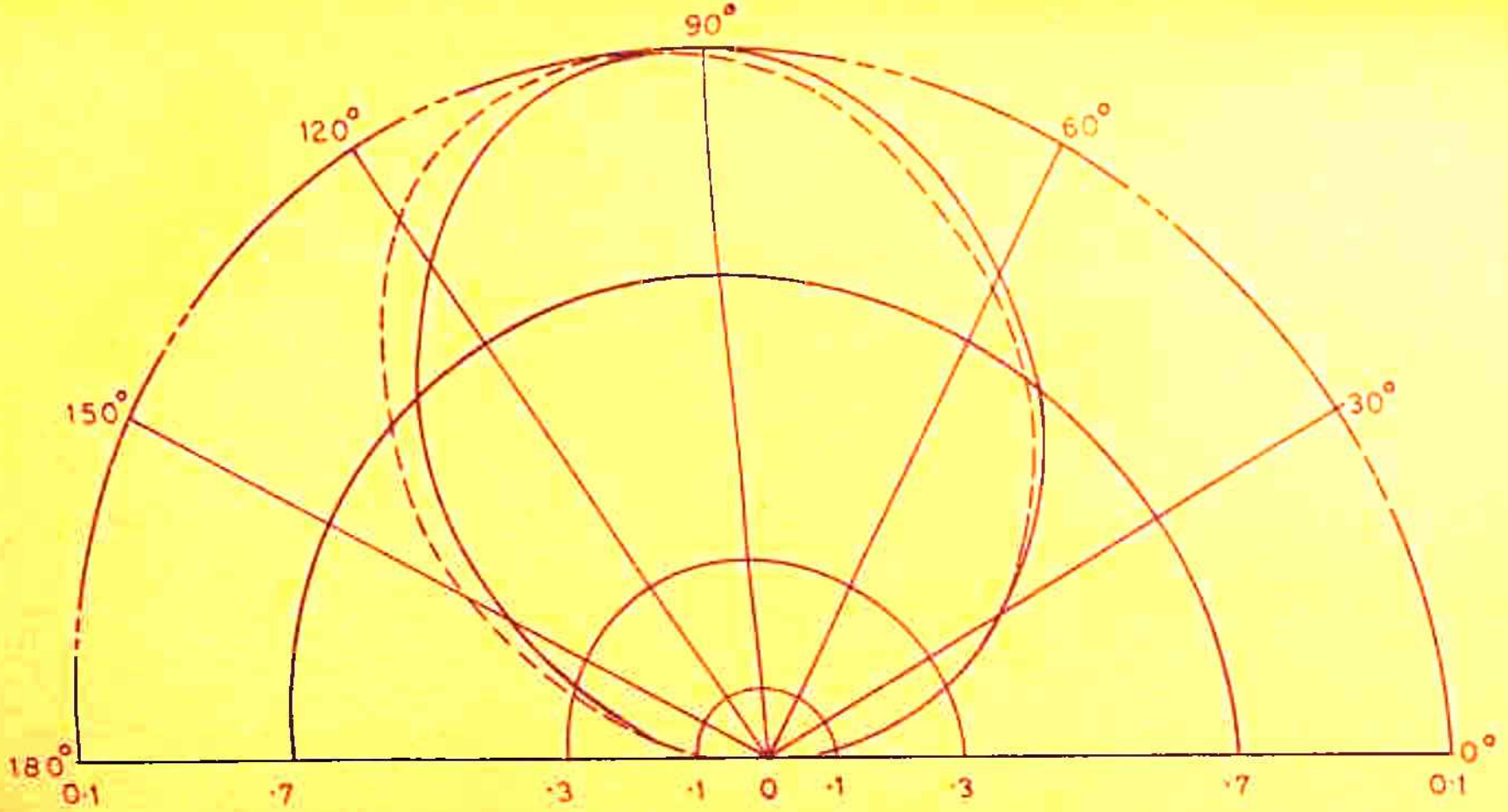

FIG.(6.1e) E AND H-PLANE PATTERNS (ELECTROMAGNETIC MODE) FOR TRANSVERSELY DISPLACED ASYMMETRIC DIPOLE ANTENNA FOR $\beta = \beta_e$

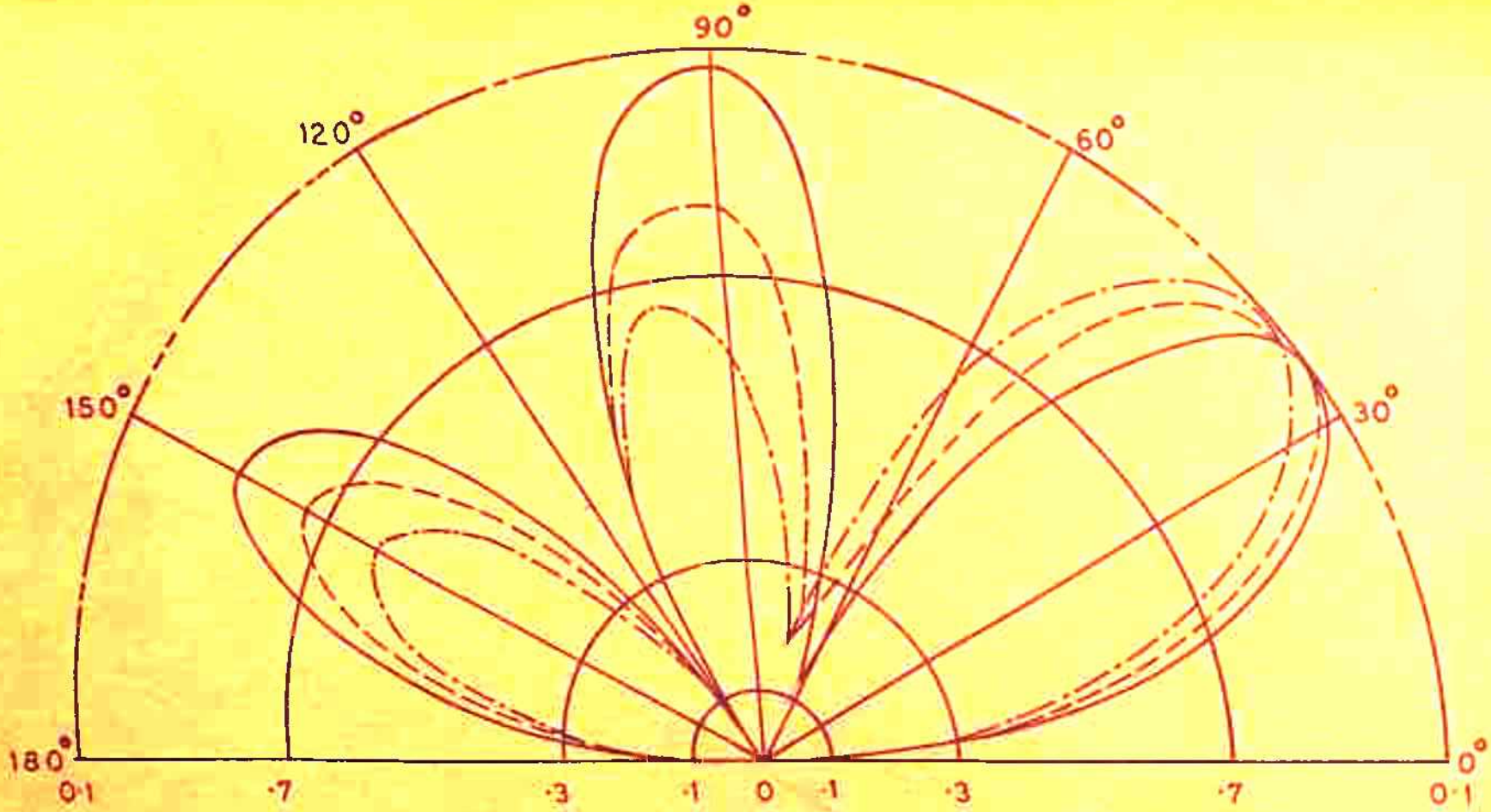

FIG (6·14) E AND H-PLANE PATTERNS (ELECTROMAGNETIC MODE) FOR ARBITRARILY DISPLACED ASYMMETRIC DIPOLE ANTENNA FOR $\beta = \beta_p$

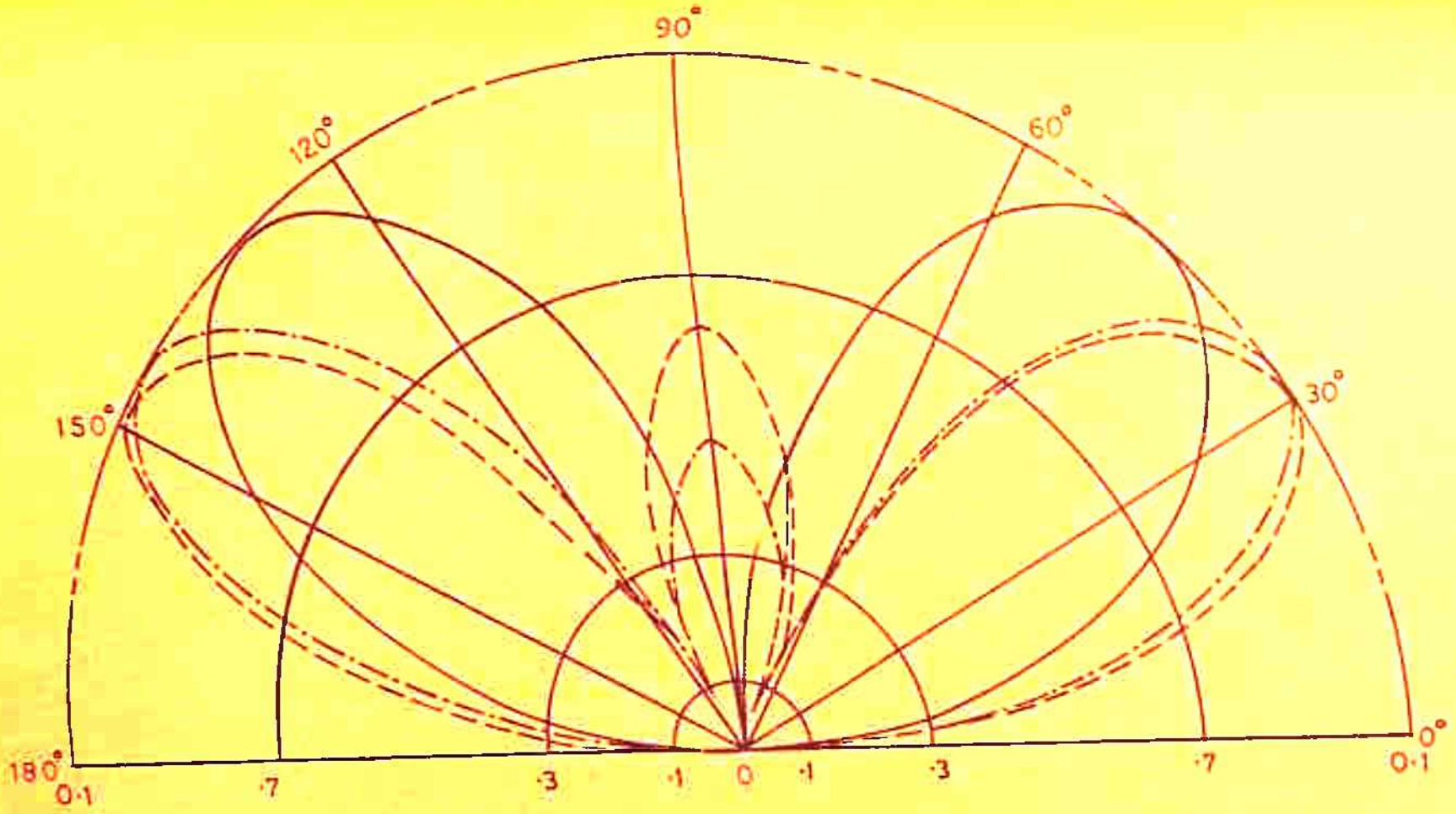

FIG.(6·18) E AND H-PLANE PATTERNS (ELECTROMAGNETIC MODE) FOR AXIALLY DISPLACED ASYMMETRIC DIPOLE ANTENNA FOR $\beta = \beta_0$

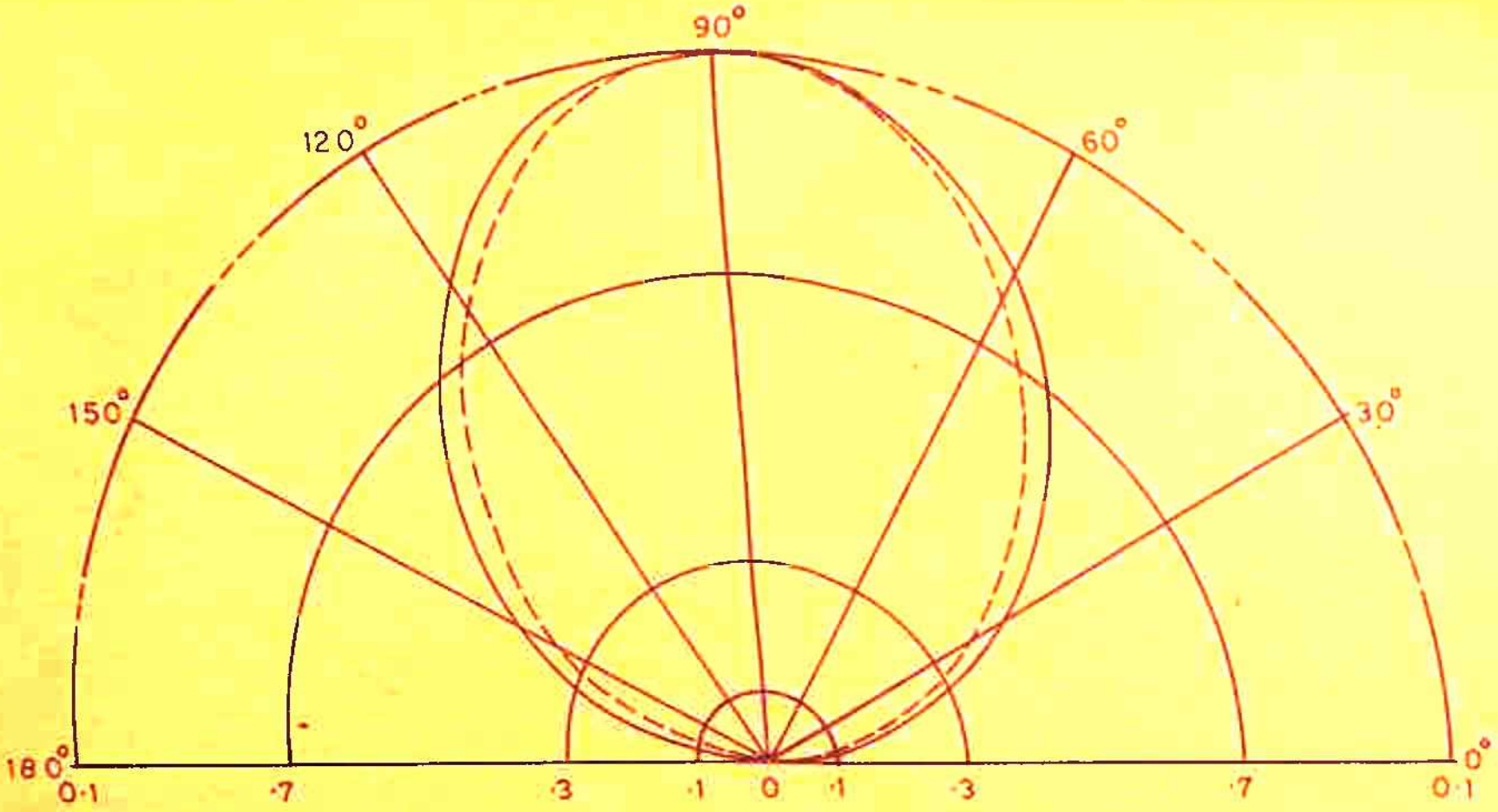

FIG. (6·1k) E AND H-PLANE PATTERNS (ELECTROMAGNETIC MODE) FOR AXIALLY DISPLACED ASYMMETRICE DIPOLE ANTENNA FOR $\beta = \beta_e$

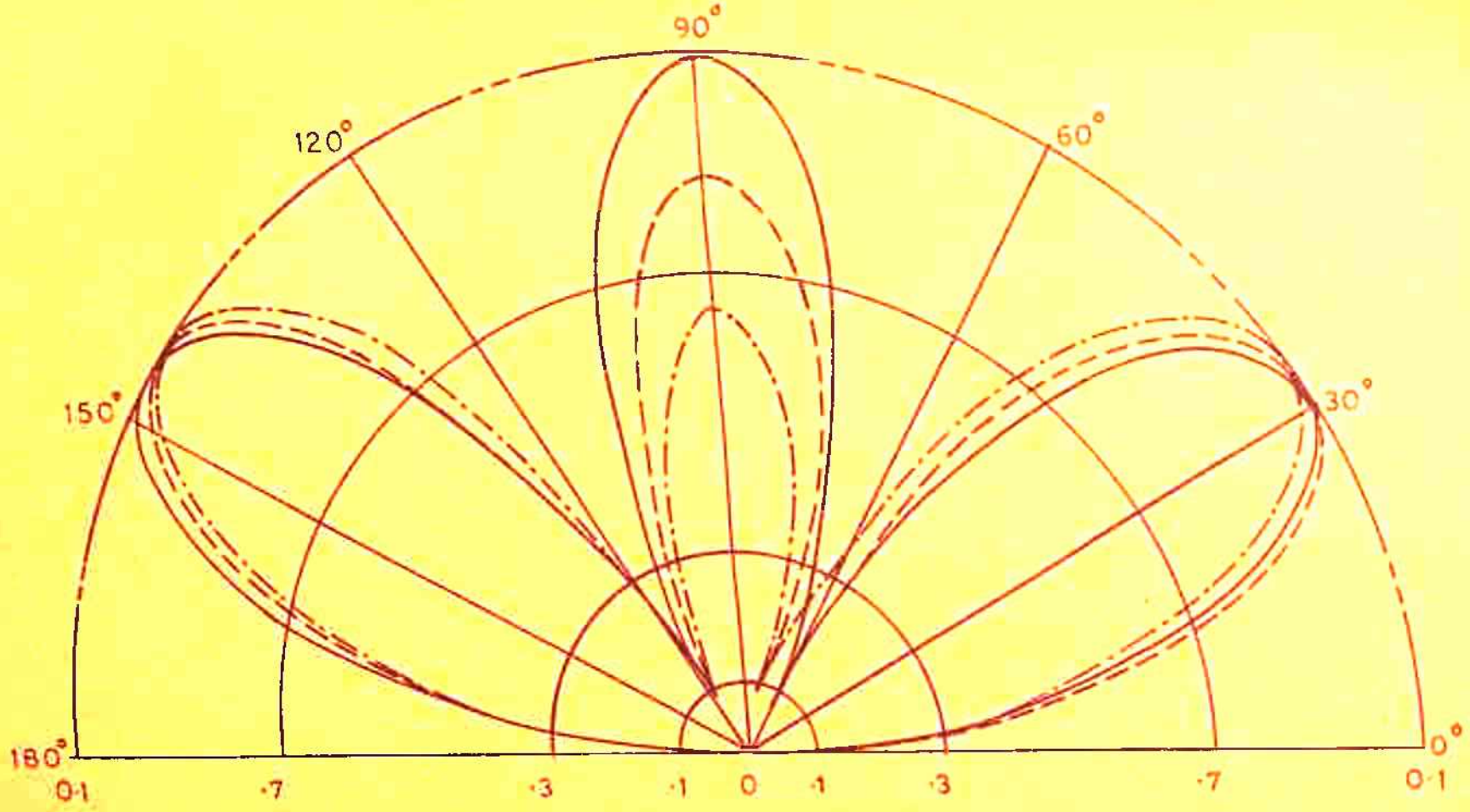

FIG. (6.11) E AND H-PLANE PATTERNS (ELECTROMAGNETIC MODE) FOR AXIALLY DISPLACED ASYMMETRIC DIPOLE ANTENNA FOR $\beta = \beta_p$

Following data has been used for computation:

$\phi_1 = \phi_2 = 90^\circ$

$h_1/\lambda = 0.25$

$h_2/\lambda = 0.75$

$\frac{\omega}{2\pi} = 5.6 \times 10^{10}$ c.p.s.

$\frac{\omega_p}{2\pi} = 5.6 \times 10^{8}$ c.p.s.

$\frac{c}{v_o} = 10^3$

$v_o = 0.3 \times 10^8$ cms./sec.

$\theta_1 = \theta_2 = 0^\circ$ (for axial displacement)

$\theta_1 = \theta_2 = 90^\circ$ (for trans. displacement)

$\theta_1 = \theta_2 = 45^\circ$ (for arbitrary displacement)

$2R/\lambda = 0.05, 0.1, 0.2$

§ 6.3 CONCLUSIONS AND DISCUSSIONS

From the theoretical plots shown in figures(6.1a-6.1 for E and H-plane patterns, following conclusions may be drawn:

Axial Displacement

(i) $\beta = \beta_o$, two lobes of equal amplitude with a smaller lobe at 90° are obtained. The two main lobes are symmetrically situated for $2R/\lambda = 0.05$. However, as $2R/\lambda$ is increased, these lobes shift to 30° on one side and 150° on the other side of 90° axis. Also the lobes at 90° become smaller.

(ii) $\beta = \beta_e$, single lobed pattern is obtained for $2R/\lambda = 0.05$ to 0.2. 3dB beam width decreases from 77^0 to 70^0 as $\frac{2R}{\lambda}$ is increased from 0.05 to 0.2.

(iii) $\beta = \beta_p$, three lobes at 30^0, 90^0 and 145^0 are obtained for $\frac{2R}{\lambda} = 0.05$. As $2R/\lambda$ is increased upto 0.2, the lobes at 30^0 and 145^0 shift to 35^0 and 140^0 respectively while the lobe at 90^0 remains fixed and becomes smaller and smaller as $\frac{2R}{\lambda}$ increases.

Transverse Displacement

(i) $\beta = \beta_o$, one major lobe at 50^0 and a side lobe at 135^0 are observed. As $2R/\lambda$ increases upto 0.2, the major lobe as well as the side lobe shift from their observed positions and also another small lobe is observed near 150^0. This side lobe decreases as $2R/\lambda$ increases upto 0.2.

(ii) $\beta = \beta_e$, as in the case of axial displacement, single lobed pattern is observed but the position of the beam maximum shifts by 5^0 as $2R/\lambda$ increases upto 0.2. 3dB beam width increases from 78^0 to 82^0 as $2R/\lambda$ is increased upto 0.2.

(iii) $\beta = \beta_p$ one major lobe at 95^0 and side lobes at 30^0 and 150^0 are obtained. With the increase of $\frac{2R}{\lambda}$ upto 0.2, the major lobe at 90^0 becomes smaller and shifts its position from 95^0 to 105^0 while the side lobe at 30^0 becomes larger and also shifts to 40^0. However, the smaller lobe at 150^0 remains fixed and

becomes smaller and smaller as $2R/\lambda$ is increased upto 0.2.

Arbitrary Displacement

(i) $\beta = \beta_o$, one major lobe at 50° and a side lobe at 135° are observed for $2R/\lambda = 0.05$. As $2R/\lambda$ is increased upto 0.2, major lobe shifts to 35° and the amplitude of the minor lobe decreases and shifts to 150°. In addition, for $2R/\lambda = 0.1$ and 0.2, there are additional lobes appearing near 90° which decrease as $2R/\lambda$ is increased.

(ii) $\beta = \beta_e$, a single lobed pattern is obtained which shifts its maximum position from 90° to 100° as $2R/\lambda$ increases. 3dB beam width decreases from 83° to 73° with the increase in feed point displacement.

(iii) $\beta = \beta_p$, two lobes (at 35° and 90°) of almost the same amplitude and a smaller lobe at 150° are observed for $2R/\lambda = 0.05$. As $2R/\lambda$ is increased to 0.2, the lobe at 35° shifts to 40° while the one at 90° shifts to 100° and becomes smaller. However, the side lobe at 150° remains fixed, but decreases in amplitude as $2R/\lambda$ goes upto 0.2.

It may be noted that, though, the general phase shift constant has been studied into three cases, namely, $\beta = \beta_o$, $\beta = \beta_e$ and $\beta = \beta_p$, all the three modes (β_o, β_e and β_p) are simultaneously present on the conductor.

C H A P T E R - 7

CONCLUSIONS AND DISCUSSIONS

§ 7.1 DISCUSSIONS

The theoretical and experimental studies of the displaced asymmetric dipole antenna are discused in chapter-2. In deriving various expressions for such a system, following assumptions were made:

i) The dipole is extremely thin

ii) The current distribution is strictly sinusoidal

iii) The coupling between the dipole and the feeder line is negligible

iv) The radiation from the ends is also negligible.

Above assumptions are only ideal conditions which are difficult to be realised in practical design of the displaced antenna system, specially for larger values of feed point displacement R. Some of the main difficulties which arise while verifying the theory of the displaced dipoles are:

i) The unavoidable coupling between the displaced system and the feeder line becomes more and more prominent with the increase in the feed point displacement

ii) The change in the distribution of the e.m. field in the feed-point region as R is increased

iii) The resulting change in the current distribution which may no longer remain strictly sinusoidal as R is increased.

However, attempts were made to verify the theoretical predictions for two displaced configurations, namely, the transversely displaced and the axially displaced systems. From the experimental and theoretical curves given in various figures of chapter-2, it may be seen that the discrepancy becomes prominent after $2R = 0.16\lambda$. Similar discrepancies are observed in the theoretical and experimental results shown in graphs of chapter-3. It may be recalled that in the solution of the wave equation (right hand side of equation (3.5)) the term $V_o/2$ is derived assuming that the scalar potential ϕ is constant across the line and δ function generator is applied. When the displacement is considered, ϕ may not any longer be a constant across the line. Because of the change in distribution of ϕ in the gap region, the current distribution also changes. However, from the experimental studies made so far, it has been found that usually a displacement $\leq 0.16\,\lambda$ does not effect adversely the assumed sinusoidal current distribution and hence the theoretical results derived on such an assumption agree reasonably good with the experimental results.

Experimental curves for the voltage distribution on a centre fed transversely displaced dipole antenna have been reported for various values of R by Kosta (31). A comparision of the current distribution shown in fig.(2.11a) with that given by Kosta shows that a sinusoidal distribution is a reasonably good assumption for smaller values of R($R \leq 0.08$).

The theoretical results derived for various parameters in chapters 4 and 5 for the log-periodic structure show a disagreement with the experimental variation of these paramenters (radiation pattern, gain, input impedance and effective aperture). It may be remembered that the basic element of the LPD array ($\phi \neq 0^{\circ}$) are the dipoles with their feed points displaced transverse to their axis (first term in square brackets of equation (4.1) and the term given by equation (5.2) respectively). The displacement in the feed points of the elements employed in an LP array is given by $R_n \sin(\phi/2)$. Obviously, as ϕ increases, the feed point displacement also increases. Hence, beyond a certain limit (usually ϕ 50° to 60°) the displacement becomes so large that the field in the gap changes appreciably. Consequently the assumption of strictly sinusoidal current distribution breaks. As a result, the various theoretically derived paremeters, namely, the input impedance,

Such studies will find their immense use in multichannel communication systems needed both for entertainment (TV systems) and the space research (space vehicles).

APPENDIX - 1

DESIGN AND FABRICATION OF LPD ANTENNA

Important characteristics for design consideration

Any electronic system which uses free space as the medium of propagation needs antenna, essentially to serve two purposes - matching impedance of transmission line to the free space and directing the radiations in the desired direction. So the characteristics of major importance for designing an antenna are its input impedance and its directional properties. Depending upon the application we are interested in designing an antenna which has given directivity and input impedance over a given frequency band.

Not only these electrical properties, i.e., directivity and input impedance, but some non-electrical requirements also play an important role in the design of an antenna. The other factors of importance which govern the design and fabrication of an LPDA antenna are as follows:-

(i) The band width of the antenna array: This may be made arbitrarily wide by extending the geometry of the antenna structure. The band width limit of a given design is determined by non-electrical restriction ; size of the antenna governs the low frequency limit, and precision of construction governs the high frequency limit.

(ii) Size, weight, compactness and portability of the antenna: The size and weight of the antenna array should be such that it may be supported by a boom and mounted on a single mast with facilities for rotational adjustment.

Details of the antenna to be designed

A pyramidal log-periodic dipole array antenna is designed and fabricated. This is shown in fig. 1 . The important design parameters - ϕ , the separation angle between the two booms ; α , the spread angle between the plates ; τ , the ratio of the lengths of the successive elements - are shown in the figure. A third angle β represents the spread angle for each boom in preceeding from apex to the rear of the antenna. In general β is not a significant design constant. A dependent variable, called the relative spacing factor σ , is defined as the distance in the wavelengths between the half wavelength dipole and its next smaller neighbour, and is given by

$$\sigma = \frac{1}{4}(1 - \tau) \cot \alpha \qquad (1)$$

This may be noted that LPDA antenna may be derived from this antenna by letting β zero and folding the two booms such that angle ϕ approaches zero.

Characteristics of the antenna to be designed Vs. parameters

There is no theoretical formulation upon which the design of LPDA is based. The design has to be based on logical experimental methods. The design data here have been extracted from

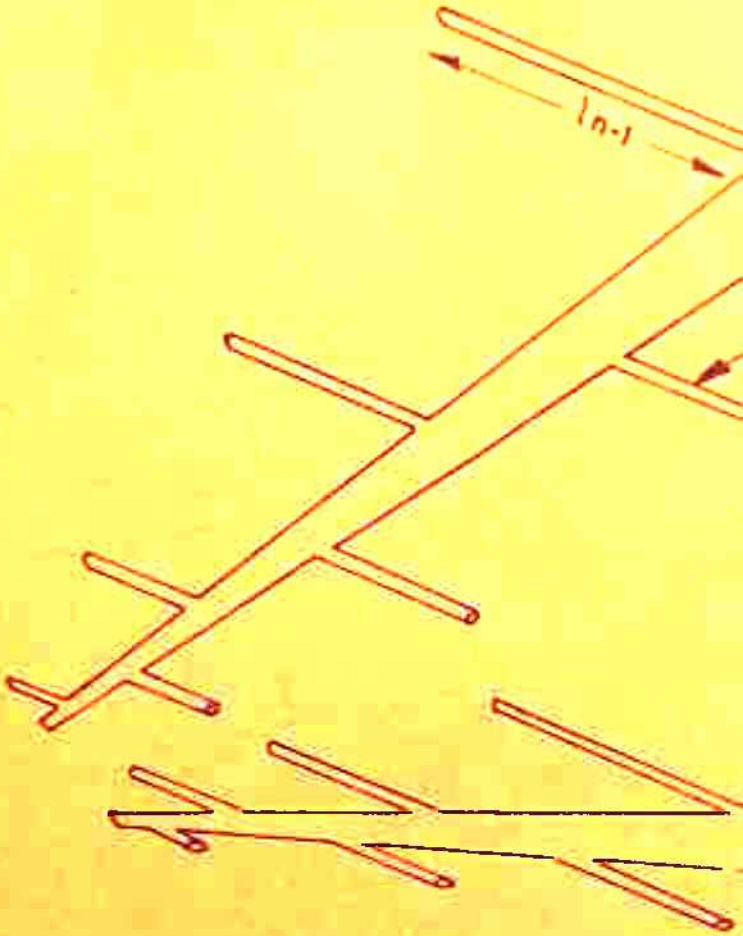

FIG. 1. PYRAMIDAL

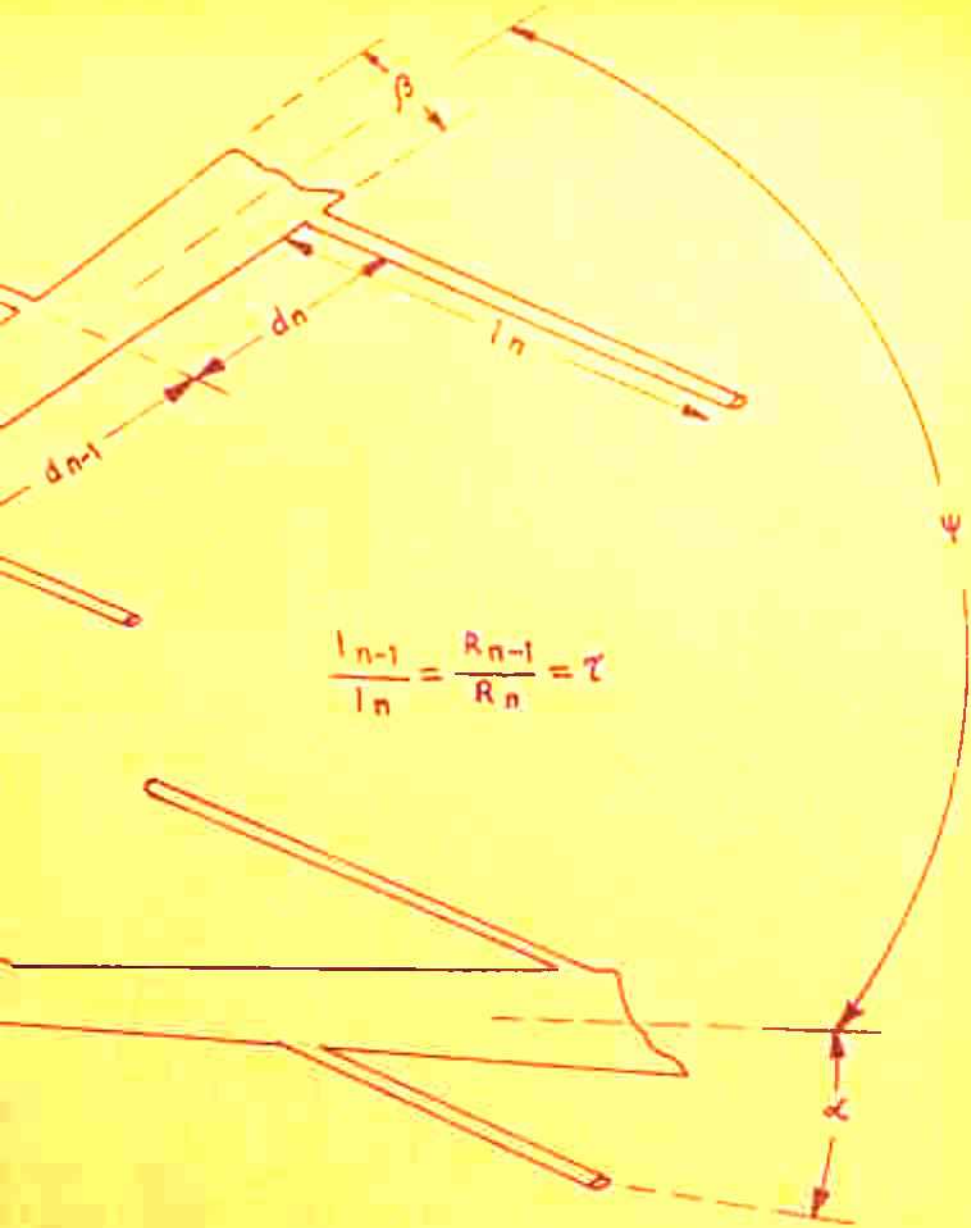

$$\frac{l_{n-1}}{l_n} = \frac{R_{n-1}}{R_n} = \tau$$

LP DIPOLE ARRAY

the result of investigations of Carrel (28). The experimental results of investigations of Carrel and others are shownin figs. (2a, 2b, 2c). These graphs indicate the variation of input impedance and directivity with τ , α and σ . The study of these curves reveals two facts:

1) As τ approaches unity, the directive gain increases and number of dipoles required also increases but the feed point impedance decreases.

2) On the other hand as α increases, both directive gain and input impedance decrease. As α decreases, directivity increases, but the spacing and thus the length of the boom increases.

If the active region has got no width, the operating bandwidth B would be given by the ratio of the length of the largest element to the length of the smallest element on the antenna. This is called the bandwidth of the structure, B_s

$$B_s = \frac{l_1}{l_N} = \tau^{1-N}$$

Since the active region has got some bandwidth it is apparent that the operating bandwidth B is always less than the structure by a factor B_{ar}, bandwidth of the active region,

$$B_s = B \times B_{ar} \qquad (2)$$

A graph of B_{ar} Vs. α for general values of τ is given in fig.(2c).

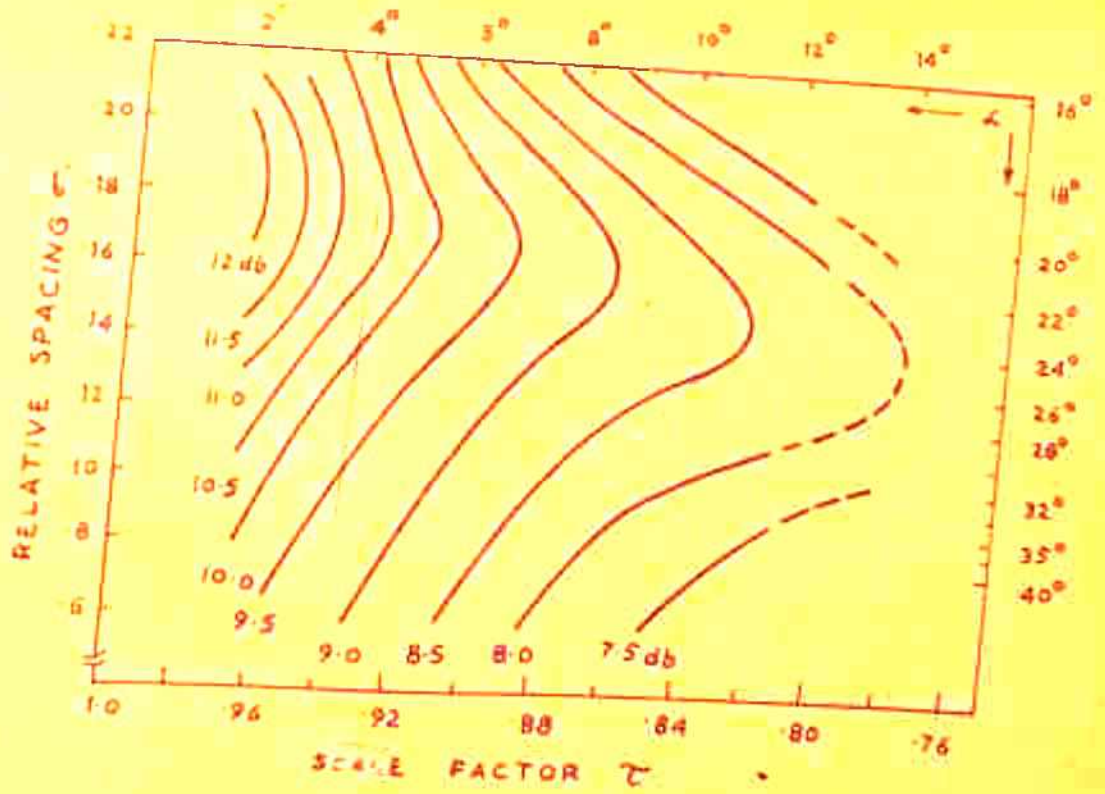

FIG.(2a) CONSTANT DIRECTIVITY CONTOURS Vs τ, σ, α.

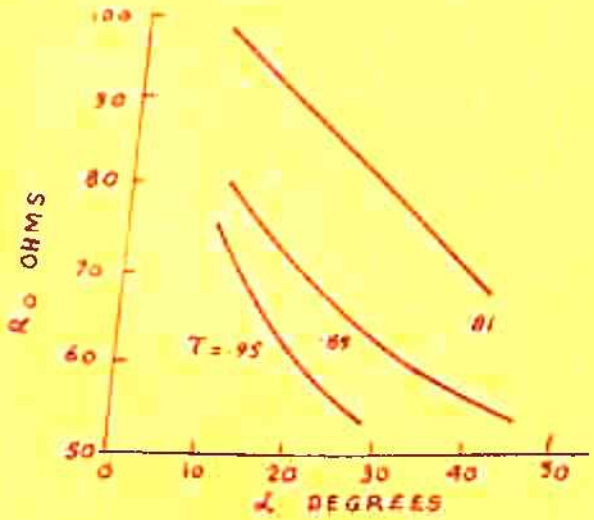

FIG.(2b) MEAN RESISTANCE R_0 Vs α

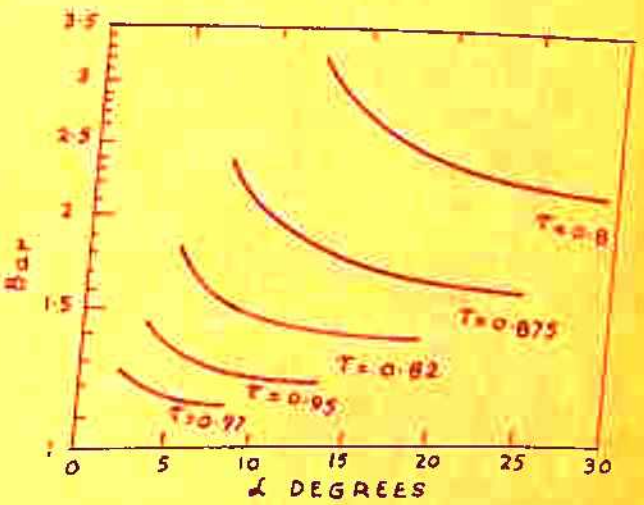

FIG.(2c) BAND WIDTH OF ACTIVE REGION Bar Vs α.

FIG. 2. ANTENNA CHARCTERISTIC VS PARAMETERS

Design procedure

Design procedure involves a judicious choice of the principal pattern parameters, α and τ, to be established to meet the given requirements of directivity and impedance. Once these electrical properties are specified we have to decide a relative importance of reducingthe number of elements or size and weight of the antenna.

With these facts in mind a preliminary choice of τ and σ or α can be made from the curve of fig. (2a). To determine the boom length and number of elements, the bandwidth of the structure must be found. Let fig. (2) be consulted to determine the bandwidth B_{ar} for the given values of τ and α. The bandwidth of the structure can then be found from

$$B_s = B \times B_{ar}$$

where B is the required bandwidth. The geometry of the LPDA antenna now provides a relation between boom length relative to the longest operative wavelength, λ_{max}. Since the length of the first element is always made equal to $\lambda_{max}/4$,

$$\frac{L}{\lambda_{max}} = \frac{1}{4}\left(1 - \frac{1}{B_s}\right) \cot \alpha \qquad (3)$$

where L is the boom length between the largest and smallest elements. A monograph of the equation is given in fig. (3a).

The number of elements required is found from the

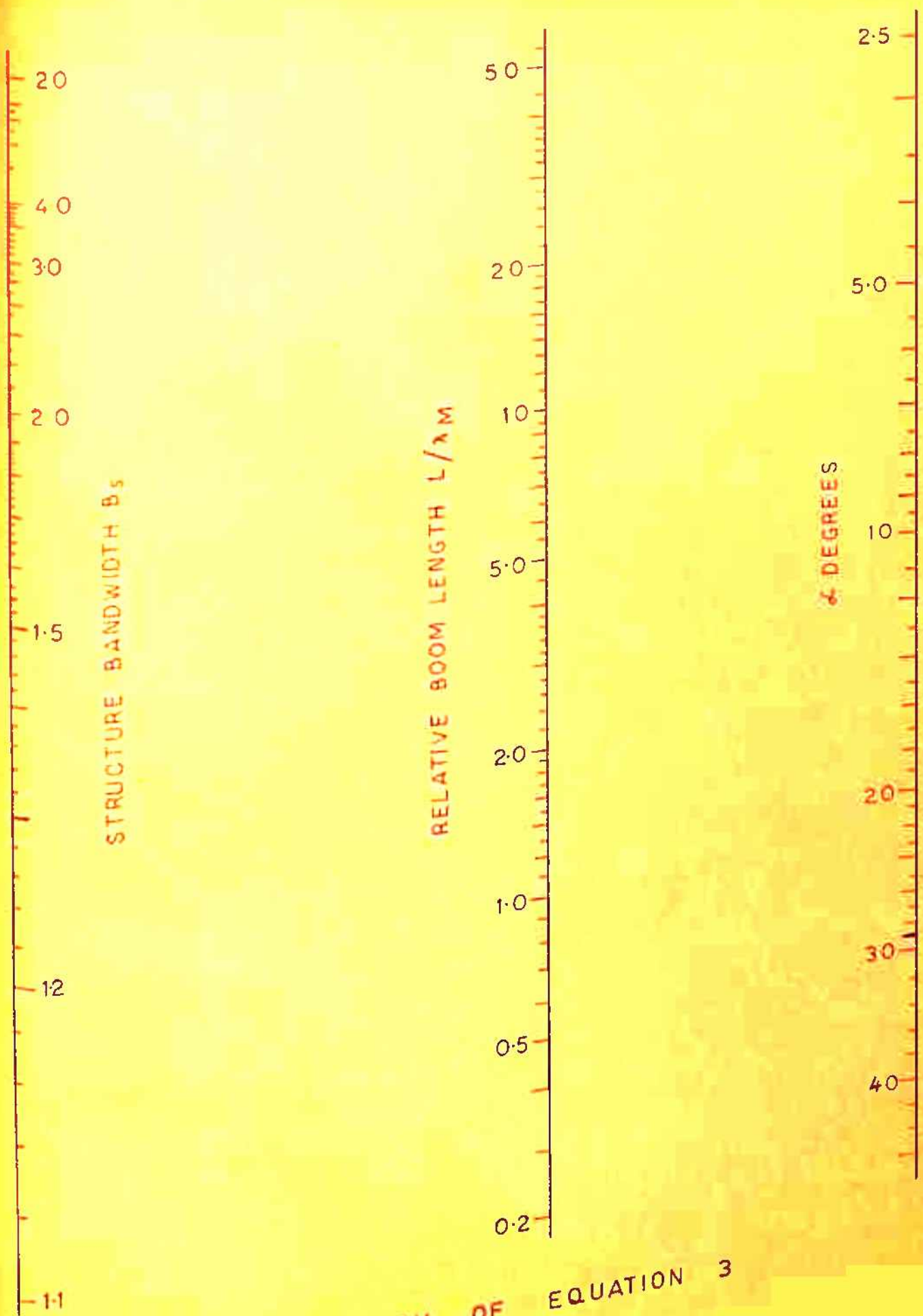

FIG.(3a) MONOGRAPH OF EQUATION 3

equation

$$N = 1 + \frac{\log B_s}{\log 1/\tau} \qquad (4)$$

a monograph of which is given in fig. (3b).

The design procedure for the principal LPDA parameters is now complete. It is likely that the first estimate of τ and α will lead to a longer boom length than necessary. So revision must be made in τ and α and above procedure must be repeated several times until minimum boom length is found.

A pyramidal LPDA antenna has been designed to meet the following requirements

Directive gain - ~~7.5~~ db, bandwidth ratio of 1:5 between lowest and highest frequency (300 MH_z/S and 1.5 GH_z), input impedance - 75 ohms, λ_{max} - 100 cms, Values of $\tau = 0.9$ and $\alpha = 25^0$ were selected from curves of fig. (2). The bandwidth of the active region B_{ar} for $\alpha = 25^0$ is 1.5 from fig. (2). This means that thebandwidth of the structure must be 6.5. The relative boom length for $B_s = 6.5$ and $\alpha = 25^0$ is 0.46 from fig. (3a), and $N = 19$ from fig. (3b). The height of element number one is $\lambda_{max}/4$ = 25 cm. The antenna was then fabricated with these data.

Fabrication of antenna

Fabrication of components designed for any experiment is one of the most important factors The accuracy upto which the fabrication of the designed component can be achieved is set by

4
EQUATION
OF
MONOGRAPH
FIG.(3b)
1·1
1·2
1·4
Bs
2·0
3·0
5·0
10
20
1
2
5
10
20
50
100
160
NUMBER OF ELEMENTS N
·70
·80
·90
·94
96
98
SCALE FACTOR T

the facilities available. As the LPDA antenna has varying dimensions in length and spacings of the dipoles, the fabrication poses a problem towards the high frequency end. The size of the dipoles and the distance between them become too small towards high frequency end to build with accuracy, and it is the precision of construction that determines and limits the high frequency operation of the antenna.

The fabrication of pyramidal LPDA antenna was simplified by the fact that two halves of the structure were identical. One half of the structure is shown in fig. 4 . The boom was cut out of a brass plate of 0.2 cm thickness. The bottom plate and two side plates were cut separately and welded together. The length of the bottom plate, along the axis was 46.4 cm., the width at high frequency end was 1.1 cm and 7.6 cm at low frequency end, the two sides subtending an angle 8° at their extended meeting point. Copper tubing of 0.8 cm outer diameter and 0.6 cm inner diameter was chosen for dipoles elements. The largest element was equal to $\lambda_{max}/4$, i.e., 25 cm long with successive elements satisfying LP criterion with $\tau = 0.9$. Holes of 0.8 cm diameter were drilled in the side plates at the spacings shown in the figure and dipole elements through the holes were brazed along the centre line of the boom. A schematic diagram of the complete half structure is shown in the fig. 5 .

The two half structures were hinged at high frequency end and a bracket with a slot and nut and bolt system was attached at

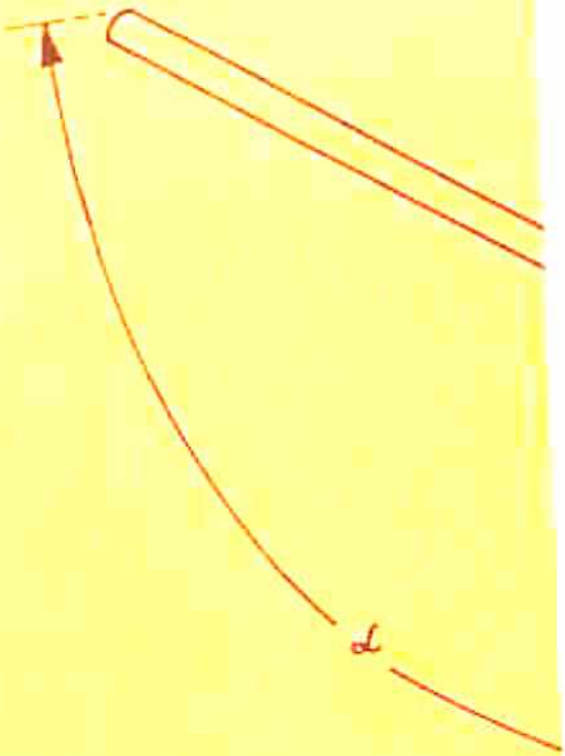

FIG. 4.

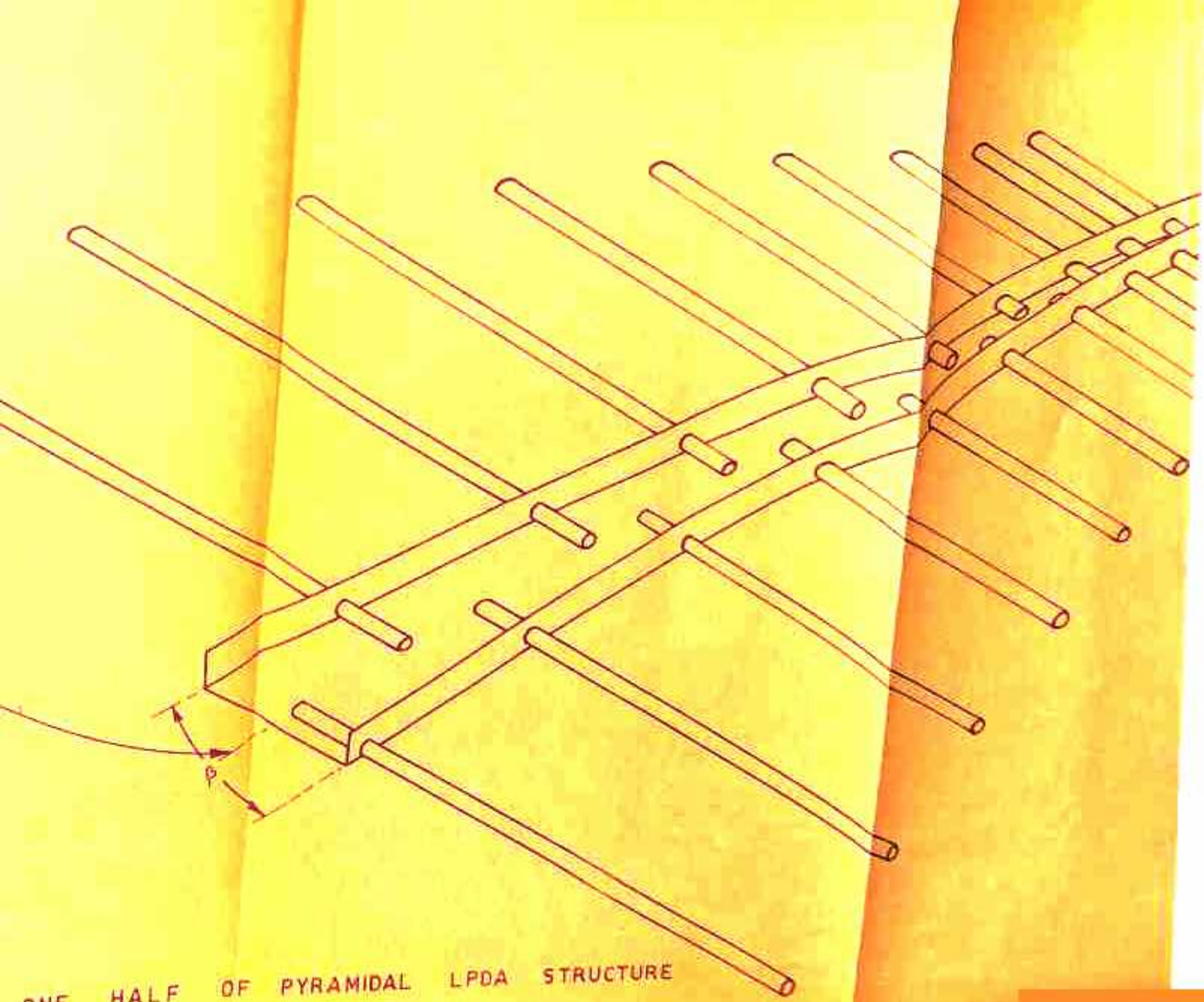

ONE HALF OF PYRAMIDAL LPDA STRUCTURE

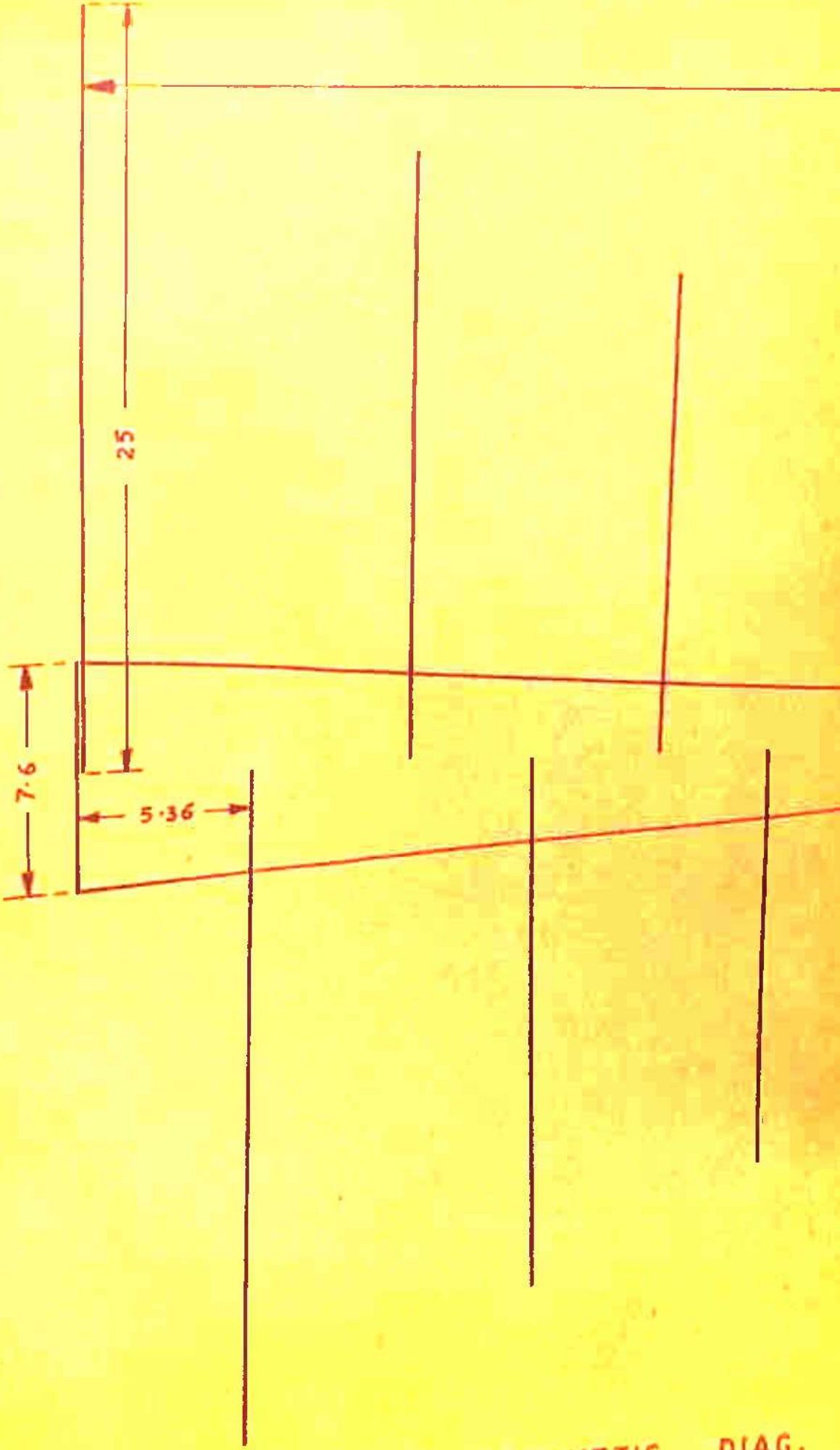

FIG. 5. SCHEMETIC DIAG.

46·2

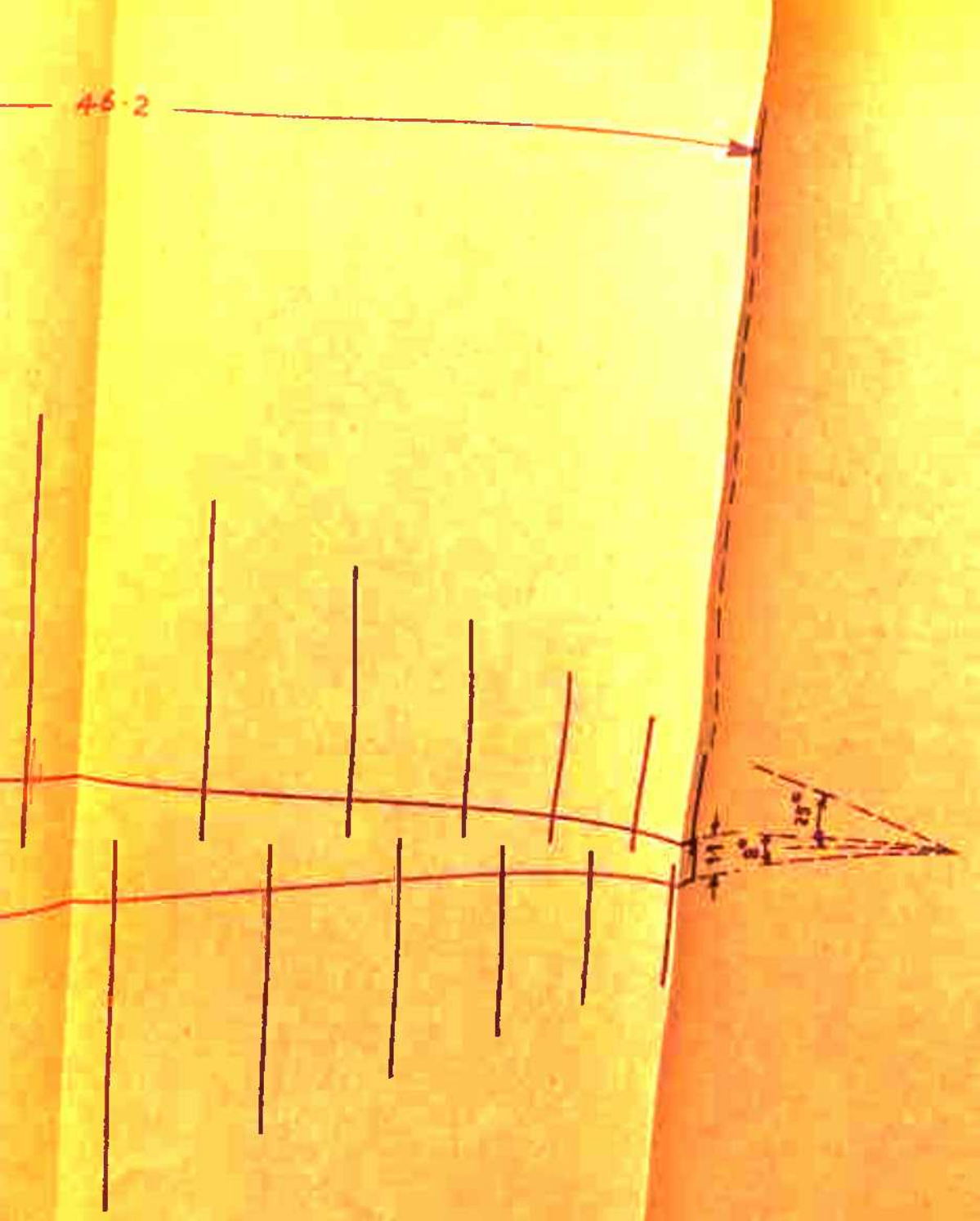

(ALL DIM. IN Cm.)

OF HALF STRUCTURE

the far end to provide a variable ϕ , the separation angle between the two booms. The antenna was fed by a 75 ohms coaxial cable, connecting inner conductor to one boom and outer to the other at high frequency end.

Two identical antennas were fabricated, one to be used as the radiator and other as the receiver. Both receiving and transmitting antennas were mounted on the masts fabrication of which has been described in chapter-2.

APPENDIX- 2.

LIST OF PUBLICATIONS

1. Banerjee, P. K., et al., "UNBALANCED CENTRE FED DIPOLE WITH ARBITRARILY DISPLACED FEED POINTS", Jan.'72, No. 5, Vol. 52, Pt. ET-3, pp. 161-63.

2. Banerjee, P. K., et al., "ON THE INPUT IMPEDANCE AND GAIN OF THE LOG-PERIODIC DIPOLE ANTENNA", Presented at the International Symposium on Antennas and Propagation held in Tokyo, Japan in Sept., '71.

3. Banerjee, P. K., et al., "INPUT IMPEDANCE AND GAIN OF THE LOG-PERIODIC DIPOLE ANTENNA", NTZ Comm. Jr., Vol. 25, May 1972, pp. 247-248.

4. Banerjee, P. K., et al., "ANALYSIS OF AN ASYMMETRIC DIPOLE ANTENNA WITH DISPLACED FEED POINTS", Jr. of ITE, Vol. 18, No. 5, May, '72, pp. 211-214.

5. Banerjee, P. K., et al., " A NEW LOG-PERIODIC STRUCTURE WITH ASYMMETRIC DIPOLE ELEMENTS", Accepted for Publication in Nov. issue of Jr. ITE.

6. Banerjee, P. K., et al., "THE INPUT IMPEDANCE, RADIATION RESISTANCE AND GAIN OF THE LOG-PERIODIC DIPOLE ANTENNA WITH ASYMMETRIC DIPOLE ELEMENTS", Accepted for publication in Indian Journal of Pure and Applied Physics.

REFERENCES

1. King, R. W. P., "THE THEORY OF LINEAR ANTENNAS", Harvard University Press, Cambridge, Mass, 1956.

2. Kraus, J. D., "ANTENNAS", Mc Graw-Hill Book Company, 1950.

3. Schelkunoff, S. A. and Fris, H. T., "ANTENNA THEORY & PRACTICE", John Willey & Sons Inc., 1952.

4. Jordan, E. C. "ELECTROMAGNETIC WAVES & RADIATING SYSTEMS", Englewood Cliff, N. J., Prentice Hall, 1950.

5. Smith, R. A., "AERIALS FOR METRE & DECIMETER WAVELENGTHS", Cambridge University Press, 1949, pp. 3-5.

6. Smith, R. A., and Smith, C. H., "THE ELIMINATION OF ERRORS FROM CROSSED-DIPOLE DIRECTION FINDING SYSTEMS", JIEE, 93, IIIA, 1946, p. 575.

7. Schelkunoff, S. A. and Fris, H. T., "ANTENNA THEORY & PRACTICE", John Willey & Sons Inc., 1952, pp. 349-51.

8. Kosta, S. P., "THEORETICAL INVESTIGATIONS ON THE CENTRE FED DIPOLE ANTENNA WITH FEED POINTS DISPLACED TRANSVERSE TO DIPOLE AXIS", Proc. IEEE, Oct., 1967, pp. 1760-61.

9. Du-Hamel, R. H. and Isbell, D. E., "BROAD BAND LOGARITHMICALLY PERIODIC ANTENNA STRUCTURE", IRE Nat. Conv. Rec., Pt. 1, 1957, pp. 119- 28.

10. Isbell, D. E., "NON-PLANAR LOGARITHMICALLY PERIODIC STRUCTURE", Tech. Report 30, Contract AF-33(616)-6220, Antenna Laboratory, University of Illinois, Urbana, 1958.

11. Du-Hamel, R. H., and Ore, F. R., "LOGARITHMICALLY PERIODIC ANTENNA DESIGN", IRE Nat. Conv. Rec. Pt. 1, 1958, pp. 139-51.

12. Isbell, D. E., "LOG-PERIODIC DIPOLE ARRAYS", IRE Trans. on Antennas and Propagation, Vol. AP-8, 1960, pp. 260-67.

13. Radford, M. F. and Wolos-Zezuk, E. W., "LOGARITHMIC AERIALS IN COMMUNICATION SYSTEMS", Point to Point Telecommunication- 7, 1967, pp. 24-39.

14. Rumsey, V. H., "FREQUENCY INDEPENDENT ANTENNAS", Academic Press, New York, 1966, pp. 73-87.

15. Carrel, R. L., "ANALYSIS AND DESIGN OF LOG-PERIODIC ANTENNAS", Tech. Report No. 52, Antenna Laboratory, University of Illinois, Urbana, 1961.

16. Mitra, R. and Jones, K. E., "THEORETICAL BRILLOUIN (k/β) DIAGRAMS FOR MONOPOLE AND DIPOLE ARRAYS AND THEIR APPLICATIONS TO LOG-PERIODIC ANTENNAS", IEEE Trans. on Antennas and Propagation, Vol. AP-12, No. 3, 1964, pp. 533- 40.

17. Mayes, P. E., Deschamps, G. A. and Patton, W. T., "BACKWARD WAVE RADIATION FROM PERIODIC STRUCTURES AND APPLICATION TO THE DESIGN OF FREQUENCY INDEPENDENT ANTENNAS", Proc. IRE, No. 49, 1961, pp. 962- 63.

18. Kosta, S. P., "A THEORY OF LOG-PERIODIC DIPOLE ANTENNA", Int. J. Elec., Vol. 23, No. 5, 1967, pp. 473- 83.

19. Cohen, M. H., 1961, Phys. Rev., 123, 711, 1962, Ibid., 126, 389, 393.

20. Chen, K. M., Judson, H. and Lin, C. C., "EXPERIMENTAL STUDY OF AN ELECTROSTATIC WAVE EXCITED BY AN ANTENNA IN A HOT PLASMA", Proc. IEEE, 55, 1956, 1967.

21. Talekar, V. L. and Gupta, B. K., "RADIATION FROM LINEAR RESONANT ANTENNA IN WEAKLY IONIZED PLASMA", Int. J. Elec., Vol. 21, No. 5, 1966, pp. 443- 55.

22. Kosta, S. P. et al, "THEORETICAL STUDY OF CENTRE FED DIPOLE ANTENNA WITH DISPLACED FEED POINTS IN PLASMA MEDIUM", Journal of ITE, Vol. 16, No. 11, 1970, pp. 799-802.

23. Monsor, C. J., "PRACTICAL LOG-PERIODIC ANTENNA DESIGN", Electronics, Vol. 37, No. 15, 1964, pp. 91-94.

24. Jordan, E. C., "ELECTROMAGNETIC WAVES AND RADIATING SYSTEMS", Prentice Hall of India (New Delhi), 1969, pp.323

25. Kraus, J. D., "ANTENNAS", New York, Mc Graw -Hill Book Company Inc., 1950, p. 136.

26. Page, H., "PRINCIPLES OF AERIAL DESIGN", Iliffe Ltd., 1966.

27. Choong, W. M. and King, R. W. P., "LOG-PERIODIC DIPOLE ANTENNA", Radio Sci., Vol. 2, 1967, pp. 1315-1325.

29. Carrol, R. L., "THE DESIGN OF LOG-PERIODIC DIPOLE ANTENNAS", IRE Conv. Rec., Pt. 1, 1961, pp. 61-75.

29. Sengupta, D. L., "ON THE PHASE VELOCITY OF WAVE PROPAGATION ALONG AN INFINITE YAGI STRUCTURE", IRE Trans. on Antennas and Propagation, Vol. AP-7, 1959, pp. 235-239.

30. Jordan, E. C., "ELECTROMAGNETIC WAVES AND RADIATING SYSTEMS", Prentice Hall of India (New Delhi), 1969, p. 548.

31. Kostu, S. P., "EXPERIMENTAL STUDY OF A DIPOLE WITH FEED-POINTS DISPLACED TRANSVERSE TO DIPOLE AXIS", Int. J. Elec., No. 4, April, 1963, pp. 365- 372.

***